LUND UNIVERSITY

Clues to galaxy evolution from spectroscopic observations of Galactic centre stars

Thorsbro, Brian

2020

Clues to galaxy evolution from spectroscopic observations of Galactic centre stars

BRIAN THORSBRO

DEPT. OF ASTRONOMY AND THEORETICAL PHYSICS | LUND UNIVERSITY 2020
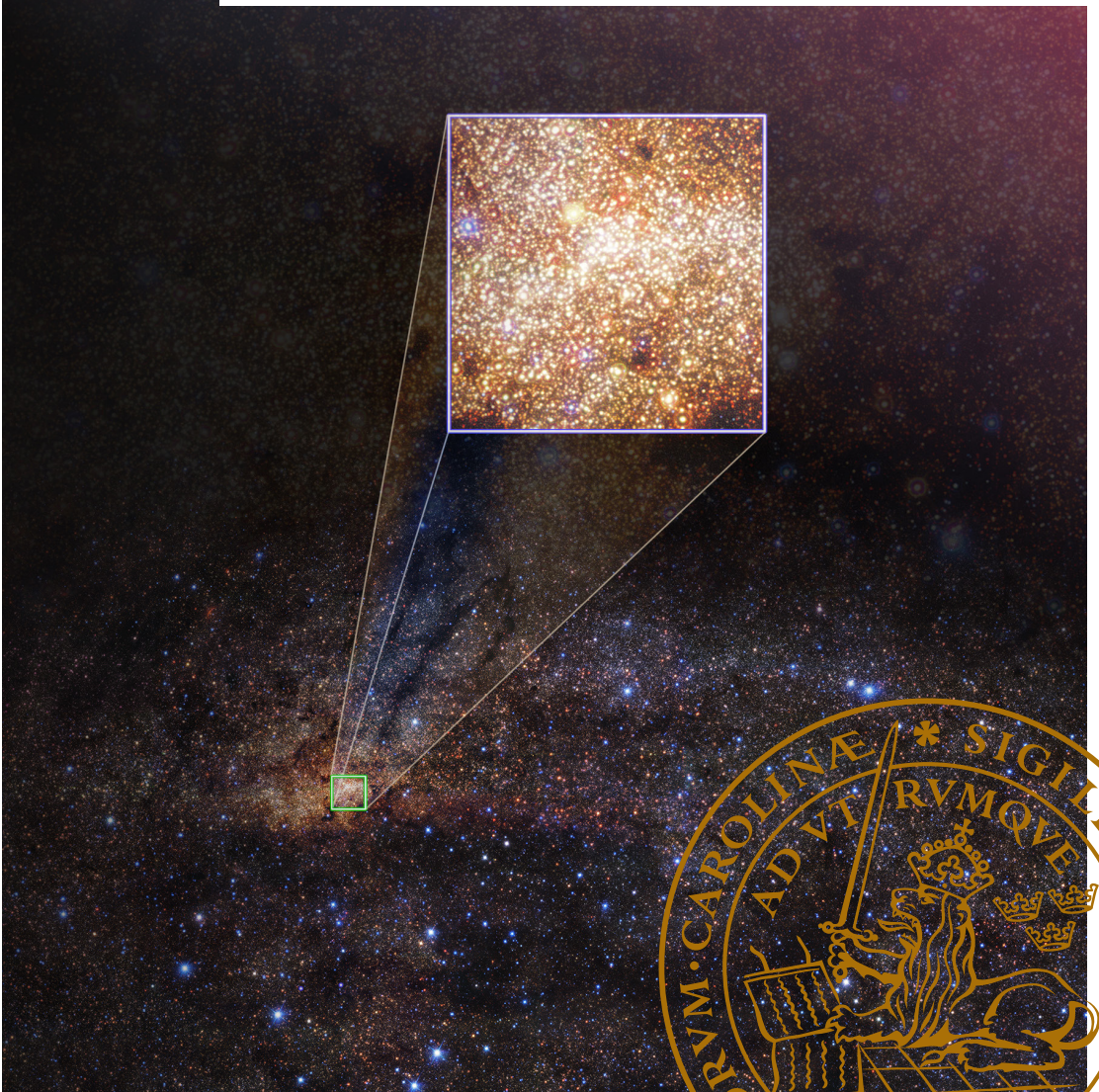
Clues to galaxy evolution from spectroscopic observations
of Galactic centre stars

Clues to galaxy evolution from spectroscopic observations of Galactic centre stars

Brian Thorsbro

LUND
UNIVERSITY

Thesis for the degree of Doctor of Philosophy

Organization		Document name	
Organization LUND UNIVERSITY		**Document name** DOCTORIAL DISSERTATION	
Department of Astronomy and Theoretical Physics Box 43, SE-22100 Lund, Sweden		**Date of issue** 2020-08-31	
Author(s) Brian Thorsbro		Sponsoring organization	

Title and subtitle
Clues to galaxy evolution from spectroscopic observations of Galactic centre stars

Abstract

In this work we present results from spectroscopic observations of Galactic centre stars. High resolution stellar spectroscopy can be used to determine accurate stellar metallicities and abundances. Observing stars in the Galactic centre is challenging due to extreme extinction. However, observing bright M giants in the K band is viable with 10 m telescopes, which is what has been carried out in this work using the Keck II telescope at W. M. Keck Observatory, Hawai'i.

We provide a metallicity distribution of a sample of stars observed in the Galactic centre and show that the sampled stars on average have a metallicity comparable to the Sun, with a subset of the sample having a very high metallicity. We also investigate the silicon abundance of the stars as an alpha tracer, and show that in general there is a similarity between the Galactic centre stars and stars further out. However, for the high metallicity subsample stars in the Galactic centre, there is evidence for a possible alpha enrichment beyond what is found elsewhere in the Galaxy.

Alpha enrichment is a powerful diagnostic as it is central to chemical evolution models giving constraints important for the development of galactic formation and evolution theories. We model the determined alpha enrichment and suggest that there might have been a recent starburst event, or maybe there was a pause in star formation between 3 and 12 Gyr ago. We model different pause scenarios. Further observations of a larger number of stars, and other tracers of alpha elements, are required to verify this result.

We also investigate claims of increased scandium abundances in the Galactic centre and find that the extremely strong scandium lines could be explained by a better understanding of the atomic physics properties of scandium, rather than a high scandium abundance. We find similarly strong scandium lines in stars further out in the Galaxy.

We have thus demonstrated that the determination of abundances of Galactic centre stars is now possible and that future investigation of more stars and more elements will provide necessary and strong constraints to theories of how the Galactic centre have formed and evolved.

Key words
Chemical abundances; Late-type stars; Star clusters; Galactic center; Galaxy chemical evolution; Chemical enrichment

Classification system and/or index terms (if any)

Supplementary bibliographical information	**Language** English
ISSN and key title	**ISBN** ISBN: 978-91-7895-568-8 (print) ISBN: 978-91-7895-569-5 (pdf)

Recipient's notes	**Number of pages** 111	Price
	Security classification	

I, the undersigned, being the copyright owner of the abstract of the above-mentioned dissertation, hereby grant to all reference sources permission to publish and disseminate the abstract of the above-mentioned dissertation.

Signature _B. Thorsbro_   Date 2020-07-07

Clues to galaxy evolution from spectroscopic observations of Galactic centre stars

Brian Thorsbro

LUND
UNIVERSITY

Faculty Opponent

Prof. Catherine A. Pilachowski
Department of Astronomy, lndiana University,
Bloomington, IN, USA

Evaluation Committee

Docent Magnus Axelsson
Astronomiska lnstitutionen, Stockholms universitet
Stockholm, Sweden

Dr. Paola Di Matteo
GEPI, L'Observatoire de Paris,
Paris, France

Dr. Alejandra Recio-Blanco
UMR Lagrange, L'Observatoire de la Côte d'Azur,
Nice, France

To Kristina Arnrup Thorsbro

Contents

List of publications

This thesis is based on the following peer-reviewed publications:

I   **Detailed abundance analysis of a metal-poor giant in the Galactic Center**
    Ryde, N.; Fritz, T. K.; Rich, R. M.; **Thorsbro, B.**; Schultheis, M.; Origlia, L.; Chatzopoulos, S. (2016)
    The Astrophysical Journal, Volume 831, Issue 1, Article 40 (8 pp.)

II **Detailed Abundances for the Old Population near the Galactic Center. I. Metallicity Distribution of the Nuclear Star Cluster**
    Rich, R. M.; Ryde, N.; **Thorsbro, B.**; Fritz, T. K.; Schultheis, M.; Origlia, L.; Jönsson, H. (2017)
    The Astrophysical Journal, Volume 154, Issue 6, Article 239 (15 pp.)

III **Evidence against anomalous compositions for giants in the Galactic Nuclear Star Cluster**
    Thorsbro, B.; Ryde, N.; Schultheis, M.; Hartman, H.; Rich, R. M.; Lomaeva, M.; Origlia, L.; Jönsson, H. (2018)
    The Astrophysical Journal, Volume 866, Issue 1, Article 52 (9 pp.)

IV **Atomic Data Needs in Astrophysics: The Galactic Center "Scandium Mystery"**
    Thorsbro, B. (2020)
    Atoms, Volume 8, Issue 1 (4 pp.)

V   **Detailed Abundances in the Galactic Center: Evidence of a Metal-rich Alpha-enhanced Stellar Population**
    Thorsbro, B.; Ryde, N.; Rich, R. M.; Schultheis, M.; Renaud, F.; Spitoni, E.; Fritz, T. K.; Mastrobuono-Battisti, A.; Origlia, L.; Matteucci, F.; Schödel, R. (2020)
    The Astrophysical Journal, Volume 894, Issue 1, Article 26 (11 pp.)

Papers I, II, III and V are reproduced with permission from The Astrophysical Journal. Atoms is an open access journal and copyright on paper IV is thus retained by Brian Thorsbro.

Work not included in the thesis

Peer-reviewed publications not included in this thesis:

I   **Chemical characterization of the inner Galactic bulge: North-South symmetry**
     Nandakumar, G.; Ryde, N.; Schultheis, M.; **Thorsbro, B.**; Jönsson, H.;
     Barklem, P. S.; Rich, R. M.; Fragkoudi, F. (2018)
     Monthly Notices of the Royal Astronomical Society, Volume 478, Issue 4,
     p. 4374-4389 (16 pp.)

II   **Abundances of disk and bulge giants from high-resolution optical spectra. III. Sc, V, Cr, Mn, Co, Ni**
     Lomaeva, M.; Jönsson, H.; Ryde, N.; Schultheis, M.; **Thorsbro, B.** (2019)
     Astronomy & Astrophysics, Volume 625, Article 141 (25 pp.)

III **The inner two degrees of the Milky Way. Evidence of a chemical difference between the Galactic Center and the surrounding inner bulge stellar populations**
     Schultheis, M.; Rich, R. M.; Origlia, L.; Ryde, N.; Nandakumar, G.;
     Thorsbro, B.; Neumayer, N. (2019)
     Astronomy & Astrophysics, Volume 627, Article 152 (9 pp.)

IV   **Stellar population astrophysics (SPA) with the TNG. Identification of a sulphur line at λair = 1063.6 nm in GIANO-B stellar spectra.**
     Ryde, N.; Hartman, H.; Oliva, E.; Origlia, L.; Sanna, N.; Rainer, M.;
     Thorsbro, B.; Dalessandro, E.; Bono, G. (2019)
     Astronomy & Astrophysics, Volume 631, Letter 3 (5 pp.)

V   **Fluorine in the Solar Neighborhood: The Need for Several Cosmic Sources**
     Ryde, N.; Jönsson, H.; Mace, G.; Cunha, K.; Spitoni, E.; Afşar, M.; Jaffe,
     D.; Forsberg, R.; Kaplan, K.; Kidder, B.; Lee, J.; Oh, H.; Smith, V.; Sneden,
     C.; Sokal, K.; Strickland, E.; **Thorsbro, B.** (2020)
     The Astrophysical Journal, Volume 893, Issue 1, Article 37 (12 pp.)

Positions of trust undertaken during the PhD education:

1. Secretary of the PhD student union at the Faculty of Science, 2017/18.

2. Chair of the PhD student union at the Faculty of Science, 2018/19, representing approximately 450 PhD students.

3. Chair of the PhD student union at Lund University, 2019/20, representing approximately 2100 PhD students.

> *"An easily governed university is no university at all."*
> (Boulton & Lucas, 2008)

Popular summary

Exploring the world we live in is intrinsic to human curiosity. In astronomy this means observing the stars in the Universe around us and trying to understand how it came to be the way it is.

In the work presented in this thesis we have observed stars in the centre of our Galaxy, The Milky Way. We know from studies of other galaxies, that the centre of a galaxy can tell us something about the rest of the galaxy as a whole. This suggests that galactic centres may have coevolved together with the rest of their galaxy.

Since the centre of the Milky Way is the closest galactic centre to us it is the one that we can study in the most detail. Assuming the mediocrity principle, i.e. that we are not special, the detailed observations of our own Galactic centre and how it is connected to the rest of the Galaxy can provide a better basis for our fundamental understanding of how galaxies are connected to their centres.

In our work we find both similarities and differences between the stars found in the centre of the Milky Way and stars found further out in the Galaxy. Stars mostly consist of hydrogen and helium, but will be enriched with other chemical species to varying degrees depending on their formation history. Similarly enriched stars exist in both the centre of the Galaxy and further out. For the extremely enriched stars we find a divergence, with the Galactic centre stars containing more silicon than the stars further out in the Galaxy. This suggests that there may have been different formation histories between the two locations.

If these results can be confirmed by future studies they can be an important part of the bigger question on how our Galaxy formed and evolved. Furthermore, this knowledge can be extrapolated to other galaxies, and perhaps in the end provide important clues to galaxy evolution and formation in general.

Populärvetenskaplig sammanfattning

Att utforska världen vi lever i är en del av människans nyfikna natur. Inom astronomi använder vi denna nyfikenhet till att observera universums stjärnor för att försöka förstå hur allt blev till och hur allt hänger samman. I arbetet som presenteras i denna avhandling har vi observerat stjärnor belägna i centrum av vår galax, Vintergatan. Från studier gjorda på andra galaxer vet vi att centrum av en galax hänger samman med hur hela galaxen ser ut och beter sig. Detta samband pekar på att mittpunkten och galaxen som helhet troligtvis utvecklats parallellt.

Då Vintergatan och dess centrum är den mest närbelägna galaxen vi har, kan vi studera dess egenskaper i stor detalj, jämfört med andra galaxcentra. Om vi antar att Vintergatan är varken mer eller mindre speciell än andra galaxer, kan en god förståelse för Vintergatan och dess centrum lägga grunden för en större förståelse för hur galaxer i allmänhet hänger samman med sina centra.

I vårt arbete hittar vi både likheter och skillnader mellan stjärnorna som finns i Vintergatans centrum respektive längre ut. Stjärnor består främst av väte och helium men kan även vara berikade med andra grundämnen, beroende på hur och när de har bildats. Både i centrum och längre ut i galaxen hittar vi stjärnor som haltmässigt ser ut att vara lika. Men när det kommer till de mest berikade stjärnorna finns det tydliga skillnader, där centrumstjärnorna har en högre halt kisel jämfört med stjärnor längre ut. Detta kan vara en indikation på att dessa regioner har bildats och utvecklats på olika sätt. Denna kunskap, om man lyckats bekräfta resultaten i framtida studier, är en viktig byggsten i vår förståelse kring Vintergatans utveckling. Som en förlängning kan även denna kunskap användas på andra galaxer och förhoppningsvis ge viktiga ledtrådar till galaxbildning och galaxutveckling i allmänhet.

Acknowledgements

I'm deeply indebted to my lovely wife, Kristina Arnrup Thorsbro, without whom this thesis wouldn't exist. Quitting my well paid job and becoming a student is not a decision you take lightly. Kristina did not so much as flinch at my crazy idea and has been at my side and supporting me every step of the way on this journey.

I would also like to extend my deepest gratitude to my supervisor Nils Ryde, who with his extreme generosity has included me in his scientific collaborations from day one and has trusted me to lead the work on several occasions. Nils Ryde and my co-supervisors, Hampus Nilsson and Henrik Jönsson, have deep knowledge of the field, which they have shared willingly and patiently in spite of my constant questioning. For this I am very grateful.

For the writing of my thesis I am deeply indebted to Colin Carlile, Florent Renaud, Rebecca Forsberg and Kasper Brandt Nyegaard; Colin for his meticulous and thorough effort to help me improve my English writing skills, Florent for for being present all summer and willing to discuss all the scientific ideas that I wanted to put in my thesis, Rebecca for helping with such a good translation of my English popular summary into Swedish and Kasper for doing the layout of the front page.

Mike Rich is an inspiration to me with his great enthusiasm for astronomy and extremely wide knowledge of the field. I am especially thankful for our time together at the Keck telescope and being taught how to enjoy life on Hawai'i. I am also very grateful for the time Mike hosted me at UCLA and in his home in Bel Air, Los Angeles—I am looking forward to the next trip.

Mathias Schultheis is also an inspiration to me showing how it is possible to be a great astronomer and still keep both feet grounded on the earth. I am very grateful for the many times that Mathias has hosted me both at the observatory in Nice, but also in his home in Mougins. Who would have thought that it was so productive to sit and work at a beach café at the Côte d'Azur. I am especially thankful for the opportunity to visit and work with Mathias for a month at the observatory in Nice—I can imagine spending more time there!

I am grateful for the collaboration that I have had on the Galactic centre work; in particular Livia Origlia and Tobias Fritz have been along for the entire project and have taught me a lot. A special thanks goes out to Livia for visiting us in Lund and teaching me the ins and outs of the REDSPEC data reduction kit.

The LUMCAS collaboration on laboratory astrophysics with Malmö University has a special place in my time as PhD student. I have greatly enjoyed going almost weekly to Malmö for a fresh change of air, and I am grateful that Per Jöns-

Clues to galaxy evolution from spectroscopic observations of Galactic centre stars

1 Introduction

In astrophysics, one of the current and active research topics is understanding the formation and evolution of galaxies (Bland-Hawthorn & Gerhard, 2016). Our own galaxy, the Milky Way Galaxy, plays a crucial role, not only because it is the galaxy that we live in, but also because it is the galaxy that we can study in the most detail. Assuming the mediocrity principle, i.e. that we are not special, we can use the understanding of our own galaxy to understand galaxies at large.

Our Galaxy is often described as a barred spiral galaxy consisting of number of components, often classified as the halo, the thin and thick disks, the bulge and the Galactic centre (Bland-Hawthorn & Gerhard, 2016). Zooming in on the Galactic centre we find that the innermost parts can be described as consisting of a nuclear star cluster hosting a super-massive black hole, with the cluster itself being surrounded by a nuclear stellar disk.

The innermost environment of a galaxy is important for several reasons. Firstly, there are empirical relations between the nuclear star cluster and the entirety of the galaxy it is hosted in. For example we find an empirical relation between the mass of the nuclear star cluster and the mass of the host galaxy. Secondly, almost all galaxies that we observe are found to contain a nuclear star cluster. Thirdly, nuclear star clusters are extremely dense and bright star environments visible from a long way away (see e.g. review by Neumayer et al., 2020).

In our own Galaxy many of the individual stars of the inner Galactic centre can be resolved and observed separately. Through the technique of spectroscopy the

light emitted from these stars can be examined in extreme detail giving us insight into information about the stars, most notably the chemical composition of the stars (see e.g. Thorne et al., 1999; Hubeny & Mihalas, 2014).

All chemical species beyond the very lightest species are formed by various different fusion processes in the stars, or in some cases during the merger processes of stars (Kobayashi et al., 2020). Thus, the observation of different chemical species are a consequence of, and hence a witness to, the existence of these fusion processes. Which fusion process happens is dependent on several factors, most notably the mass of the star and whether or not the star is part of a binary star system, described in more detail in stellar evolution theories (see e.g. Prialnik, 2000). Chaining together the lives of many stars accumulates a production of chemical species that eventually combines into a mixture of chemical species that we can observe today. The chemical species mixtures are thus fingerprints of the history of the given environments the mixtures are observed in.

In other words, by observing the chemical composition of stars, we are able to set constraints on, or provide clues to, how the environments that stars reside in, have formed and evolved.

In Section 2 galaxy formation and evolution theories and how they relate to the work in this thesis are described briefly and in Section 3 an overview of basic chemical evolution is given. Following in Section 4 is an account of the observations that have provided the data. Finally, in Section 5 the methodology of spectroscopy, which is the foundation of the work done in this thesis, is described in more detail. In the second part of this thesis the author's contributions to the scientific articles are described and the articles themselves are included.

2   Galaxy formation and evolution

Firstly an introduction to galaxies is given, and afterwards galactic formation and evolution models are considered. This is followed with a discussion on how the theories form predictions that call for observations to constrain the theories.

2.1   Galaxies

Galaxies have been called the building blocks of the Universe and are in general seen as the home of stars. Knowing a few basic facts about galaxies, and in particular our own galaxy, the Milky Way, is beneficial to getting an idea of the overarching astronomical context of the work discussed in this thesis.
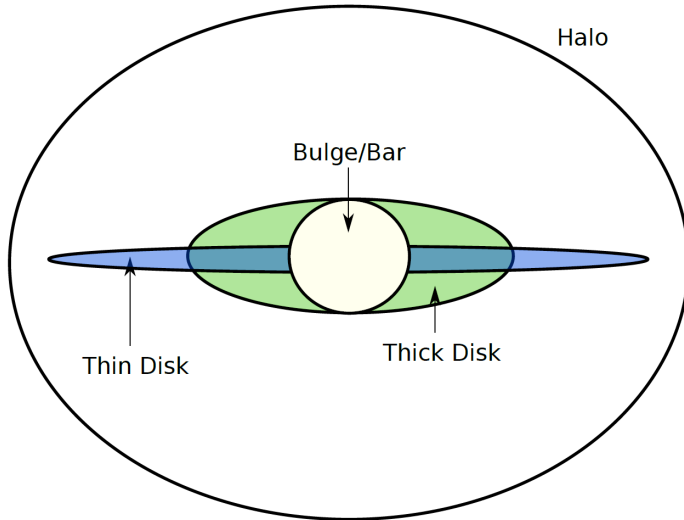
Figure 1: A schematic illustration of the stellar components of the Milky Way. The thick disk is illustrated in green, the thin disk in blue and the bulge/bar in beige. The stellar halo surrounding it all is in white. Adapted from Christensen (2020) with permission.

A galaxy typically has a radius of the order of several kpc and a mass, not including dark matter, between $10^7\,\mathrm{M_\odot}$ and $10^{12}\,\mathrm{M_\odot}$ and is self gravitating. The Milky Way galaxy is estimated to have a radius of about $25 \pm 10\,\mathrm{kpc}$ with the Sun located about 8 kpc from the centre and has a mass of stars and other baryonic material of about $6 \cdot 10^{10}\,\mathrm{M_\odot}$. Extending the radius out to about 200 kpc and including the dark matter halo the mass of the Milky Way reaches upwards to $10^{12}\,\mathrm{M_\odot}$ (Bland-Hawthorn & Gerhard, 2016).

Galaxies come in various forms and shapes and the two dominant classifications are spherical and spiral galaxies, often called respectively early type and late type galaxies. The classifications can further be subdivided, for example a spiral galaxy can have a bar or not, and there can be several disk components. The Milky Way is considered to be be a barred spiral galaxy with a bulge and both a thin and thick disk surrounded by a halo, as illustrated in Figure 1. The bulge is thought to have a mass of about $1.8 \cdot 10^{10}\,\mathrm{M_\odot}$, the thin disk about $3.5 \cdot 10^{10}\,\mathrm{M_\odot}$, the thick disk about $6 \cdot 10^9\,\mathrm{M_\odot}$ and the stellar halo about $4\text{-}7 \cdot 10^8\,\mathrm{M_\odot}$ (Bland-Hawthorn & Gerhard, 2016).

Almost all galaxies we observe have a bright stellar nucleus, a so-called nuclear

star cluster, at their centre (Neumayer et al., 2020). The Milky Way is no exception, and has a nuclear star cluster with a radius of about 5 pc having a mass of about $2.5 \cdot 10^7 \, M_\odot$. Surrounding the nuclear star cluster is a nuclear stellar disk that extends out towards 150-200 pc radius and has a mass of about $1.5 \cdot 10^9 \, M_\odot$ (Bland-Hawthorn & Gerhard, 2016). Note, that the distances are now of the orders of pc instead of kpc, which serves to illustrate that these regions have a very high density of stars. At the centre of the nuclear star cluster in the Milky Way lies a supermassive black hole with the mass of about $4.2 \cdot 10^6 \, M_\odot$ (Bland-Hawthorn & Gerhard, 2016). Supermassive black holes have been detected in many galaxies, but are not as ubiquitous as nuclear star clusters (Neumayer et al., 2020).

Nuclear star clusters have been found to have empirical relations with their host galaxy, suggesting that nuclear star clusters may have coevolved with their host. Studying nuclear star clusters thus potentially becomes key in understanding the galaxies they are located in, which is particularly interesting as nuclear star clusters are very dense star environments making them bright targets that can be observed from much further away compared to other parts of their host galaxy. One particularly interesting relationship is that between the mass of the nuclear star cluster and the mass of its host. The mass relationship is shown in Figure 2.

In Figure 2 in the left pane, the masses of the nuclear star clusters are shown in relation to the masses of their host galaxies. The disks and stars represent two different studies. The star symbols refer to a study done by Erwin & Gadotti (2012) where the mass of the studied nuclear star clusters either have been dynamically measured or obtained by fitting multiple single stellar populations to high resolution spectra. The disks represent studies where multiple single stellar populations have been fitted to colours obtained through photometry (Georgiev et al., 2016; Spengler et al., 2017; Ordenes-Briceño et al., 2018; Sánchez-Janssen et al., 2019).

Fitting the total sample to a linear relationship gives the dashed line seen in Figure 2, given by Neumayer et al. (2020) as

$$\log M_{\text{NSC}} = 0.48 \log \left(\frac{M_{\text{host}}}{10^9 M_\odot} \right) + 6.51. \tag{1}$$

More simply put the mass of nuclear star clusters are proportional to the square root of the mass of their host galaxy. If one considers the methods used by Erwin & Gadotti (2012) to be more accurate and precise then there more uncertain photometric based methods used by the other authors, and focus on late-type galaxies (i.e. spiral galaxies like the Milky Way) the relationship looks rather different, which is marked by the dashed-dotted line in Figure 2, given by Neumayer
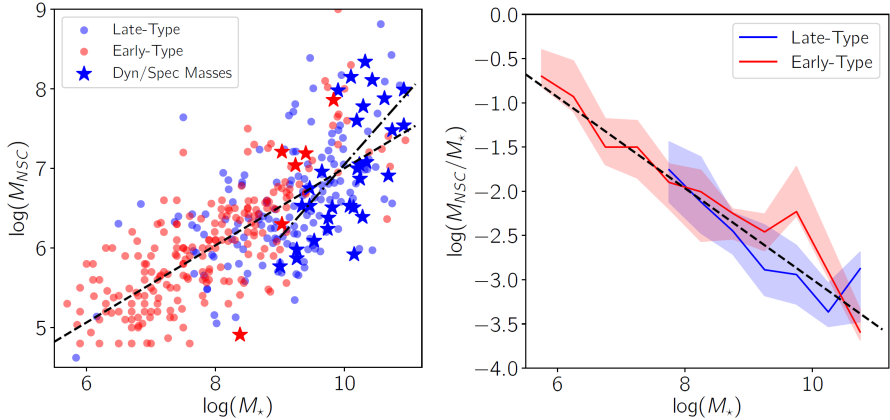
Figure 2: The masses of nuclear star clusters (NSCs) correlate with galaxy masses, but higher-mass galaxies have a lower fraction of their mass in their NSC. *Left –* NSC mass vs. Galaxy mass $(M_\star)$. The disks and stars represent different methods of determining the masses of the NSCs, see the text for more information. The full sample is fitted to the dashed line, while the dashed-dotted line is a fit to the subset marked with blue stars. Galaxies have been divided by their Hubble types into early (red) and late (blue) types. *Right –* The mass fraction of galaxies in NSCs as a function of galaxy mass, using the data from the left panel. The line indicates the median galaxy within each mass bin, while shaded regions show the 25th and 75th percentiles of the distribution. Adapted from Neumayer et al. (2020) with permission.

et al. (2020) as

$$\log M_{\mathrm{NSC}} = 0.92 \log \left(\frac{M_{\mathrm{host}}}{10^9 \mathrm{M_\odot}} \right) + 6.13. \tag{2}$$

Here the relation between the mass of the nuclear star clusters and their host galaxies is almost linear.

Examining these relationships using the Milky Way data shows good agreement with either of the relations. They both adequately describe the relation between the mass of the Milky Way nuclear star cluster, $2.5 \cdot 10^7 \, \mathrm{M_\odot}$, and the mass of the Milky Way itself, $6 \cdot 10^{10} \, \mathrm{M_\odot}$. In Figure 2, the Milky Way would be plotted near the intersection of the two lines.

With an overview of galaxies in place, from a viewpoint that focuses on their centres, we turn our attention to their formation and evolution.

2.2 Formation and evolution of galaxies

Theories of formation and evolution of galaxies should be able to explain the galaxies we observe today, particularly the Milky Way, where observations provide much greater detail.

With the advent of strong computational power in the last two decades, numerical simulations using first principles of fundamental physical laws combined with appropriate physical modelling have become one of the dominant methods for investigating galaxy formation and evolution (see e.g. review by Naab & Ostriker, 2017).

The starting point for any theory of formation and evolution is the initial conditions. Modern cosmological models describe the Universe after the Big Bang and also how the structure of the Universe was initially formed. The initial baryonic matter in the Universe is described as a primordial gas consisting of hydrogen and helium, with helium having a mass fraction of about 24% (Schneider, 2006). The density of the primordial gas is not perfectly uniform initially, leading to the overdensity regions amplifying with gravity over time to form the large scale structures, and finally the galaxies (e.g. Mo et al., 1998).

In simulations based on cosmological models a Milky Way–like galaxy is typically formed by mergers of smaller galaxy fragments early on. Examples of such simulations are the EAGLE simulation (Schaye et al., 2015; Crain et al., 2015), the AURIGA simulation (Grand et al., 2017) and the recent VINTERGATAN simulation (Agertz et al., 2020; Renaud et al., 2020b,a).

The limiting factor for simulations is computational power, and thus the different simulations vary in both the volume of space they cover and the shortest distances they can resolve in their simulated space. Furthermore, the simulations can be run multiple times to explore different initial conditions and increase statistics. The EAGLE simulation covers a very large volume of space, enough to contain about 10,000 Milky Way–mass galaxies, but has poor resolution (~ 1 kpc). The AURIGA simulation focuses on simulating a single Milky Way–like galaxy, with intermediate resolution (~ 200 pc), and runs the simulation 30 times with varying initial conditions to build up statistics. The VINTERGATAN simulation also focuses on simulating one Milky Way–like galaxy, having only one instance, but at very high resolution (~ 20 pc).

Alternatively, one can start with one large gas cloud and form a galaxy from that without accounting for the cosmological context, as a means of studying an isolated galaxy, which arguably the Milky Way could be. A recent example of such a simulation with multiple realisations has been done by Khoperskov et al. (2020),

having a high resolution ($\sim 50\,\text{pc}$).

A major goal of the simulations mentioned above is to show how galaxies with a Milky Way–like morphology can be formed. While this is undoubtedly an important diagnostic, there are also other diagnostics available to us. One such diagnostic is the chemical composition of the atmospheres of the stars found in various parts of a galaxy. The underlying theories for this diagnostic are covered in more depth in Section 3 on chemical evolution models. Common to the simulations mentioned above is that they all include this diagnostic, i.e. provide the chemical composition of the atmospheres of the stars found in the simulations.

The chemical compositions of the atmospheres of stars can be observed in the Milky Way and its satellite dwarf galaxies where it is possible to resolve individual stars and determine their chemical composition using spectroscopy. It is not possible to resolve individual stars in other galaxies than these. However, with the advent of 30-40 meter telescopes now in construction, resolving stars in the neighbouring Andromeda galaxy, M31, should become possible (see proposals by e.g. Escala, 2020). This diagnostic is an example of how the greater detail of the Milky Way available to us enhances the demands on the theories.

When discussing the chemical composition of the atmosphere of stars, one of the most commonly used approaches is to examine the ratio of alpha-abundance to iron-abundance of a star vs. the metallicity of the same star. The alpha-elements are the stable atoms with a nucleus comprised of a certain number of alpha-particles (2 neutrons and 2 protons), which are C, O, Ne, Mg, Si, S, Ar and Ca. The metallicity of stars is usually measured through the proxy of the ratio of iron to hydrogen abundance.

In Figure 3 and Figure 4 the alpha to iron-abundance vs. metallicity of respectively the VINTERGATAN simulation and one of the realisations from the Khoperskov et al. (2020) simulations are shown. The really interesting and essential part is to compare these simulations with observations. These abundances have been observed in a stellar sample containing close to 300,000 stars in the APOGEE survey and an updated data version was released recently (Jönsson et al., 2020). The abundance trends of the alpha-elements O, Mg and Si, with respect to Fe are shown in Figure 5.

The notation [O/Fe] is to be understood as the abundance ratio of O to Fe logarithmically compared to the same ratio found in the Sun, as described by

$$[\text{O/Fe}] = \log\left(\frac{N_\text{O}}{N_\text{Fe}}\right)_\text{star} - \log\left(\frac{N_\text{O}}{N_\text{Fe}}\right)_\text{Sun}, \tag{3}$$

where N_O and N_Fe are the number densities of O and Fe atoms respectively. The
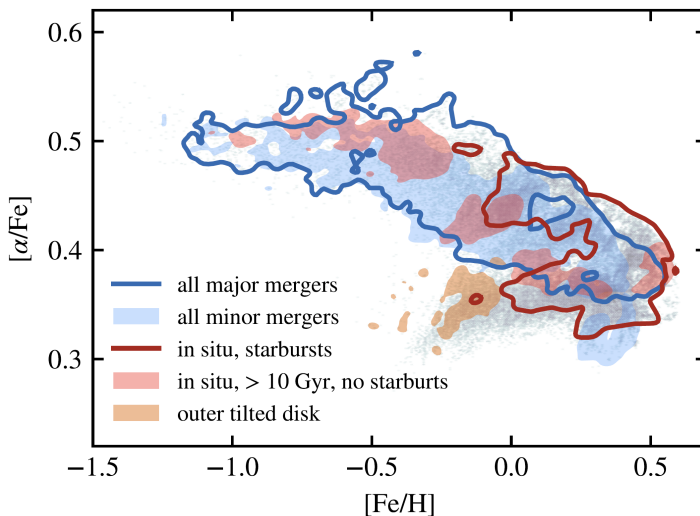
Figure 3: Alpha-elements to iron abundances vs. metallicity, see text for explanation of notation. The grey dots in the background shows the chemical composition of stars found in the simulations with the coloured contours and regions mapping out the origin of their formation. Adapted from Renaud et al. (2020b) with permission.
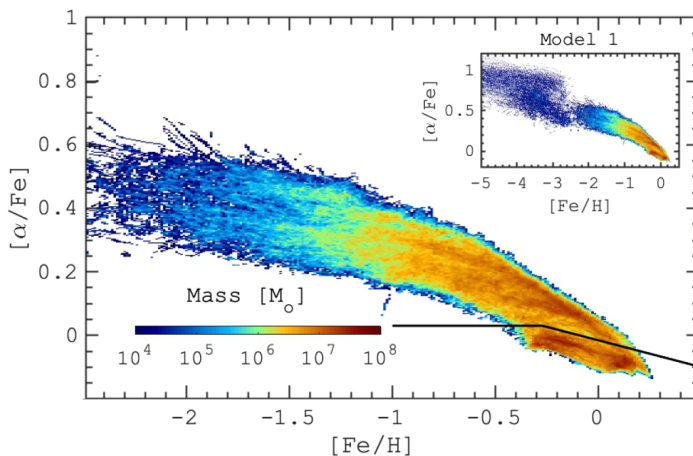
Figure 4: Alpha-elements to iron abundances vs. metallicity, colour-coded by the stellar mass, see text for explanation of notation. The frame in the top right is an overview of all the data in the simulation with the main figure itself a zoom-in. The black line separates two major stellar populations with low and high alpha-abundances. Adapted from Khoperskov et al. (2020) with permission.
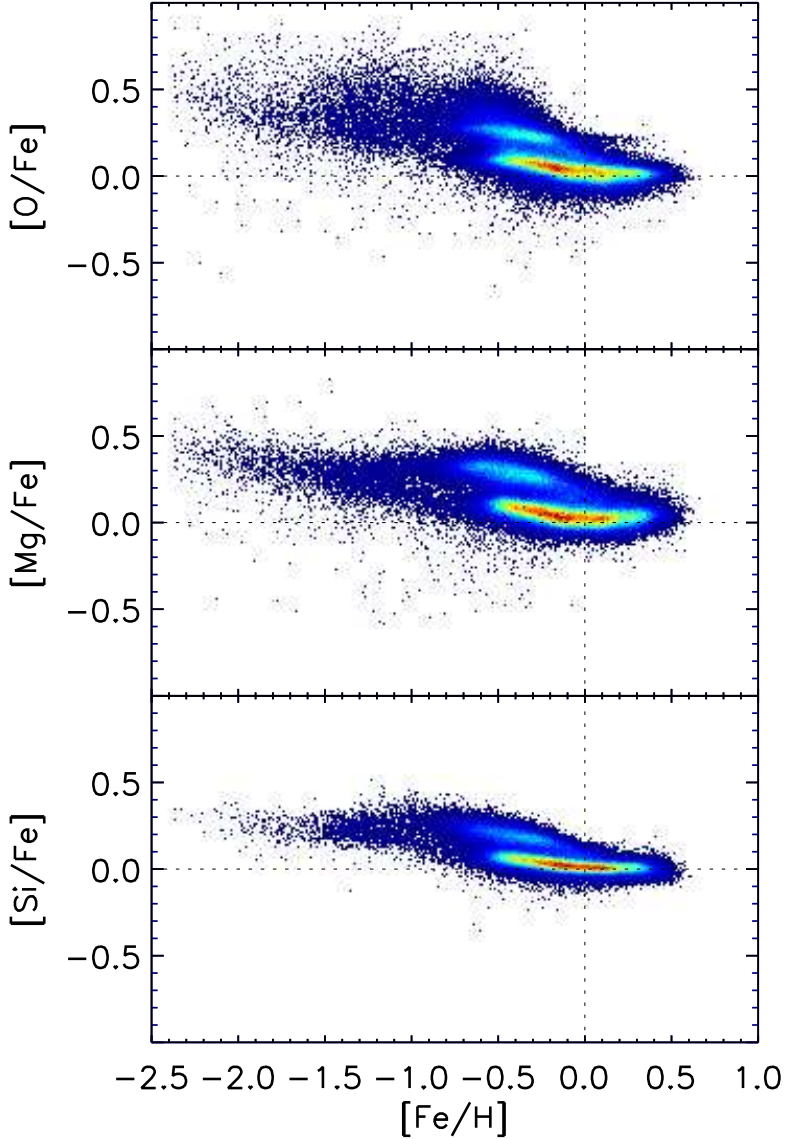
Figure 5: Alpha-elements to iron abundances vs. metallicity, colour-coded by the stellar number density, see text for explanation of notation. The stars were observed as part of the APOGEE survey (Jönsson et al., 2020), and shown here are the trends from giant stars for the three alpha-elements, O, Mg and Si. Figure from H. Jönsson (private communication).
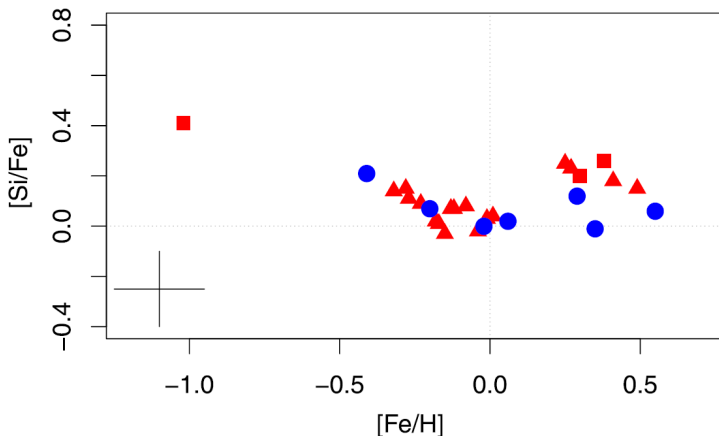
Figure 6: Alpha-elements to iron abundances vs. metallicity, here traced by Si, see text for explanation of notation. Red triangles and squares are abundances of stars found in the nuclear star cluster and nuclear stellar disk of the Milky Way; blue circles are stars found in the Milky Way disk. Adapted from Thorsbro et al. (2020) with permission.

Sun is therefore located at the origin in the abundance plots. In Figure 3 [α/Fe] is traced by [O/Fe] in the simulation, while in Figure 4 [α/Fe] is traced by the average of [O/Fe], [Mg/Fe] and [Si/Fe].

Comparing the trends in Figures 3 and 4 to the trends in Figure 5 shows the same high ratios that recede as the metallicity increases. In particular, the simulation can offer explanations for how the bimodal nature of the abundance trends arises from an evolution of the star formation activity in the galactic host. This is driven both by the transition from a merger-dominated growth phase in the early Universe to a quiescent evolution later, and the joint intrinsic evolution of the disks. Such matters are out of the scope of this thesis (for details, see Renaud et al., 2020b).

The work in this thesis aims at adding observations of the Galactic centre to the available data. The data we have obtained is presented in the accompanying papers. One of our central results is shown here in Figure 6. To our knowledge, there are currently no numerical simulations that have attempted to simulate the formation and evolution of the Galactic centre with a sufficient resolution to make a comparison to our data. In our Paper V we compare the data with chemical evolution models to offer possible interpretations of our data. It is our hope that with the availability of data like ours more theoretical work can be done to better understand the Galactic centre.

3   Chemical evolution models

In the previous section much attention is given to the diagnostic of alpha-elements and iron abundances. It is not a coincidence that this diagnostic of alpha-elements and iron abundances is both targeted by observers and included in the theoretical models. We take a closer look on first nucleosynthesis and then chemical evolution models to better understand why this diagnostic is interesting.

3.1   Nucleosynthesis

As mentioned in the previous section, the primordial gas initially present in the Universe shortly after the Big Bang mostly consists of hydrogen and helium (with a whiff of lithium and beryllium). All chemical species found today that are heavier than helium are therefore due to some fusion of the material originally found in the primordial gas. This is basically the domain of the stars. In astronomy all chemical species heavier than helium are called metals, and the metallicity of a gas is the amount of metal compared to hydrogen. Often the metallicity is traced by using the ratio of the abundance of iron atoms to hydrogen atoms (as we saw in the previous section with [Fe/H]), which has the underlying assumption that the distribution of metals in the given material is scaled to the distribution of metals we find in the Sun (see e.g. Grevesse et al., 2007).

Explaining how stars can form metals through various fusion processes is the domain of nucleosynthesis models, which is a vast scientific topic in itself (see e.g. Burbidge et al., 1957; Woosley & Weaver, 1995; Kobayashi et al., 2020). Here we focus on two production channels that are central for choosing the diagnostics discussed in the previous section. In these production channels metals are created through fusion and later released into the interstellar medium by either a supernova type II (SNII) or a supernova type Ia (SNIa) event.

An SNII event happens towards the end of the life of a massive star with eight or more solar masses (see e.g. Prialnik, 2000). In such a massive star there is a significant production of the alpha-elements, which are then released to the inter-stellar environment through the SNII event. An alpha-particle is the nucleus of a helium atom, consisting of four nucleons, two protons and two neutrons. The alpha-particle is relevant because it has a particularly high binding energy per nucleon compared to the nuclei of other atoms, i.e. it is very tightly bound. This makes it a favoured product in fusion processes and as a consequence the combination of multiple alpha-particles also becomes favoured fusion products. In an SNII we see a strong production of several such alpha-elements, in particular the

elements: O, Ne, Mg, Si, S, Ar, Ca and Ti.

In comparison an SNIa event happens in binary systems, where one star has first developed into a white dwarf, and where the other star is undergoing its final stages of life and is transferring mass to the white dwarf. If enough mass is transferred to the white dwarf it collapses and ignites an SNIa event (see e.g. Prialnik, 2000). In an SNIa there is also the generation of alpha-elements, but the circumstances are such that the fusion processes are mainly focused around the production of iron and elements close to iron with respect to the number of protons, the so-called iron-peak elements: Ti, V, Cr, Mn, Fe, Co and Ni. Hence, an SNIa is seen as outputting iron, albeit a bit "delayed" as the two stars both have to go through their evolutionary stages before the output is seen.

Ti requires more neutrons than protons to be stable and is therefore not really a true alpha-element, but since it is often produced together with the alpha-elements in type II supernovae it is sometimes considered to be an alpha-element by astronomers. An interesting side-effect of the unstable Ti created in an SNII is that it beta-decays to Sc, perhaps rendering Sc a better SNII tracer than Ti (Clayton, 2003). However, the nucleosynthesis production channels are still under debate to this day, so one has to be careful about making definite statements.

3.2 Chemical evolution

In chemical evolution theories the basic premise is that stars are formed from the gas found in the interstellar medium (ISM). Over time the stars produce metals and return them to the ISM, which then forms the foundation for future generations of stars. Therefore the metallicity, [Fe/H], in a way becomes a proxy for cosmic time. How fast the [Fe/H] increases is dependent on the star formation rate (SFR) (see e.g. Matteucci, 2012).

When gas infalls and starts producing stars, the mass distribution of the newly born stars can be described by the so-called initial mass function (IMF). The first IMF developed was by Salpeter (1955), though there have been several revisions of this work since (see e.g. historical overview by Kroupa & Jerabkova, 2019). It is interesting to note that while these IMFs have a theoretical foundation they have been fine-tuned to fit observations of the Milky Way.

Since massive stars over-produce alpha-elements compared to other elements the ratio of alpha-elements to iron depends on the fraction of high mass stars created. However, over time the enhanced iron production from SNIa systems kicks in, at which the point the ratio of alpha-elements to iron drops. This leads to the famous "alpha-knee plot" first identified by Matteucci & Brocato (1990). An
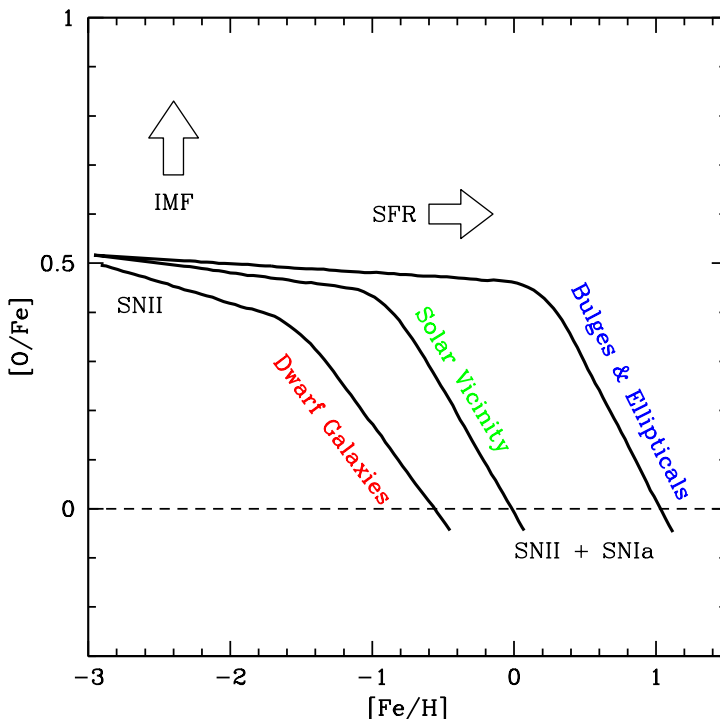
Figure 7: Matteucci & Brocato (1990) predicted that the knee in the trend of [O/Fe] with [Fe/H] depends on the star formation rate (SFR): High SFR systems, such as bulges and elliptical galaxies, should show enhanced [O/Fe] to high [Fe/H], whilst the low SFR dwarf galaxies show reduced [O/Fe] relative to the Solar vicinity. Also shown is the direction of the [O/Fe] plateau with an enhanced fraction of massive stars, marked as the initial mass function (IMF), which over-produce oxygen. Adapted from McWilliam (2016) with permission.

updated version of the figure, with IMF and SFR illustrated, is shown in Figure 7.

Figure 7 demonstrates how the ratio of alpha-elements to iron vs. metallicity can be a diagnostic that provides a lot of information on the formation and evolutionary process that a stellar population has experienced.

So far the evolution scenarios have been rather restricted to the simple infall of a gas cloud. Several advanced scenarios can be considered. For instance if a second gas cloud is accreted into the system, what happens then? Or what if there is a pause in the star formation process due to some event that suppresses star formation? These are some of the questions we explore in our work, which is

explored in more detail in the accompanying papers.

Or course, before such considerations can be taken into account, the actual observational data has to be gathered, which is the topic of the next section.

4   Observations

It is hard to imagine the discipline of astronomy progressing without the science and engineering of instrumentation making high precision observations a reality. We have described in the earlier sections how observations are essential to constrain our theories. In this section the observations performed as part of the work done in this thesis are covered in some detail.

The data analysed in this thesis has been obtained using the Keck II telescope during three observation visits at the W. M. Keck Observatory located on the volcano Mauna Kea on the island of Hawai'i (aka The Big Island), in the state of Hawaii in the U.S.A. We recognise and acknowledge the very significant cultural role and reverence that the summit of Mauna Kea has always had within the indigenous Hawaiian community. We have been most fortunate to have had the opportunity to conduct observations from this mountain.

The Keck II telescope has a primary mirror of $\sim 10\,\mathrm{m}$ in diameter and comprises 36 hexagon segments that work together as a single unit. A photograph of the primary mirror taken during the first observational visit is shown in Figure 8. The telescope is constructed such that different instruments can be mounted to analyse the light that the telescope is capturing. For our work we have used the NIRSPEC spectrometer (McLean et al., 1998).

Observing the stars in the Galactic centre is particularly challenging because of the dust lying between the Sun and the Galactic centre. In the optical wavelength regime nearly all light is blocked. However, in the infrared wavelength regime around 2 micron about 15% of the light penetrates through, which makes observations with large telescopes feasible. In our work we exposed the stars for about 40 minutes each on the Keck II telescope to reach a good signal to noise around 70 to 100. This is also the reason why we observe M giants, since they are very bright stars, with an apparent Ks magnitude around 11.

The NIRSPEC spectrometer is a single slit spectrometer with a resolution of about R = 23,000. This is what we consider to be a necessary resolution for high quality abundance analyses. The slit of the spectrometer is placed on the star being observed, as illustrated in Figure 9. We are interested in the light from the star, however the light passing through the rest of the slit can be used to quantify
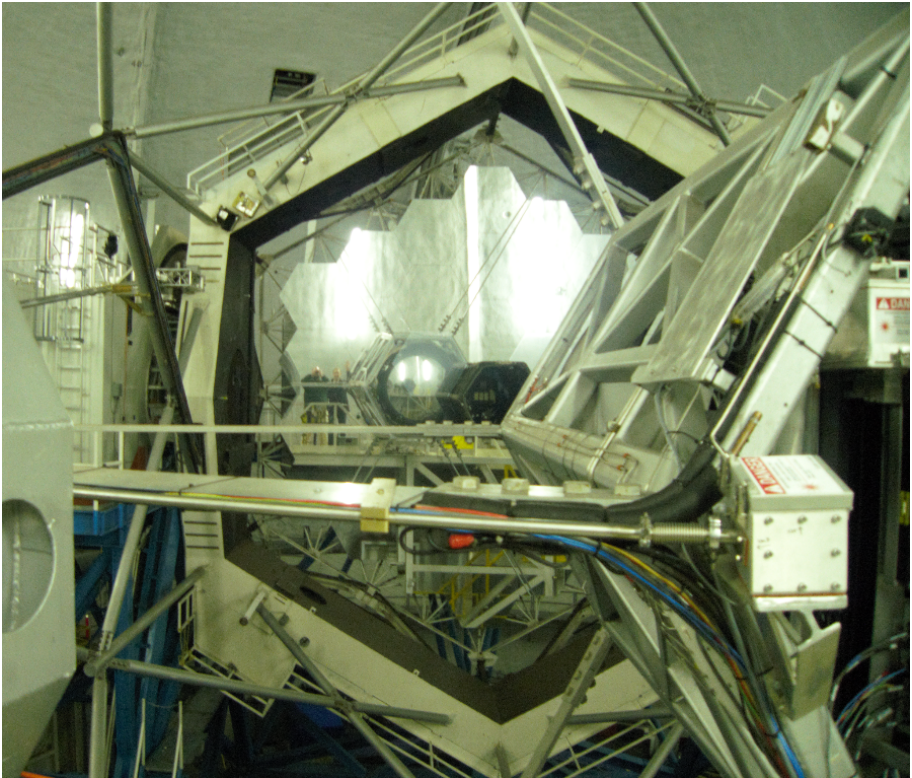
Figure 8: A photograph of the primary mirror of the Keck II telescope. The mirror is about 10 m in diameter, illustrated by the size of the two people seen in the reflection (from the left Brian Thorsbro and Nils Ryde). The secondary mirror, which resides inside the metal box on the front right of the photograph, can be seen reflected in the primary mirror. The black hexagon, seen to the right of the reflection of the secondary mirror, is the focal point of the telescope where the captured light is gathered. From there the captured light is sent off to one of the mounted instruments. For our observations we used the NIRSPEC spectrometer that was mounted in one of the so-called Nasmyth/bent Cassegrain foci, located on the side of the telescope. Photograph by Brian Thorsbro.
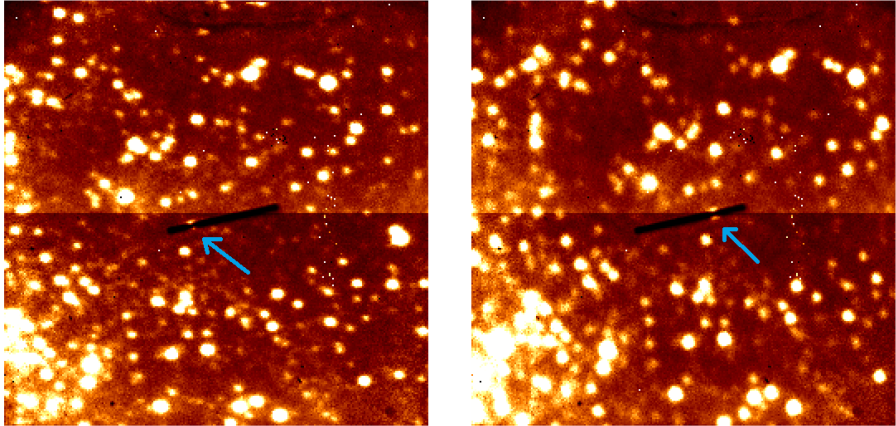
Figure 9: Image taken with the Keck II telescope to verify that the target star, in this case the star named GC 13727 in our work, is located correctly under the slit used to pass light on to the spectrometer. The blue arrows have been added to point out where the star is located. Two observations are performed using the "nodding" technique to ensure that it is also possible to obtain suitable background images for error subtraction.
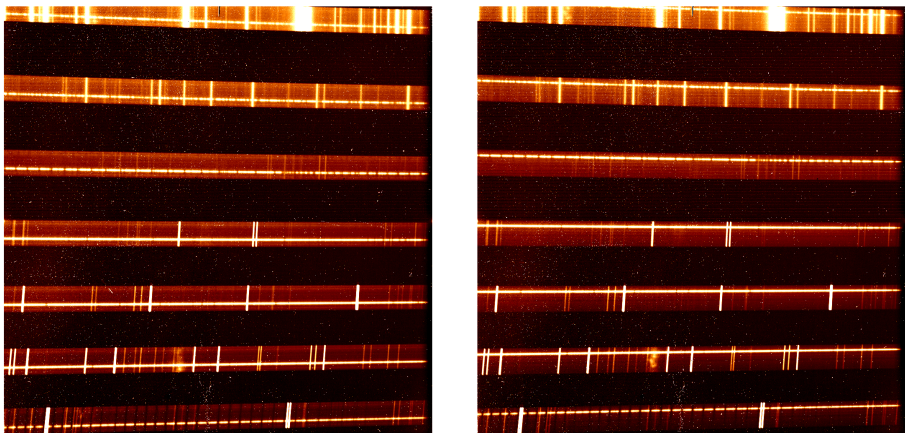
Figure 10: Observed cross-dispersed spectra of the same star, GC 13727, as seen in Figure 9. Absorption features can be seen as black "Fraunhofer" lines in various parts along the horizontal lines, which are the dispersed starlight. The vertical lines are OH emission lines from the Earth's atmosphere.

the background light. Subtracting background light allows for the reduction of systematic errors. This is especially important in the infrared, which is the wavelength region where we observe, since the thermal background is rather bright. Furthermore, there can be imperfections in the instrument that varies along the slit, so it is important to capture a background at the same slit location as the star, and to achieve this the telescope is "nodded", such that two observations are made. This way there will be two locations on the slit where the star is observed and for the same two slit positions there will also be a background observation. This "nodding" approach is shown in Figure 9 where blue arrows points to the location where the star is covered by the slit recording the light.

The NIRSPEC spectrometer is a so-called cross-dispersed echelle spectrometer. This enables transverse dispersion of the recorded spectrum, such that a square detector array can be used more efficiently. In other words, the high resolution spectrum is cut up in parts and shifted vertically on the detector. An example of the image of a spectrum cut up in this way can be seen in Figure 10. In this figure the horizontal lines are the spectrum of the observed star, and if one looks more closely it is possible to see black "Fraunhofer" lines, in particular in the third line from the top which displays molecular band absorption features of the molecule CO. The vertical lines are OH emission lines from Earth's atmosphere.

In order to analyse the observed spectrum the spectral data has to be extracted from the image pixels. The Collaboration responsible for the design and implementation of the NIRSPEC spectrometer has made a software package available, called REDSPEC, which helps with this task (Kim et al., 2015). The basic idea is to map out a curve that follows the spectrum across the pixels in the detector array and read out the intensity values along the curve. At the same time the software carries out background subtraction and divides out flat fields. The exact procedure will not be detailed here.

Using the REDSPEC pipeline on the recorded image data we thus obtain a spectrum with an approximate wavelength calibration. Given that we observe in the infrared wavelength region around 2 microns we have many telluric features in the spectrum, which is both a blessing and a curse. It is helpful in improving the accuracy of the wavelength calibration, but it also means that parts of the spectrum are so crowded with telluric features that it can be difficult to reconstruct the actual stellar spectrum. Improving the wavelength calibration and removing the telluric features are performed by using the IRAF software package (Tody, 1993). For the telluric line removal we observe a swiftly rotating hot star which allows for easy identification of which spectral features that are telluric lines.

However, in order to extract the abundances of chemical species, from the spectra that we observe we now turn to the field of stellar spectroscopy.

5   Stellar Spectroscopy[1]

Spectroscopy was already founded in the 19th century when the dark Fraunhofer lines in the solar spectrum were identified to be the absorption of light caused by the presence of chemical species in the solar photosphere. The discovery was facilitated by shining light through different chemical species in a laboratory and recording at which wavelengths the light was absorbed. Up to the present day laboratory measurements are still a fundamental ingredient for the continued development of stellar spectroscopy (Atkins & Baranov, 2013).

Although the recording of the spectra of stars is important, an understanding is not reached until the underlying physics is well enough known to be able to reproduce the observed stellar spectra using physical modelling. The input needed for good modelling can broadly be categorised as

- Atomic and molecular physics,

- Stellar photospheres, and

- Radiation transport.

A knowledge of these topics allows us to carry out abundance analyses of the observed stars. The topics are discussed in turn next, followed by a few pertinent comments on abundance analysis and astrophysical line lists.

5.1   Atomic and molecular physics

In modern atomic physics the state of an electron is described in a quantum mechanical way via a wave function. The energy level transition in an atom whereby an electron moves from one energy level to another is considered as a state change from one wave function to another. The electron has an electric charge and as the two wave functions have different probability distributions for the position of the electron there is a charge distribution difference between them, and thus there exists an electric dipole moment.

This dipole interacts with the radiation field around the atom, and if the radiation field resonates with the natural frequency of the dipole then energy can

---

[1]This section is based on a similar section from the licentiate thesis of Thorsbro (2018).

be put into the atom in form of absorption or removed from the atom in form of stimulated emission. The natural frequency is also known as the wavelength of the transition. Knowing this to high precision is necessary to identify the lines in a spectrum.

The dipole also has an oscillator strength, which can be hard to understand intuitively, but in a way it represents the probability that a transition will happen. The higher the chance for a transition the stronger the oscillator is said to be, and in the spectrum this manifests itself as a stronger line.

In molecules there are similar energy transitions if the electrons in the atoms move around, but there are also energy transitions when switching between different rotational and vibrational modes of the molecule itself. The interactions of rotational and vibrational modes often gives rise to molecular bands, which consists of a large number of spectral lines grouped near each other in the spectrum.

If one tries to identify all possible energy transitions that exist in our 92 naturally occurring elements, it amounts to a staggering number. On top of that the molecular data needs to be taken into account. In the infrared wavelength range, very few laboratory measurements have in fact been carried out, which makes stellar spectroscopy particularly challenging.

One approach to obtaining usable atomic physics data is by employing theory to calculate the values. There are promising results showing that if theory is calibrated using measurements from the laboratory it can provide an avenue for cataloguing all this data (e.g. Pehlivan Rhodin et al., 2017a,b).

An important property of atoms with an odd number of nucleons, in particular if the number of protons is odd, is nuclear spin, which gives rise to hyperfine structure. If the nucleus of an atom has a nuclear spin the electronic energy levels in the atom are affected, and this has to be taken into account when calculating theoretical energy level transitions.

5.2   Stellar photospheres

The physical region in the star from where the radiation escapes is aptly named the photosphere and it is the region that determines the shape of the spectrum that we observe. Principally, the energy is generated in the interior of the star and is transported up to the photosphere through radiation transport and convection.

The key parameters we are interested in are the temperature and pressure gradients of the photosphere, since they govern which chemical species can be detected. For simplicity, the photosphere is often only modelled in the radial direction, with so called 1D models, which provide a temperature and pressure stratification. Do-

ing full 3D modelling would enable a higher fidelity on the heat transport from convection, which affects the temperature distribution. However, by employing mixing length theory this can be approximated to a good degree for stars like M giants, which has been shown by comparing 3D models with 1D models for giant stars (Černiauskas et al., 2017).

Performing a full 3D model would also enable us to understand the particle velocity fields in the photosphere, which is known to affect the spectra of the stars. However, for most stars we can not resolve the surface in any case, and the effect of the velocity fields can be approximated by introducing some heuristic parameters to the 1D modelling, usually denominated the micro- and macro-turbulence.

Temperature is not an inherently unique property. In the same patch of space, the temperature described by the Maxwellian velocity distribution of particles is not necessarily the same temperature described by the Saha-Boltzmann equation, which is governed by the distribution of electrons in energy levels of chemical species. However, when the particle density is high, and collisions between particles dominate the energy distribution compared to the photon interactions from radiation fields, the system is said to be in local thermodynamic equilibrium (LTE). In LTE the radiation field becomes the Planck black body radiation field, and the temperature becomes unique.

LTE is a very powerful assumption that enables physical modelling to be simplified tremendously. For stars like M giants most of the photosphere can be said to be in LTE. However, the outer parts of the photosphere can be sparse and cause the LTE condition to fall away. To a first order the non-LTE (or NLTE) condition can be modelled with perturbation theory, adding so-called departure coefficients to the Saha-Boltzmann equation.

NLTE calculations for M giants have only been done to a limited extent. We did some calculations on Si for Paper V together with our collaborator Anish Amarsi showing the departure coefficients to be insignificant for our analysis. Other elements are now being calculated (see e.g. Amarsi et al., 2020), and will be published as they are completed.

5.3 Radiation transport

Radiation transport is quite simple in concept, namely that along a beam of light with a certain frequency, ν, the change of intensity, I, of the radiation is governed by the intensity added and removed from the beam at a given position along the

beam axis, s,

$$\frac{\mathrm{d}I(\nu, s)}{\mathrm{d}s} = I_{\mathrm{added}}(\nu, s) - I_{\mathrm{removed}}(\nu, s).\qquad(4)$$

However, the intensities added and removed can originate from many different sources and sinks depending on the fidelity of the physical modelling.

In LTE the intensity added to the light beam is described by the Planck black body radiation function. However, in NLTE the intensity added could depend on the radiation field, which in turn could depend on the intensity of the light beam, making a circular dependence that increases the difficulty of solving the radiation equation.

The absorption of light at different frequencies varies, which leads to variations in how easy it is for the light to escape from the star as a function of frequency. If there are no chemical species to interact with the light of a given frequency the photon escaping the star could come from relatively deep regions of the star. If on the other hand the frequency of light matches a strong energy transition, most of the light at that frequency is absorbed, and only the photons from the very top of the star's surface are able to escape. The term opacity is used to describe how strongly light is being absorbed, and is a function of frequency.

In cool stars the amount of free electrons and neutral hydrogen atoms are so plentiful that they interact with significant cross-sections in the following two absorption processes, which are respectively called H^- bound-free and H^- free-free (John, 1964)

$$H^- + \gamma \longrightarrow H + e^- \qquad(5)$$
$$H + e^- + \gamma \longrightarrow H + e^- \qquad(6)$$

In both cases the energy of the photon is transferred to the electron. The photon absorption by these two processes are both weak functions of the photon frequency and set a minimum opacity for the star. Such an opacity is often dubbed the continuum opacity. For stars like M giants, and incidentally also stars like the Sun, the continuum opacity in the optical and infrared wavelength ranges is dominated by the H^- bound-free and free-free absorption processes (Wildt, 1939; Chandrasekhar & Elbert, 1958). In general such a continuum opacity sets the limits on how deep we can probe into a star by observing escaped light.

For transitions between energy levels in chemical species, and even for a change of rotational and vibrational modes for molecules, we call the process bound-bound absorption. In the frequency range where strong energy transitions exist the opacity becomes very high, which causes a strong spectral line to be present

in the spectrum. The assumption that we can make is that the continuum and weaker spectral lines are created deeper in the photosphere, while the stronger absorption lines, in particular the core of these lines, are created further out in the photosphere.

This means that for the continuum and the weaker lines we can normally assume that the LTE conditions hold, but for the stronger lines we need to be concerned whether NLTE conditions need to be taken into account, and if so, to what degree.

5.4 Abundance analysis

The spectral lines of chemical species are affected not only by the oscillator strength of a given transition, but also by the abundance of said species. Knowing both the oscillator strength and the abundance allows a spectral line to be modelled. However, as mentioned earlier, when the line becomes strong other considerations enter into the modelling, not only NLTE issues, but also saturation issues.

Restricting ourselves to weak lines, a knowledge of the atomic and molecular physics of the chemical species and their abundances suffices to model the spectral line. This emphasises the importance of having the correct atomic and molecular physics information since it directly affects the abundance determination.

Excellent tools exist that combine atomic physics data and stellar photosphere models, and solve the radiation equation using a set of stellar parameters and abundances of chemical species. For the atomic physics data one can download the dataset organised by the VALD3 Collaboration (Ryabchikova et al., 1997), and for stellar photosphere models the excellent MARCS models are a good choice (Gustafsson et al., 2008). A tool that has been utilised many times throughout the work presented in this thesis is the code called Spectroscopy Made Easy, SME (Valenti & Piskunov, 1996, 2012; Piskunov & Valenti, 2017).

5.5 Astrophysical line list

A challenge with the data found in the VALD3 collaboration (Ryabchikova et al., 1997) is that large parts of the data have been calculated theoretically and have yet to be verified by laboratory measurements. This is a particular problem in the infrared wavelength regime. The theoretical calculations are very good, but aim at being correct on a statistical level to support opacity calculations for creating stellar atmosphere models, like the MARCS models (Gustafsson et al., 2008).

For stellar spectroscopy it is, however, necessary to verify every data point for

every single spectral line. Assuming the abundances in the Sun are well known, one can produce model spectra of the Sun and compare to observations. Any deviation in line strength between model and observation can then be attributed to imprecise theoretical calculations in the oscillator strengths.

Adjusting the oscillator strength to make the model spectra fit the observation of the Sun thus produces a new data set of oscillator strengths. These oscillator strengths are called astrophysical oscillator strengths to signify their non-laboratory origin.

Another challenge with the data found in VALD3 is that the wavelength of a spectral line has an uncertainty associated with it, this goes not only for the theoretical calculations, but also for the laboratory measurements. Making accurate theoretical energy calculations is extremely difficult and requires very good physical modelling and often increases the reach of the problem beyond what can feasibly be calculated even with the most powerful computers today (see e.g. Fischer et al., 2016). The wavelength measurements obtained from laboratory experiments are not always as precise as we would like for high resolution spectroscopy, in particular because we need not only to assign the spectral lines to a given species, but also to be able to fit models to observations for abundance analysis.

When comparing model spectra of the Sun with observations it becomes clear that, as with oscillator strengths, adjustments to the wavelength of a spectral line can be needed to fit model to observation. By combining the astrophysical oscillator strengths and the wavelength adjustments, an astrophysical line list is created.

A major part of our work in this project has been to develop an astrophysical line list in the infrared wavelength regime around 2 microns. In total we identified more than 700 interesting spectral lines for our project and slightly modified about 570 of them (Thorsbro et al., 2017).

6   Outlook

The nuclear star cluster of the Milky Way is still poorly investigated with high resolution spectroscopy, which is needed for an accurate and precise abundance determination. Expanding our stellar sample to 100 stars or more would allow us to determine metallicities and abundances to a much higher degree, allowing us to confirm or reject the result suggested in Paper V. If the nuclear star cluster indeed is different from other stellar populations found elsewhere in the Galaxy, it is important to collect a good high resolution sample to map out the differences.

It is possible to increase the resolution beyond the 23000 we have used, since

for example NICRSPEC on the Keck telescopes has recently been upgraded to 38000, and other spectrometers exist, like IGRINS with a resolution of about 56000. IGRINS is also able to capture the H band (~ 1.5 micron) in addition to the K band (~ 2 micron), opening up an abundance analysis of many more chemical speciecs, though the higher extinction in the H band is a problem with current telescopes. The higher resolution will allow for higher fidelity in line detection and blend analysis.

We are also interested in the exploration of the nuclear stellar disk. It is about 100 times more massive than the nuclear star cluster, and could be a more important component to study than the nuclear star cluster. We are planning on embarking on such a project with our collaborator R. M. Rich.

In our current collected data set we have a few stars still under investigation that we are curious about (Thorsbro et al., in prep.). These stars are different from the stars included in our published work in that they are most probably young stars found in the nuclear star cluster. Their presence opens up the possibility of mapping the more recent star formation. Compared to earlier studies of these stars it is possible that we can advance our understanding of these stars by having more accurate and precise metallicity and abundance determinations from high resolution spectroscopy.

We have also noticed a particularly high light element abundance in the stars we have observed, most likely nitrogen (Thorsbro et al., in prep.). It will be interesting to study this in further detail and determine if there is an actual difference between stars in the Galactic centre and stars further out in this respect. If this turns out to be an additional difference it will be another interesting observation that needs to be explained by theories.

Finally, with the new large telescopes, 30 m or more in diameter, new observation targets becomes available to us. Apart from seeing things further away, like stars in the Andromeda galaxy, M31, they can also be used for observing shorter wavelength regimes in dust-extincted regions compared to what we are able to do today. Being able to observe the nuclear star cluster in the H band could open up the abundance analysis of elements that do not have spectral lines in the K band.

The future is bright.

References

Agertz, O., Renaud, F., Feltzing, S., et al. 2020, arXiv e-prints, arXiv:2006.06008. https://arxiv.org/abs/2006.06008

Amarsi, A. M., Grevesse, N., Grumer, J., et al. 2020, A&A, 636, A120, doi: 10.1051/0004-6361/202037890

Atkins, J. F., & Baranov, P. V. 2013, Nature, 503, 437, doi: 10.1038/503437a

Bland-Hawthorn, J., & Gerhard, O. 2016, ARA&A, 54, 529, doi: 10.1146/annurev-astro-081915-023441

Boulton, G., & Lucas, C. 2008, What are universities for?, Leuven, Belgium: League of European Research Universities, Accessed: 2020-07-09. https://www.leru.org/files/What-are-Universities-for-Full-paper.pdf

Burbidge, E. M., Burbidge, G. R., Fowler, W. A., & Hoyle, F. 1957, Rev. Mod. Phys., 29, 547, doi: 10.1103/RevModPhys.29.547

Chandrasekhar, S., & Elbert, D. D. 1958, ApJ, 128, 633, doi: 10.1086/146576

Christensen, I. B. 2020, Accurate Abundances of Giant Stars in the Local disk: A manual analysis of IR APOGEE spectra, Lund University Student Paper

Clayton, D. 2003, Handbook of Isotopes in the Cosmos (Cambridge University Press)

Crain, R. A., Schaye, J., Bower, R. G., et al. 2015, MNRAS, 450, 1937, doi: 10.1093/mnras/stv725

Do, T., Kerzendorf, W., Konopacky, Q., et al. 2018, ApJL, 855, L5, doi: 10.3847/2041-8213/aaaec3

Do, T., Kerzendorf, W., Winsor, N., et al. 2015, ApJ, 809, 143, doi: 10.1088/0004-637X/809/2/143

Erwin, P., & Gadotti, D. A. 2012, Advances in Astronomy, 2012, 946368, doi: 10.1155/2012/946368

Escala, I. A. 2020, arXiv e-prints, arXiv:2008.01636. https://arxiv.org/abs/2008.01636

Feldmeier-Krause, A., Kerzendorf, W., Neumayer, N., et al. 2017, MNRAS, 464, 194, doi: 10.1093/mnras/stw2339

Fischer, C., Godefroid, M., Brage, T., Jönsson, P., & Gaigalas, G. 2016, Journal of Physics B: Atomic, Molecular and Optical Physics, 49, doi: 10.1088/0953-4075/49/18/182004

Georgiev, I. Y., Böker, T., Leigh, N., Lützgendorf, N., & Neumayer, N. 2016, MNRAS, 457, 2122, doi: 10.1093/mnras/stw093

Grand, R. J. J., Gómez, F. A., Marinacci, F., et al. 2017, MNRAS, 467, 179, doi: 10.1093/mnras/stx071

Grevesse, N., Asplund, M., & Sauval, A. J. 2007, SSRv, 130, 105, doi: 10.1007/s11214-007-9173-7

Gustafsson, B., Edvardsson, B., Eriksson, K., et al. 2008, A&A, 486, 951

Hubeny, I., & Mihalas, D. 2014, Theory of Stellar Atmospheres (Princeton University Press)

John, T. L. 1964, MNRAS, 128, 93, doi: 10.1093/mnras/128.1.93

Jönsson, H., Holtzman, J. A., Allende Prieto, C., et al. 2020, arXiv e-prints, arXiv:2007.05537. https://arxiv.org/abs/2007.05537

Khoperskov, S., Haywood, M., Snaith, O., et al. 2020, arXiv e-prints, arXiv:2006.10195. https://arxiv.org/abs/2006.10195

Kim, S., Prato, L., & McLean, I. 2015, REDSPEC: NIRSPEC data reduction, Astrophysics Source Code Library. http://ascl.net/1507.017

Kobayashi, C., Karakas, A. I., & Lugaro, M. 2020, arXiv e-prints, arXiv:2008.04660. https://arxiv.org/abs/2008.04660

Kroupa, P., & Jerabkova, T. 2019, Nature Astronomy, 3, 482, doi: 10.1038/s41550-019-0793-0

Matteucci, F. 2012, Chemical Evolution of Galaxies (Springer Berlin Heidelberg), doi: 10.1007/978-3-642-22491-1

Matteucci, F., & Brocato, E. 1990, ApJ, 365, 539, doi: 10.1086/169508

McLean, I. S., Becklin, E. E., Bendiksen, O., et al. 1998, in Society of Photo-Optical Instrumentation Engineers (SPIE) Conference Series, Vol. 3354, Infrared Astronomical Instrumentation, ed. A. M. Fowler, 566–578, doi: 10.1117/12.317283

McWilliam, A. 2016, PASA, 33, e040, doi: 10.1017/pasa.2016.32

Mo, H. J., Mao, S., & White, S. D. M. 1998, MNRAS, 295, 319, doi: 10.1046/j.1365-8711.1998.01227.x

Naab, T., & Ostriker, J. P. 2017, ARA&A, 55, 59, doi: 10.1146/annurev-astro-081913-040019

Neumayer, N., Seth, A., & Böker, T. 2020, A&A Rv, 28, 4, doi: 10.1007/s00159-020-00125-0

Ordenes-Briceño, Y., Puzia, T. H., Eigenthaler, P., et al. 2018, ApJ, 860, 4, doi: 10.3847/1538-4357/aac1b8

Pehlivan Rhodin, A., Hartman, H., Nilsson, H., & Jönsson, P. 2017a, A&A, 598, A102, doi: 10.1051/0004-6361/201629849

Pehlivan Rhodin, A., Belmonte, M. T., Engström, L., et al. 2017b, MNRAS, 472, 3337, doi: 10.1093/mnras/stx2159

Piskunov, N., & Valenti, J. A. 2017, A&A, 597, A16, doi: 10.1051/0004-6361/201629124

Prialnik, D. 2000, An Introduction to the Theory of Stellar Structure and Evolution (Cambridge University Press)

Renaud, F., Agertz, O., Andersson, E. P., et al. 2020a, arXiv e-prints, arXiv:2006.06012. https://arxiv.org/abs/2006.06012

Renaud, F., Agertz, O., Read, J. I., et al. 2020b, arXiv e-prints, arXiv:2006.06011. https://arxiv.org/abs/2006.06011

Ryabchikova, T. A., Piskunov, N. E., Kupka, F., & Weiss, W. W. 1997, Baltic Astronomy, 6, 244

Salpeter, E. E. 1955, ApJ, 121, 161, doi: 10.1086/145971

Sánchez-Janssen, R., Côté, P., Ferrarese, L., et al. 2019, ApJ, 878, 18, doi: 10.3847/1538-4357/aaf4fd

Schaye, J., Crain, R. A., Bower, R. G., et al. 2015, MNRAS, 446, 521, doi: 10.1093/mnras/stu2058

Schneider, P. 2006, Extragalactic Astronomy and Cosmology (Springer-Verlag Berlin Heidelberg)

Spengler, C., Côté, P., Roediger, J., et al. 2017, ApJ, 849, 55, doi: 10.3847/1538-4357/aa8a78

Thorne, A., Litzen, U., & Johansson, S. 1999, Spectrophysics (Springer-Verlag Berlin Heidelberg New York)

Thorsbro, B. 2018, Spectroscopic Investigations of Cool Giant Stars in the Galactic Centre, Lund University Licentiate Thesis

Thorsbro, B., Ryde, N., Rich, R. M., et al. 2017, Proceedings of the International Astronomical Union, 13, 372–373, doi: 10.1017/S1743921317009851

Thorsbro, B., Ryde, N., Rich, R. M., et al. 2020, ApJ, 894, 26, doi: 10.3847/1538-4357/ab8226

Tody, D. 1993, in ASP Conf. Ser. 52: Astronomical Data Analysis Software and Systems II, ed. R. J. Hanisch, R. J. V. Brissenden, & J. Barnes, 173

Černiauskas, A., Kučinskas, A., Klevas, J., et al. 2017, A&A, 604, A35, doi: 10.1051/0004-6361/201630305

Valenti, J. A., & Piskunov, N. 1996, A&AS, 118, 595

—. 2012, SME: Spectroscopy Made Easy. http://ascl.net/1202.013

Wildt, R. 1939, ApJ, 90, 611, doi: 10.1086/144125

Woosley, S. E., & Weaver, T. A. 1995, ApJS, 101, 181, doi: 10.1086/192237

Scientific publications

Paper summaries and author contributions

A summary of each paper is presented here, and my contributions clarified.

Paper I

In this paper we have gone through the first part of our dataset taken from the first observation trip. In the dataset we found a metal poor star in the hotter end of M giants with an effective temperature of about 3800 K. This means that its spectrum was devoid of most of the molecular features that we find in the other stars in our dataset. Hence, the star's spectrum was easier to analyse.

Careful orbit analysis of the star suggests that the star is a member of either the nuclear star cluster (NSC) or the nuclear stellar disk (NSD). The orbit does not show signs of it being a stray star from the bulge that has been captured, though we cannot rule out that the star may originally have formed in a globular cluster that had fallen into the Galactic centre.

That the star is metal poor, $[Fe/H] \sim -1.0$, meaning that it could be similar to globular cluster stars. Other studies of the Galactic centre are finding 5–10% low metalliticy stars (Feldmeier-Krause et al., 2017; Do et al., 2015), so our one star out of the 20 in our sample agrees with that.

We find that $[\alpha/Fe] \sim 0.4$, which is similar to what is found elsewhere in our Galaxy for stars with the same metallicity. The study of this one star does not give reason to claim any differences between the Galactic centre and other parts of the Galaxy.

My contribution to paper I

I took part in the observations, having led some of the time. I was responsible for the data reduction. I developed the astrophysical line list used for the spectroscopy

analysis and carried out the abundance analysis in close collaboration with Nils Ryde. I contributed to writing the article.

Paper II

In this paper we present a metallicity distribution function (MDF) of stars found in the nucleus of our Galaxy, either NSC or NSD. The stars seem to show two peaks in the MDF, one centred around [Fe/H] ~ -0.25 and one centred around [Fe/H] ~ 0.4.

Because of patchy extinction towards the Galactic centre, it turned out to be really difficult to get proper photometric $\log g$ values for all of the stars in the dataset. Given that we have targeted old stars we we were able to make use of the fact that isochrone tracks for M giants are insensitive to age for ages above 5 Gyr. This means we have a function linking the three stellar parameters: effective temperature, [Fe/H] and $\log g$. Performing an iterative metallicity determination including the constraints from this developed function made it possible to determine the metallicities of the stars.

This method was verified against a subsample of giant stars in the APOGEE data set having effective temperatures between 3500 K and 4500 K so as to be as comparable to the M giants in our sample as possible. We also did the analysis using the photometric $\log g$ determinations, even though we had problems with the patchy extinction. The photometric results are in good agreement with the isochrone $\log g$ for many of the stars but, as expected, exhibit larger deviations for some of the stars.

We investigated many of the strong spectral lines belonging to scandium, titanium, vanadium and calcium. However, we found many lines to be very temperature sensitive and further suspected NLTE to be an issue, so we did not trust our abundance analysis of these lines.

My contribution to paper II

I took part in the observations, having led some of the time. I was responsible for the data reduction. I used the previously developed astrophysical line list and did the abundance analysis in close collaboration with Nils Ryde. I developed the isochrone method required for finding the metallicity distribution. I contributed to writing the article.

Paper III

After our paper II had been published, a publication (Do et al., 2018) appeared claiming unusual scandium, vanadium and yttrium abundances in the Galactic centre. We thus decided that it was necessary to return to the strong spectral lines we had ignored in Paper II and reconsider our data.

Our dataset also includes observations of M giants further out in the Galaxy that we use as a control sample. This allowed us to make a differential studies, where a lot of the systemic uncertainties are eliminated.

Comparing our Galactic centre stars and stars further out in the Galaxy, we found that these strong lines are also present further out in the Galaxy. Therefore, the strong lines are likely to be intrinsic to the cool stars that we are probing and not due to the stellar population or environment where the stars live.

We took a closer look at scandium, since we had recently measured its atomic properties in the lab. Many of the atomic physics properties of scandium were at the time not included in the database VALD3, and including them actually could explain partially the strong spectral lines. In particular temperature sensitivity due to ionisation and the hyperfine splitting properties of scandium are both significant contributors. Further investigation of the temperature sensitive NLTE effects will be needed to enable determination of Sc abundance from these lines.

My contribution to paper III

I took part in the observations, having led some of the time. I was responsible for the data reduction. I used the previously developed astrophysical line list and isochrone method and carried out the Sc abundance determinations. I modelled scandium with and without hyperfine structure. I led the paper writing.

Paper IV

This paper is unusual in that it started as a conference proceeding but, for some reason, it was assigned no less than three referees. Thanks to the comments from the referees it took off from there to become a work that focused on making the astrophysical results from the previous articles available to the atomic physics community.

My contribution to paper IV

I was wholly responsible for this paper.

Paper V

Since the publication of Paper II we have concentrated on finding good alpha lines to investigate. There are several good silicon lines and, after doing a thorough investigation into identifying molecular features of cool stars, we were able to compile a good set of silicon lines that could be used for abundance analysis.

After we had demonstrated the temperature sensitivity of scandium lines in Paper III we used this to implement a temperature determination function, rather similar to the CO bandhead one we have used in Paper II. It turned out that the temperatures determined from the scandium lines were generally in good agreement with the temperature from the CO bandhead method, which has increased our confidence in the determined effective temperatures of the stars.

Using the updates on molecular blending and the slightly improved temperatures, we redid the MDF analysis. It is quite similar to the MDF we found in Paper II, although the new MDF shows even more strongly the bimodality in the MDF suggested in Paper II.

We also investigated the silicon abundance as a tracer element for alpha elements and we find, curiously enough, a slightly enhanced silicon abundance for the metal-rich end of our dataset. We investigated possible systematics to be confident with the results. NLTE calculations showed that NLTE corrections are not a significant concern for our choice of silicon lines.

We entered into a collaboration with the community working on chemical evolution models and, in this paper, offer two possible explanations for the enhanced silicon abundances in metal-rich stars.

My contribution to paper V

I took part in the observations, having led some of the time. I was responsible for the data reduction. I developed a scandium temperature determination method to improve on our temperatures. I used the previously developed astrophysical line list and isochrone method and performed the updated metallicity distribution and the abundance analysis. I investigated line blending by modelling theoretical spectra to minimise the impact of CN blending. I led the paper writing, including the coordination of contributions from the new collaborators.

Paper I

DETAILED ABUNDANCE ANALYSIS OF A METAL-POOR GIANT IN THE GALACTIC CENTER

N. RYDE[1], T. K. FRITZ[2], R. M. RICH[3], B. THORSBRO[1], M. SCHULTHEIS[4], L. ORIGLIA[5], AND S. CHATZOPOULOS[6]
[1] Lund Observatory, Department of Astronomy and Theoretical Physics, Lund University, Box 43, SE-221 00 Lund, Sweden; ryde@astro.lu.se
[2] Department of Astronomy, University of Virginia, 3530 McCormick Road, Charlottesville, VA 22904, USA
[3] Department of Physics and Astronomy, UCLA, 430 Portola Plaza, Box 951547, Los Angeles, CA 90095-1547, USA
[4] Observatoire de la Côte d'Azur, CNRS UMR 7293, BP4229, Laboratoire Lagrange, F-06304 Nice Cedex 4, France
[5] INAF—Osservatorio Astronomico di Bologna, Via Ranzani 1, I-40127 Bologna, Italy
[6] Research Center for Astronomy, Academy of Athens, Soranou Efessiou 4, GR-115 27 Athens, Greece
Received 2016 June 21; revised 2016 August 18; accepted 2016 August 19; published 2016 October 26

ABSTRACT

We report the first results from our program to examine the metallicity distribution of the Milky Way nuclear star cluster connected to Sgr A*, with the goal of inferring the star formation and enrichment history of this system, as well as its connection and relationship with the central 100 pc of the bulge/bar system. We present the first high-resolution ($R \sim 24,000$), detailed abundance analysis of a $K = 10.2$ metal-poor, alpha-enhanced red giant projected at 1.5 pc from the Galactic center, using NIRSPEC on Keck II. A careful analysis of the dynamics and color of the star locates it at about 26^{+54}_{-16} pc line-of-sight distance in front of the nuclear cluster. It probably belongs to one of the nuclear components (cluster or disk), not to the bar/bulge or classical disk. A detailed spectroscopic synthesis, using a new line list in the K band, finds [Fe/H] ~ -1.0 and [α/Fe] $\sim +0.4$, consistent with stars of similar metallicity in the bulge. As known giants with comparable [Fe/H] and alpha enhancement are old, we conclude that this star is most likely to be a representative of the $\sim$10 Gyr old population. This is also the most metal-poor-confirmed red giant yet discovered in the vicinity of the nuclear cluster of the Galactic center. We consider recent reports in the literature of a surprisingly large number of metal-poor giants in the Galactic center, but the reported gravity of log g ~ 4 for these stars calls into question their reported metallicities.

Key words: Galaxy: center – stars: abundances – stars: late-type

1. INTRODUCTION

The predominance of late-type M giants in the bulge has been known since the work of Nassau & Blanco (1958) and in fact had marked the bulge as a metal-rich, disk population in the 1957 Vatican meeting on stellar populations. The evolved stellar content was known early on to be very different from that of the halo and globular clusters, even though Baade's (1951) discovery of RR Lyrae variables in the bulge offered one population in common. The lack of metal-poor giants with [Fe/H] ~ -1 was evident from the earliest abundance distributions (Rich 1988) and was confirmed in all subsequent studies (e.g., Fulbright et al. 2006; Zoccali et al. 2008; Johnson et al. 2011, 2013, 2014; Ness et al. 2013). While aspects of the microlensed dwarf population remain in debate, especially the age distribution, Bensby et al. (2013) agree with results based on giants in finding very few stars with [Fe/H] < −1. These studies all consider bulge fields with $b < -4°$, although the lack of a metal-poor population inward of $b = -4°$ continues to be confirmed in the GIBS survey (Gonzalez et al. 2015). Extremely metal-poor stars (e.g., [Fe/H] < −3) are known in the bulge, but they are so rare that wide-field surveys must be undertaken to discover them (see, e.g., Howes et al. 2015), and while they are in the bulge, they are considered to have an origin apart from most of the bulge (Koch et al. 2016). Simply based on an assessment of the nature of the bulge, known abundance gradients in external galaxies, and the well-established presence of massive clusters and young stars toward the Galactic center, it would be expected that few if any metal-poor stars might be found within 300 pc of the nucleus.

Indeed, at the Galactic center, Ramírez et al. (2000b), Carr et al. (2000), and Davies et al. (2009) found, by analyzing red supergiants, a metal-rich population narrowly distributed around the solar metallicity. Similar results are found by Ryde & Schultheis (2015) for M giants. Recently, though, Schultheis et al. (2015) found the presence of a metal-poor population beyond 70 pc from the nuclear cluster, which has a radius of approximately 7 pc (Fritz et al. 2016). Do et al. (2015) also reported a significant population of metal-poor stars in the nuclear cluster.

Here we report on the first high-resolution spectroscopy of a red giant with [Fe/H] ~ -1 to be found in the vicinity of the nuclear cluster, at a projected distance of 1.5 pc from the Galactic center. We have performed a detailed abundance analysis based on high-resolution, K-band spectra. Observing at K band makes such investigations possible due to the much lower extinction at higher wavelengths (Cardelli et al. 1989). The K-band extinction toward the central parsec is only $A_{K_S} = 2.74$ with a variation of ±0.30 due to spatial variations (Schödel et al. 2010).

2. TARGET SELECTION

We selected a list of Galactic center giants from spectra observed with the integral field spectrometer SINFONI (Bonnet et al. 2003; Eisenhauer et al. 2003) on the Very Large Telescope, providing a K-band resolution of $R = 4000$ or $R = 1500$. The selection for the target group, to which the observed star belongs, was done according to the following criteria: a K_S magnitude range of $10 < K_S < 11$, an angular distance from the Galactic center of R_c(Sgr A*) > 25″, and excluding stars with neighbors too close for seeing-limited high-resolution spectroscopy. Initially, SINFONI spectra were only used to ensure qualitatively that the objects are cool in the sense that the CO bandheads exist, but we have not imposed any initial cuts based on the CO band strength or derived
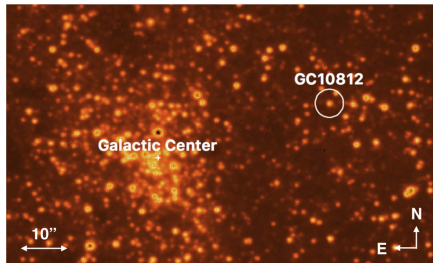
1

Figure 1. UKIDSS finding chart of the Galactic center (Lawrence et al. 2013). GC10812 is marked with a circle.

effective temperature. We also used the catalogs of Blum et al. (2003) and Matsunaga et al. (2009) to exclude some known asymptotic giant branch/long-period variable stars, such as Miras, and known red supergiants. The aim of this sample is to develop a relatively unbiased, large sample of old Galactic center stars that we will use in our study of the metallicity distribution. A more detailed discussion of our full sample is in preparation.

In Figure 1 we present a finding chart (Lawrence et al. 2013) with our observed target, the giant GC10812, indicated (see also Table 1). The star lies at an angular distance of $38\rlap{.}''4$ from the Galactic center. This corresponds to a projected galactocentric distance of $R_c = 1.5$ pc, adopting the distance to the Galactic center of 8.3 kpc (Chatzopoulos et al. 2015a; Bland-Hawthorn & Gerhard 2016).

The K_S magnitude of GC10812 is 10.25 ± 0.05 from Nishiyama et al. (2009), and its color is $H - K_S = 1.63 \pm 0.07$. Using the extinction law of Fritz et al. (2011), this leads to an extinction of $A_{Ks} = 1.94 \pm 0.10$. The absolute magnitude of GC10812 is $M_{Ks} = -6.48 \pm 0.12$. This is close to the approximate tip of the RGB with $M_{bol} = -3.5$ (see also Tiede et al. 1995; Omont et al. 1999). Compared to all stars with $M_{Ks} = -5.5$ from Nishiyama et al. (2009) within $100''$ of Sgr A*, the star is clearly bluer, -0.84 bluer than the median color. That means that only 21 of 1067 stars are bluer than GC10812. There are also extinction variations over the Galactic center (Schödel et al. 2010). To account for them, we measure relative color locally using Gemini AO data.[7] We use stars with $K_S < 16$ and account for intrinsic color differences. Dependent on the comparison scale ($3''$ or $6''$) and including other error sources like scatter and photometry uncertainty for the target, we obtain that GC10812 is 0.75 ± 0.10 bluer than the local median. Over the full Galactic center $3.6^{+2.7}_{-1.9}\%$ of all stars are that blue or bluer. The $H - K_S$ color excess corresponds to an extinction difference of $A_{Ks} = 1.01 \pm 0.14$ between the $A_{Ks} = 1.94$ measured for this star and $A_{Ks} = 2.95$ measured as the average for all stars in this region. That is more dust than the $A_{Ks} \approx 0.4$ that Chatzopoulos et al. (2015b) find within $r = 100''$ of Sgr A*. However, there is also extinction variation in the plane of sky (Schödel et al. 2010); at some places up to $A_{Ks} \approx 0.8$ was found. Further, the model of Chatzopoulos et al. (2015b) is very insensitive to dust at greater distances.

To constrain the line-of-sight position, we use the Galactic center model of Chatzopoulos et al. (2015a) and derive how much a star needs to be placed in front of Sgr A* in order for it to be bluer than $3.6^{+2.7}_{-1.9}\%$ of its stars. We obtain a distance of $D_c = 26^{+54}_{-16}$ pc. That is in principle a slight underestimate of the distance because the model includes no bar/bulge or Galactic disk. This contribution is, however, probably small; Launhardt et al. (2002) show that in this part of the nuclear disk the space density due to the bar/bulge is more than 40 times smaller than the contribution due to the nuclear disk. Its absolute extinction also argues for a location within the nuclear disk; an extinction of $A_{Ks} \approx 2$ is unusual for old stars outside the nuclear disk (Schultheis et al. 2014). Whether it is possible that the star still is around the outer rim of the nuclear cluster or not depends on the precise distance and nuclear cluster definition (Schödel et al. 2014; Chatzopoulos et al. 2015a; Fritz et al. 2016). It is, however, clear that the star is currently within a nuclear component, because the nuclear disk extends to an outer radius of 230 pc (Launhardt et al. 2002).

The dynamics measured in Fritz et al. (2016) are $\mu_l = 2.31 \pm 0.27$ mas yr^{-1}, $\mu_b = -3.12 \pm 0.27$ mas yr^{-1}, and $v_{rad} = -51 \pm 5$ km s^{-1} (which we confirm in our measurement of the star's heliocentric velocity from the NIRSPEC high-resolution spectra of -56.4 ± 1.0 km s^{-1}; see Table 1). These velocities are rather typical for a Galactic center star; see Figure 2. The positive velocity in l and the lower extinction fit as the extinction to a star in front of the Galactic center (Chatzopoulos et al. 2015b).

We calculate the orbit for the stars using the potential of Chatzopoulos et al. (2015a). This potential includes the supermassive black hole, nuclear cluster, and cluster disk. Three orbits are shown in Figure 3. For small current distances (black and red orbits in the figure) the average distance of GC10812 from the Galactic center is somewhat larger than the current distance from the Galactic center. That makes membership in the nuclear cluster unlikely, and excludes it nearly certainly if the cluster is assumed to have a Sérsic-like cutoff, which results in a half-light radius of about 5 pc (Schödel et al. 2014; Fritz et al. 2016). If it is instead assumed that the outer slope follows a power law (Chatzopoulos et al. 2015a), a membership in the nuclear cluster is still possible. When the star is currently at large distance (blue orbit in Figure 3), the star does not move much further away on its orbit. We conclude that the star most likely resides within the nuclear disk and is unlikely to experience any excursions into the bulge or halo. We conclude based on the distance and kinematics that GC10812 is probably a nuclear disk star.

3. OBSERVATIONS

We observed the giant GC10812 on 2015 April 27 with the NIRSPEC spectrometer McLean (2005) mounted on Keck II, at a resolution of $R \sim 24{,}000$ in the K band, using the $0\rlap{.}''432 \times 12''$ slit and the NIRSPEC-7 filter. The retrieved spectra range from 21100 to 23300 Å, using five orders and therefore obtaining about 50% spectral coverage. We observed in an ABBA nodding scheme with a throw of $6''$ on the slit, to achieve proper background and dark subtraction. A total exposure time on target was 960 s. The data were reduced with the NIRSPEC software `redspec` (Kim et al. 2015), providing final 1D wavelength-calibrated spectra. IRAF (Tody 1993) was subsequently used to normalize the continuum, eliminate obvious cosmic-ray hits, and correct for telluric lines (with

---

[7] We use H-continuum and K (long) continuum images from program Gs-2013A-Q-15, avoiding data in which the target is saturated.

2

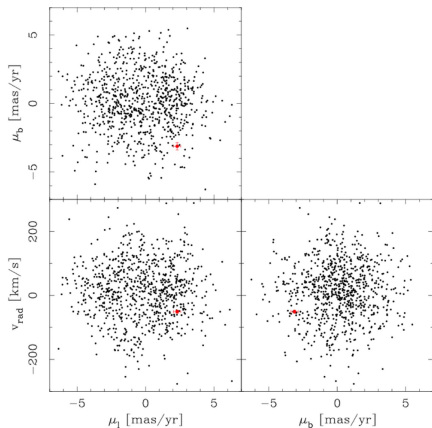| Data	R.A. (h:m:s)	Decl. (d:m:s)	(l, b) (deg)	R_c (pc)	D_c (pc)	$v_{\rm rad}^{\rm helio}$ (km s^{-1})	μ_l (mas yr^{-1})	μ_b (mas yr^{-1})
GC10812	17:45:37.229	−29:00:16.62	(359.9, −0.035)	1.5	26	−56.5	2.31	−3.12
Uncertainties	⋯	⋯	⋯	±0.1	$^{+54}_{-16}$	±1.0	±0.27	±0.27

Figure 2. Velocity of GC10812 (red) in comparison with other Galactic center stars. The other stars are in 0.8–3.6 pc projected distance from Sgr A*.
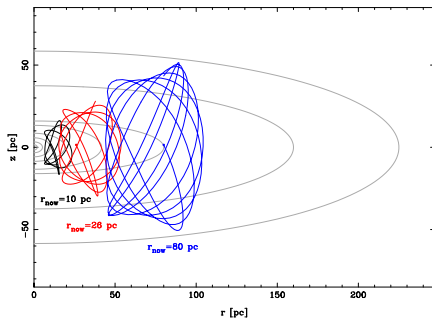

Figure 3. Orbit of GC10812. The red curve shows it for the most likely distance in front of the Galactic center (26 pc), while the other two curves show the orbit when the star would be at the outer/inner edge of the 1σ interval. The gray curves show equal star surface density of contours of the nuclear disk from Fritz et al. (2016) and Launhardt et al. (2002). The outermost curve marks roughly the outer edge of the nuclear disk.

telluric standard stars). We estimate S/N = 90 per pixel in our reduced spectra. A portion of the observed spectrum is shown in Figure 4.
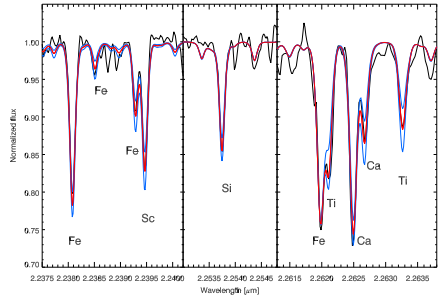

Figure 4. Examples of spectra covering a few of the lines used for the abundance determination. The black curves are the observations; the red one is the best-fit model. The blue spectra correspond to ±0.2 dex in the corresponding abundances, in order to show the sensitivity of these lines to the determined abundances.

4. ANALYSIS

We analyze our spectra, deriving detailed chemical abundances, by calculating synthetic spectra, given the star's fundamental parameters, i.e., effective temperature ($T_{\rm eff}$), surface gravity (log g), metallicity ([Fe/H]), and microturbulence ($\xi_{\rm mic}$), and a suitable line list in the K band (see Section 4.2).

4.1. The Stellar Parameters

The derived $T_{\rm eff} = 3817 \pm 150$ K is determined from integrating the strength of the 2.3 μm CO (2–0) band in the SINFONI spectra[8] and using the relation between the CO band strength and the $T_{\rm eff}$ given in Schultheis et al. (2016). They have shown that this relation works very well in the temperature range between 3200 and 4500 K and in the metallicity range between 0.5 and −1.2 dex with a typical dispersion of about 150 K.

The surface gravity, log g, is determined photometrically and assuming a mean distance of 8.3 kpc to the Galactic center, in the same manner as in Ryde & Schultheis (2015). A stellar mass of an old star of typically 1 $M_\odot$ is assumed, but the surface gravity is not very sensitive to the mass. A difference in mass of 0.2 $M_\odot$ gives 0.1 dex log g difference. In the calculation of the surface gravity we used the extinction law from Fritz et al. (2011) and the bolometric corrections from Houdashelt et al. (2000). An extinction uncertainty of $A_{Ks} = 0.1$ gives 0.2 dex error in log g, and a bolometric uncertainty of $M_{\rm bol} = 0.12$ gives 0.15 dex uncertainty in log g. The combined uncertainty is thus $\sqrt{0.1^2 + 0.2^2 + 0.15^2} = 0.27$ dex. Our derived surface gravity is thus log $g = 0.5 \pm 0.3$ (dex).

---

[8] The SINFONI spectrum is from program 087.B-0117.

Table 2
Stellar Photometry, Parameters, and Abundances

Data	K_S	$H - K_S$	T_{eff} (K)	log g (dex)	ξ_{mic} (km s^{-1})	[Fe/H]	[Mg/Fe]	[Si/Fe]	[Ca/Fe]	[Ti/Fe]	[Sc/Fe]
GC10812	10.25	1.63	3817	0.5	2.0	−1.05	0.36	0.39	0.55	0.53	0.44
Uncertainties	±0.05	±0.07	±150	±0.3	±0.5	±0.1	±0.1	±0.1	±0.2	±0.3	±0.3

Ramírez et al. (2000a) found that the combination of the CO first-overtone band with the Na I and the Ca I lines is sensitive to the surface gravity of the star. We have therefore also measured the Na I and Ca I lines in the SINFONI spectra as in Schultheis et al. (2016). Our derived value for $\log[EW(CO)/(EW(Na) + EW(Ca))] = 0.405$ for GC10812 locates our star on the RGB sequence of Ramirez et al. (1997).

We have chosen a typical value of $\chi_{mic} = 2.0 \pm 0.5$ km s^{-1} found in detailed investigations of red giant spectra in the near-IR by Tsuji (2008); see also the discussion in Cunha et al. (2007).

The location of GC10812 in the Hertzsprung–Russel diagram, using our derived effective temperature, surface gravity, and metallicity (see Table 2), is plotted with a big star symbol in Figure 5. It fits nicely on the red giant branch.

4.2. Line List

An atomic line list based on the VALD3 database (Piskunov et al. 1995; Kupka et al. 1999, 2000; Ryabchikova et al. 1997, 2015) has been constructed (B. Thorsbro et al. 2017, in preparation). Wavelengths and line strengths (astrophysical log gf-values) are updated for 575 lines in the K band using the solar center intensity atlas (Livingston & Wallace 1991). New laboratory measurements of wavelengths and oscillator strengths of Sc lines (Pehlivan et al. 2015) and newly calculated oscillator strengths of Mg lines (A. Pehlivan et al. 2016, in preparation) are included. ABO[9] line-broadening theory is included (Anstee & O'Mara 1991; Barklem & O'Mara 1998) when available. In the abundance analysis, we also include molecular line lists of CN (Jørgensen & Larsson 1990) and CO (Goorvitch 1994).

The line list is tested by determining abundances from high-quality spectra of α Boo (Hinkle et al. 1995) and five thick-disk stars. The thick-disk giants were observed with NIRSPEC in the same manner as for GC10812. The parameters and abundances of α Boo are from Ramírez & Allende Prieto (2011), and those of the thick-disk stars are from the APOGEE pipeline (Ahn et al. 2014). The parameter ranges of these test stars are $4150 < T_{eff}/K < 4750$, $1.5 < \log g < 2.5$, and $-0.5 < $ [Fe/H] < -0.1. We find an excellent agreement, to within 0.05 dex, between the abundances we determined from the K band and these reference values. The line list has not yet been tested against supersolar-metalicity stars. Thus, the line list can with confidence be used for metal-poor to solar-metallicity cool stars.

4.3. Spectral Synthesis

We derive our target star's abundances by comparing the observed spectrum with synthesized spectra using the software *Spectroscopy Made Easy*, *SME* (Valenti &

Table 3
Line List

Element	Wavelength in Air (Å)	Exc. Pot. eV	log(gf) (cgs)
Mg I	21208.106	6.73	−0.821
Si I	21195.298	7.29	−0.425
Si I	21779.720	6.72	0.418
Si I	21819.711	6.72	0.087
Si I	21874.199	6.72	−0.731
Si I	21879.345	6.72	0.384
Si I	22537.593	6.62	−0.216
Ca I	22626.786	4.68	−0.281
Sc I	21730.452	1.44	−1.880
Sc I	21812.174	1.43	−1.490
Sc I	21842.781	1.43	−1.760
Sc I	22394.695	1.43	−1.180
Ti I	22632.743	1.88	−2.760
Fe I	21124.505	5.33	−1.647
Fe I	21238.509	4.96	−1.281
Fe I	21779.651	3.64	−4.298
Fe I	21894.983	6.13	−0.135
Fe I	22380.835	5.03	−0.409
Fe I	22392.915	5.10	−1.207
Fe I	22473.263	6.12	0.483
Fe I	22619.873	4.99	−0.362

Piskunov 1996, 2012; Piskunov & Valenti 2016). This program uses a grid of model atmospheres (MARCS spherical-symmetric, LTE model atmospheres; Gustafsson et al. 2008) in which it interpolates for a given set of fundamental parameters of the analyzed star. The spectral lines, which are used for the abundance analysis, are marked with masks in the pre-normalized observed spectra. SME then iteratively synthesizes spectra for the searched abundances, under a scheme to minimize the χ^2 when comparing with the observed spectra. In order to match our synthetic spectra with the observed ones, we also convolve the synthetic spectra with a Gaussian function of FWHM of 20 ± 0.5 km s^{-1}. This broadening accounts for the instrumental spectral resolution and the macroturbulence of the stellar atmosphere.

The abundances of the elements Fe, Mg, Si, Ca, Ti, and Sc are determined from carefully chosen lines. We have restricted our analysis to lines that are on the weak part of the curve of growth, i.e., with equivalent widths of $W < 250$ Å or $\log W/\lambda < -4.9$. This means that at our resolution of $R = 24,000$, there is an upper limit to the line depth of approximately 0.75 of the continuum. Lines deeper than this will certainly be saturated and will be not as sensitive to the abundance but at the same time more sensitive to the uncertain microturbulence parameters, ξ_{mic}. Our restriction of the analysis to weak lines will ensure a good measurement of the abundances. We also require that the spectral recording around the lines and the form of the continuum is of such high quality that the continuum is traceable.

---

[9] ABO stands for Anstee, Barklem, and O'Mara, authors of the papers describing the theory in Anstee & O'Mara (1991) and Barklem & O'Mara (1998).

4

Table 4
Uncertainties due to Uncertainties in the Stellar Parameters

Parameter	[Fe/H]	[Mg/Fe]	[Si/Fe]	[Ca/Fe]	[Ti/Fe]	[Sc/Fe]
$\Delta T_{\rm eff} = \pm 150\,{\rm K}$	<0.02	$+0.07$ -0.02	-0.04 $+0.10$	$+0.16$ -0.13	$+0.28$ -0.22	$+0.27$ -0.24
$\Delta \log g = \pm 0.3\,{\rm dex}$	<0.02	<0.02	$+0.07$ -0.03	-0.05 $+0.17$	-0.03 $+0.05$	-0.03 $+0.05$
$\Delta \xi_{\rm mic} = \pm 0.5\,{\rm km\,s^{-1}}$	-0.12 $+0.10$	$+0.02$ $+0.06$	-0.01 $+0.05$	-0.08 $+0.13$	-0.02 $+0.06$	-0.06 $+0.08$

The final line list is given in Table 3. In the table the wavelengths, excitation potential, and line strengths of the lines used for the abundance determination are given. The entire line list including all lines will be published elsewhere (B. Thorsbro et al. 2017, in preparation).

Examples of synthetic spectra are shown in Figure 4, and the derived abundances are given in Table 2. The Fe, Si, and Sc abundances are determined from eight, six, and four lines, respectively, whereas the Mg, Ca, and Ti abundances are determined from only one carefully chosen line each. This means that the former abundances are observationally better determined.

The uncertainties in the determination of the abundance ratios, for typical uncertainties in the stellar parameters, are ±0.1 for [Fe/H], [Mg/Fe], and [Si/Fe], whereas it is ±0.2 dex for [Ca/Fe] and ±0.3 dex for [Ti/Fe] and [Sc/Fe]; see Table 4. In addition, we estimate random uncertainties of less than 0.05 dex due to the continuum placement. In Figure 4 we show the observed and our best-fit spectra, as well as synthetic spectra with ±0.2 dex abundance variations with respect to the best-fit solution. The figure clearly shows that we can derive abundances with overall uncertainties smaller than 0.2 dex.

5. RESULTS

Our derived stellar parameters and their uncertainties for GC10812 are given in Table 2. We find that these parameters place the star in the appropriate location on the Hertzsprung–Russel diagram, as seen in Figure 5. It lies on the red giant branch appropriate for its metallicity, as demonstrated by plotting an old population with the 10 Gyr isochrones of Bressan et al. (2012).

Our derived abundances of Fe, Mg, Si, Ca, Ti, and Sc are given in Table 2. We have normalized our derived abundances to the solar abundances of Grevesse et al. (2007): $\log \varepsilon({\rm Mg}) = 7.53$, $\log \varepsilon({\rm Si}) = 7.51$, $\log \varepsilon({\rm Ca}) = 6.31$, $\log \varepsilon({\rm Sc}) = 3.17$, $\log \varepsilon({\rm Ti}) = 5.02$, and $\log \varepsilon({\rm Fe}) = 7.45$.

Typical internal errors in the derived stellar abundances are a few hundredths of dex, while the systematic uncertainties due to different assumptions for the stellar parameters are detailed in Table 4 and, on average, amount to 0.1–0.2 dex, often dominated by one of the uncertainties in the stellar parameters.

The derived [α/Fe] abundance ratios are plotted in Figure 6, together with the corresponding measurements of different samples of giants in the bulge from Gonzalez et al. (2011) and Johnson et al. (2014) by means of optical spectroscopy, as well as measurements in low-latitude (innermost 2°) fields from Rich et al. (2007, 2012) and Ryde et al. (2016) by using H- and K-band IR spectroscopy. In Figure 6 we also reported the measurements of some low-mass giants in the Galactic center region from Ryde & Schultheis (2015) and the average abundance ratios of the three stellar populations of Terzan 5 at $(l, b) = (3°.8, +1°.7)$ from Origlia et al. (2011, 2013).

We find that the [α/Fe] abundance ratios of GC10812 are consistent with an enhancement between a factor of two and three with respect to the solar values and fully consistent with the values measured in bulge and Galactic center giants with subsolar metallicities.

6. DISCUSSION

The best constraint of the 3D location of GC10812 is at 1.5 pc distance from the Sgr A* in projected distance on the sky and 26^{+54}_{-16} pc distance in the line of sight in front of the Galactic center. The nuclear cluster has a half-light radius of $178'' \pm 51'' \sim 7 \pm 2$ pc (Fritz et al. 2016), but the nuclear disk extends to about 230 pc (Launhardt et al. 2002). The dynamics of the star is typical for a Galactic center star, and our orbit calculations show that the star's orbit is constrained within the nuclear cluster.

The kinematics strongly favor a Galactic center origin, and it is thus rather certain that the star belongs to a nuclear component. The probability of the star being a stray bulge giant is low since most bulge giants are more metal-rich and [Fe/H] ~ −1 stars are rare in the bulge (Ness & Freeman 2016). Based on the kinematics and metallicity, the probability of the star being a halo giant is also low since at least in the solar vicinity the halo metallicity in the mean is typically [Fe/H] ~ −1.6, not −1 (Ryan & Norris 1991). The relative number density of halo stars in the Galactic center is difficult to estimate, since there are no measurements of the halo quantitatively even within 8 kpc. Extrapolation can obtain a relevant mass in the center when a broken power law like, for example, that in Bland-Hawthorn & Gerhard (2016) is used. However, when other parameterizations are used, like an Einasto profile (Sesar et al. 2013; Xue et al. 2015), the obtained mass is much smaller and irrelevant. Also, from a theoretical standpoint a flatter profile is expected, since it is difficult for dwarf galaxies, which probably form the main contributor to the halo, to reach the center of the Milky Way. For example, Bullock & Johnston (2005) measure, in their model, a slope of −1 between 3 and 10 kpc, flatter than farther out. In summary, we conclude that the probability of GC10812 being a halo star is low.

The metallicity of GC10812 is lower than that of most stars in the inner bulge. Rich et al. (2007, 2012) find, for example, a dispersion of approximately 0.1 dex around [Fe/H] = −0.05 to −0.15. The more recent works of Schultheis et al. (2015) and Ryde et al. (2016) found, in addition, also some metal-poor stars with [Fe/H] ≈ −1. They are, with |b| > 0.4°, all located outside the nuclear disk. Within the nuclear components (disk and cluster) Cunha et al. (2007) find a total spread of 0.16 dex around [Fe/H] = +0.14 for the luminous giants and supergiants located within 2.2 pc of the Galactic center. Further, Carr et al. (2000), Ramírez et al. (2000b), and Davies et al. (2009) analyzed high-resolution spectra of supergiant stars in the
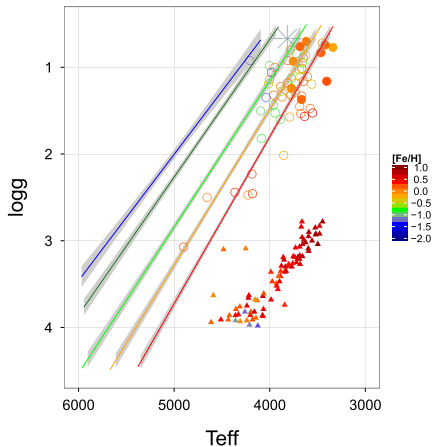
5

Figure 5. Logarithm of the surface gravities of inner bulge stars plotted vs. their effective temperatures and color-coded by their metallicities. The big star is the metal-poor star GC10812 discussed in this paper. The selection of stars in the inner 3° of the bulge from the literature are marked by open circles for the stars from Ryde et al. (2016) and Schultheis et al. (2015), by filled circles for the stars within 10 pc projected galactocentric distance from Ryde & Schultheis (2015), and by triangles for the stars discussed in Do et al. (2015). Superimposed are also the 10 Gyr PARSEC isochrones (Bressan et al. 2012) with the corresponding color of the metallicity.

Galactic center, finding near-solar metallicity. Similarly, Ryde & Schultheis (2015) at about 4.′1 distance from Sgr A* also only detect a metal-rich component with a total spread of 0.15 dex around [Fe/H] = +0.11.

The location of the [α/Fe] abundance ratios versus metallicity for the giant GC10812 is that expected for the metal-poor population in the outer bulge. The [Mg/Fe] and [Si/Fe] trends of the inner bulge are tight and are indistinguishable from the outer bulge trend, within uncertainties. Although with a larger scatter, this is also true for the [Ca/Fe] abundances for giants in the central regions (Cunha et al. 2007; Origlia et al. 2011; Johnson et al. 2014; Ryde et al. 2016). It can, however, be noted that they all follow a higher trend than that determined by Bensby et al. (2013). This might (but not necessarily) arise from greater errors ultimately attributable to the higher uncertainties based on the Ca determination based on the giant star spectra as compared with those based on dwarf spectra (see also the discussion in Gonzalez et al. 2011). Scrutinizing the Ca line used, using more Ca lines, comparing with detailed galactic chemical evolution models, and observing more stars will be needed to investigate and understand the true nature of the [Ca/Fe] trend. Our [Ti/Fe] determination also has a high uncertainty, mainly arising from the uncertainty in the effective temperature. The value is, however, consistent within errors with the other bulge stars too. Thus, within the uncertainties, the [α/Fe] we measure for GC10812 cannot be claimed to be different from the rest of the bulge.

The log g versus T_{eff} location of GC10812 is indicated in Figure 5 with a large asterisk. Superimposed are isochrones color-coded for different metallicities (Bressan et al. 2012). We

assume here an age of 10 Gyr. The red line shows the most metal-rich isochrone (+0.7 dex). Based on its apparent luminosity, its kinematic membership to one of the nuclear components, its low metallicity, our independent determination of its effective temperature and surface gravity, and its high α abundance, we are confident that GC10812 is consistent with being a low-mass, old red giant star in the vicinity of the nuclear cluster.

In the figure we also plot the locations for a sample of stars in the inner 3° from the Galactic center from Ryde & Schultheis (2015), Ryde et al. (2016), Schultheis et al. (2015), and Do et al. (2015). The typical uncertainties of temperatures are about ±150 K, while the errors in log g can be on the order of 0.3–0.5 dex as those were determined photometrically. We note that the isochrones predict too high temperatures, for a given surface gravity, for the most metal-rich stars (>0.5 dex). One should, however, be aware of the fact that everything at metallicity >+0.5 dex needs still to be understood: the metallicities themselves, model atmospheres, and isochrones are all very uncertain and mostly calibrated by extrapolation. Thus, it could be possible that the log g determination of the most metal-rich stars is ∼0.3–0.5 dex too high.

Whereas the M giants from Ryde & Schultheis (2015), Ryde et al. (2016), and Schultheis et al. (2015) are situated along the isochrone sequence in Figure 5, the location of the Do et al. (2015) stars is not compatible with the indicated location of the RGB branch from the PARSEC isochrones. These stars are plotted as triangles. As their extinction is typically that of stars in the Galactic center, we believe that their surface gravities are about two to three order of magnitudes too high. Also, the metal-poor stars discussed in Do et al. (2015) are orders of magnitude away from the expected isochrones.

The work of Do et al. (2015) obtained integral-field, moderate-resolution spectroscopy for scores of stars in the central cluster behind adaptive optics (AO). They did not claim to undertake a full high-resolution abundance analysis and were aware of potentially significant uncertainties in their methods. Their stated uncertainty in log g is 0.91 dex. The main effect of decreasing the surface gravity in a synthetic spectrum calculation is the decreased continuous opacity, which generally increases the line strengths. In the simultaneous fit of the stellar parameters by Do et al. (2015), the temperature and metallicity determinations might therefore also be affected by this large uncertainty. We agree with the assessment of Do et al. (2015) that additional observations at high spectral resolution would be required to confirm the low metallicities ([Fe/H] ∼ −1) claimed for the five stars in the nuclear cluster. Likewise, the high-metallicity stars found by Do et al. (2015), which have nominal metallicities up to [Fe/H] = +1.0 dex, need to be confirmed.

The similarity between GC10812 and the rest of the inner bulge would suggest a homogeneous star formation history in the entire bulge. There is a clear connection with the bulge and the Galactic center. Thus, our results argue for the Galactic center being in the context of the bulge over most of its history rather than very distinct.

7. CONCLUSIONS

In targeting the Milky Way nuclear star cluster we have observed the most metal-poor giant (GC10812) yet in the vicinity of the Galactic center. A careful analysis of its three-
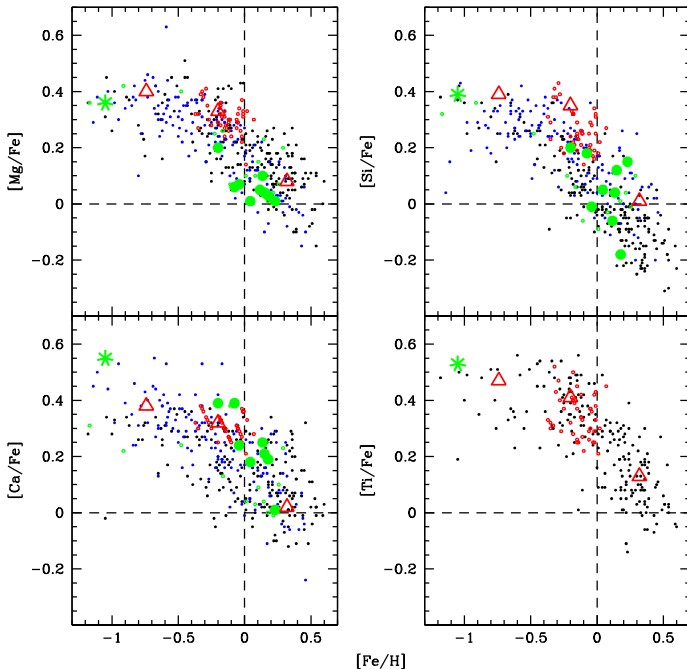
Figure 6. Abundance ratios of [Mg/Fe], [Si/Fe], [Ca/Fe], and [Ti/Fe] vs. [Fe/H] for GC10812 (big green star) and different samples of bulge and Galactic center giants: Gonzalez et al. (2011) (black dots), Johnson et al. (2014) (blue dots) in the outer bulge from optical spectroscopy, Rich et al. (2007, 2012) (red circles) and Ryde et al. (2016) (green circles) in low-latitude bulge fields, and Ryde & Schultheis (2015) (big green dots) in the Galactic center region from IR spectroscopy. The average abundance ratios of the three stellar populations of Terzan 5 from Origlia et al. (2011, 2013) (big red triangles) are also plotted for comparison. We have rescaled all the abundances to the same solar reference of Grevesse et al. (2007).

dimensional location locates it at 26^{+54}_{-16} pc in front of the Galactic center and at a projected distance of 1.5 pc to the northwest. This line-of-sight position and orbit integration make it unlikely that the star belongs in the most central component, the nuclear cluster. However, the orbit integration also shows that the star very likely does not leave the nuclear disk. Thus, the star very likely belongs to a nuclear component.

The metallicity and abundances are determined from a detailed abundance analysis based on $R = 24,000$ Keck/NIRSPEC spectra. The [Fe/H] = −1.05 ± 0.10 is the lowest measured and confirmed metallicity of a star from the nuclear components. It is unexpected and differs from earlier measurements. We can, however, still conclude that there is no evidence hitherto that there are metal-poor stars (e.g., originating in globular clusters inspiraling to the Galactic center; Tremaine et al. 1975; Capuzzo-Dolcetta & Miocchi 2008) in the nuclear star cluster. The [α/Fe]-element enhancement of ∼+0.4 follows the trend of the outer bulge.

GC10812 is by virtue of its 3D kinematics a likely member of the central disk/cluster system. It also exhibits the metal-poor, alpha-enhanced hallmarks of an old, metal-poor giant. The existence of an old population in the Galactic center has

been well established from the robust presence of a red clump population (Figer et al. 2004), as well as the analysis of star formation history by Pfuhl et al. (2011). It will be important going forward to explore the full abundance distribution of this old population, as well as that of the ∼10⁸ yr population responsible for the supergiants. Such studies will lay the foundation for applying models of chemical evolution to this very interesting region of the Milky Way.

We have demonstrated that K-band spectroscopy of individual giants at high spectral resolution offers a path forward enabling exploration of the chemistry of the central cluster. This has the potential to elucidate the system's star formation and enrichment history, as well as its relationship with the central 100 pc of the bulge/bar system.

7

REFERENCES

Ahn, C. P., Alexandroff, R., Allende Prieto, C., et al. 2014, ApJS, 211, 17
Anstee, S. D., & O'Mara, B. J. 1991, MNRAS, 253, 549
Baade, W. 1951, POMic, 10, 7
Barklem, P. S., & O'Mara, B. J. 1998, MNRAS, 300, 863
Bensby, T., Yee, J. C., Feltzing, S., et al. 2013, A&A, 549, A147
Bland-Hawthorn, J., & Gerhard, O. 2016, ARA&A, 54, 529
Blum, R. D., Ramírez, S. V., Sellgren, K., & Olsen, K. 2003, ApJ, 597, 323
Bonnet, H., Ströbele, S., Biancat-Marchet, F., et al. 2003, Proc. SPIE, 4839, 329
Bressan, A., Marigo, P., Girardi, L., et al. 2012, MNRAS, 427, 127
Bullock, J. S., & Johnston, K. V. 2005, ApJ, 635, 931
Capuzzo-Dolcetta, R., & Miocchi, P. 2008, ApJ, 681, 1136
Cardelli, J. A., Clayton, G. C., & Mathis, J. S. 1989, ApJ, 345, 245
Carr, J. S., Sellgren, K., & Balachandran, S. C. 2000, ApJ, 530, 307
Chatzopoulos, S., Fritz, T. K., Gerhard, O., et al. 2015a, MNRAS, 447, 948
Chatzopoulos, S., Gerhard, O., Fritz, T. K., et al. 2015b, MNRAS, 453, 939
Cunha, K., Sellgren, K., Smith, V. V., et al. 2007, ApJ, 669, 1011
Davies, B., Origlia, L., Kudritzki, R.-P., et al. 2009, ApJ, 694, 46
Do, T., Kerzendorf, W., Winsor, N., et al. 2015, arXiv:1506.07891
Eisenhauer, F., Abuter, R., Bickert, K., et al. 2003, Proc. SPIE, 4841, 1548
Figer, D. F., Rich, R. M., Kim, S. S., Morris, M., & Serabyn, E. 2004, ApJ, 601, 319
Fritz, T. K., Chatzopoulos, S., Gerhard, O., et al. 2016, ApJ, 821, 44
Fritz, T. K., Gillessen, S., Dodds-Eden, K., et al. 2011, ApJ, 737, 73
Fulbright, J. P., McWilliam, A., & Rich, R. M. 2006, ApJ, 636, 821
Gonzalez, O. A., Rejkuba, M., Zoccali, M., et al. 2011, A&A, 530, A54
Gonzalez, O. A., Zoccali, M., Vasquez, S., et al. 2015, A&A, 584, A46
Goorvitch, D. 1994, ApJS, 95, 535
Grevesse, N., Asplund, M., & Sauval, A. J. 2007, SSRv, 130, 105
Gustafsson, B., Edvardsson, B., Eriksson, K., et al. 2008, A&A, 486, 951
Hinkle, K., Wallace, L., & Livingston, W. C. 1995, Infrared Atlas of the Arcturus Spectrum, 0.9–5.3 microns (San Francisco, CA: ASP) (http://adsabs.harvard.edu/abs/1995iaas.book.....H)
Houdashelt, M. L., Bell, R. A., & Sweigart, A. V. 2000, AJ, 119, 1448
Howes, L. M., Casey, A. R., Asplund, M., et al. 2015, Natur, 527, 484
Johnson, C. I., Rich, R. M., Fulbright, J. P., Valenti, E., & McWilliam, A. 2011, ApJ, 732, 108
Johnson, C. I., Rich, R. M., Kobayashi, C., et al. 2013, ApJ, 765, 157
Johnson, C. I., Rich, R. M., Kobayashi, C., Kunder, A., & Koch, A. 2014, AJ, 148, 67
Jørgensen, U. G., & Larsson, M. 1990, A&A, 238, 424
Kim, S., Prato, L., & McLean, I. 2015, REDSPEC: NIRSPEC Data Reduction, Astrophysics Source Code Library, ascl:1507.017
Koch, A., McWilliam, A., Preston, G. W., & Thompson, I. B. 2016, A&A, 587, A124
Kupka, F., Piskunov, N., Ryabchikova, T. A., Stempels, H. C., & Weiss, W. W. 1999, A&AS, 138, 119
Kupka, F. G., Ryabchikova, T. A., Piskunov, N. E., Stempels, H. C., & Weiss, W. W. 2000, BaltA, 9, 590
Launhardt, R., Zylka, R., & Mezger, P. G. 2002, A&A, 384, 112
Lawrence, A., Warren, S. J., Almaini, O., et al. 2013, yCat, 2319, 0
Livingston, W., & Wallace, L. 1991, An Atlas of the Solar Spectrum in the Infrared from 1850 to 9000 cm^{-1} (1.1 to 5.4 micrometer), NSO Tech. Rep. (Tucson, AZ: National Solar Observatory, National Optical Astronomy Observatory) (http://adsabs.harvard.edu/abs/1991aass.book.....L)
Matsunaga, N., Kawadu, T., Nishiyama, S., et al. 2009, MNRAS, 399, 1709
McLean, I. S. 2005, in High Resolution Infrared Spectroscopy in Astronomy, ed. H. U. Käufl, R. Siebenmorgen, & A. F. M. Moorwood (Berlin: Springer), 25
Nassau, J. J., & Blanco, V. M. 1958, ApJ, 128, 46
Ness, M., & Freeman, K. 2016, PASA, 33, e022
Ness, M., Freeman, K., Athanassoula, E., et al. 2013, MNRAS, 430, 836
Nishiyama, S., Tamura, M., Hatano, H., et al. 2009, ApJ, 696, 1407
Omont, A., Ganesh, S., Alard, C., et al. 1999, A&A, 348, 755
Origlia, L., Massari, D., Rich, R. M., et al. 2013, ApJL, 779, L5
Origlia, L., Rich, R. M., Ferraro, F. R., et al. 2011, ApJL, 726, L20
Pehlivan, A., Nilsson, H., & Hartman, H. 2015, A&A, 582, A98
Pfuhl, O., Fritz, T. K., Zilka, M., et al. 2011, ApJ, 741, 108
Piskunov, N., & Valenti, J. A. 2016, arXiv:1606.06073
Piskunov, N. E., Kupka, F., Ryabchikova, T. A., Weiss, W. W., & Jeffery, C. S. 1995, A&AS, 112, 525
Ramírez, I., & Allende Prieto, C. 2011, ApJ, 743, 135
Ramírez, S. V., Depoy, D. L., Frogel, J. A., Sellgren, K., & Blum, R. D. 1997, AJ, 113, 1411
Ramírez, S. V., Sellgren, K., Carr, J. S., et al. 2000a, ApJ, 537, 205
Ramírez, S. V., Stephens, A. W., Frogel, J. A., & DePoy, D. L. 2000b, AJ, 120, 833
Rich, R. M. 1988, AJ, 95, 828
Rich, R. M., Origlia, L., & Valenti, E. 2007, ApJL, 665, L119
Rich, R. M., Origlia, L., & Valenti, E. 2012, ApJ, 746, 59
Ryabchikova, T., Piskunov, N., Kurucz, R. L., et al. 2015, PhyS, 90, 054005
Ryabchikova, T. A., Piskunov, N. E., Kupka, F., & Weiss, W. W. 1997, BaltA, 6, 244
Ryan, S. G., & Norris, J. E. 1991, AJ, 101, 1865
Ryde, N., & Schultheis, M. 2015, A&A, 573, A14
Ryde, N., Schultheis, M., Grieco, V., et al. 2016, AJ, 151, 1
Schödel, R., Feldmeier, A., Kunneriath, D., et al. 2014, A&A, 566, A47
Schödel, R., Najarro, F., Muzic, K., & Eckart, A. 2010, A&A, 511, A18
Schultheis, M., Chen, B. Q., Jiang, B. W., et al. 2014, A&A, 566, A120
Schultheis, M., Cunha, K., Zasowski, G., et al. 2015, A&A, 584, A45
Schultheis, M., Ryde, N., & Nandakumar, G. 2016, A&A, 590, 13
Sesar, B., Ivezić, Ž., Stuart, J. S., et al. 2013, AJ, 146, 21
Tiede, G. P., Frogel, J. A., & Terndrup, D. M. 1995, AJ, 110, 2788
Tody, D. 1993, in ASP Conf. Ser. 52: Astronomical Data Analysis Software and Systems II, ed. R. J. Hanisch, R. J. V. Brissenden, & J. Barnes (San Francisco, CA: ASP), 173
Tremaine, S. D., Ostriker, J. P., & Spitzer, L., Jr. 1975, ApJ, 196, 407
Tsuji, T. 2008, A&A, 489, 1271
Valenti, J. A., & Piskunov, N. 1996, A&AS, 118, 595
Valenti, J. A., & Piskunov, N. 2012, SME: Spectroscopy Made Easy, Astrophysics Source Code Library, ascl:1202.013
Xue, X.-X., Rix, H.-W., Ma, Z., et al. 2015, ApJ, 809, 144
Zoccali, M., Hill, V., Lecureur, A., et al. 2008, A&A, 486, 177

Paper II
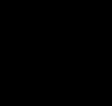
Detailed Abundances for the Old Population near the Galactic Center. I. Metallicity Distribution of the Nuclear Star Cluster

R. M. Rich[1] , N. Ryde[2] , B. Thorsbro[2], T. K. Fritz[3], M. Schultheis[4] , L. Origlia[5] , and H. Jönsson[2]

[1] Department of Physics and Astronomy, UCLA, 430 Portola Plaza, Box 951547, Los Angeles, CA 90095-1547, USA; rmr@astro.ucla.edu
[2] Lund Observatory, Department of Astronomy and Theoretical Physics, Lund University, Box 43, SE-221 00 Lund, Sweden
[3] Department of Astronomy, University of Virginia, 3530 McCormick Road, Charlottesville, VA 22904, USA
[4] Observatoire de la Côte d'Azur, CNRS UMR 7293, BP4229, Laboratoire Lagrange, F-06304 Nice Cedex 4, France
[5] INAF—Osservatorio Astronomico di Bologna, Via Gobetti 93/3, I-40129 Bologna, Italy

Abstract

We report the first high spectral resolution study of 17 M giants kinematically confirmed to lie within a few parsecs of the Galactic center, using $R \sim 24,000$ spectroscopy from Keck/NIRSPEC and a new line list for the infrared K band. We consider their luminosities and kinematics, which classify these stars as members of the older stellar population and the central cluster. We find a median metallicity of $\langle[\mathrm{Fe/H}]\rangle = -0.16$ and a large spread from approximately -0.3 to $+0.3$ (quartiles). We find that the highest metallicities are $[\mathrm{Fe/H}] < +0.6$, with most of the stars being at or below the solar iron abundance. The abundances and the abundance distribution strongly resemble those of the Galactic bulge rather than the disk or halo; in our small sample we find no statistical evidence for a dependence of velocity dispersion on metallicity.

Key words: Galaxy: center – stars: abundances – stars: late-type

1. Introduction

Only in recent years has it become feasible to explore the composition of stars that are members of the central cluster that occupies the inner parsec of the Milky Way. This region continues to be of great interest as most of its mass resides within the sphere of influence of the supermassive black hole Sgr A*. The stellar population surrounding this cluster is the bar/bulge system, which now has $\approx 10^4$ members with high resolution and high signal-to-noise ratio (S/N) optical/IR spectra. Nonetheless, one cannot assume that there is any connection between the central cluster and the bar/bulge population as a whole. While the bar/bulge population is dominated by an older stellar population (e.g., Kuijken & Rich 2002; Clarkson et al. 2008) the central cluster still has ongoing star formation (e.g., Paumard et al. 2006; Feldmeier-Krause et al. 2015). Also, microlensing studies (e.g., Bensby et al. 2013, 2017) argue for the presence of a metal-rich, intermediate-age population in the bulge. Separated from the bar/bulge by its dense structure and kinematics, its potential well defined by both Sgr A* and the stellar cluster, the central cluster might well be expected to have experienced a different and unique history of chemical evolution, leaving its own imprint of chemical abundances. This is especially true because of the presence of Sgr A*, the evidence for a complex star formation history (Pfuhl et al. 2011) suggesting cross-pollination with gas from the disk and inner bulge regions. Of additional interest is the possibility of gaining insight into the early chemical evolution of this special environment. The presence of stars older than 1 Gyr (and likely 8–10 Gyr old) within 50 pc of the Galactic center has been established since Figer et al. (2004) clearly detected the red clump, and the discovery of RR Lyrae variables near Sgr A* (Dong et al. 2017) argues for at least a significant fraction of the central cluster being globular cluster age, i.e., ~10 Gyr old. The expected compositions at this Galactic crossroads might be alpha-enhanced from an early starburst, or more toward scaled solar, reflecting the extended star formation history of this region. The reality is that we will probably find representatives of both ancient and relatively recent star formation; more complete inferences must await larger samples with analyses of additional elements.

Spectroscopy in the central parsec has focused on either the brightest stars, that are likely supergiants, or on fainter red giants that are likely to be dominated in number by the ~10 Gyr old population because lifetimes of those stars on the red giant branch are longer. Early studies emphasized the brighter red supergiants, with all stars $K < 9.5$ and $M_{bol} < -5$, with the best results from IRS7, the most luminous red supergiant (Ramírez et al. 2000; Cunha et al. 2007). These studies found a solar iron abundance with alpha enhancement for this population. High-resolution spectroscopy of nine fainter red giants by Ryde & Schultheis (2015) find a suprasolar distribution in [Fe/H] but otherwise normal [α/Fe].

Medium-resolution spectroscopy has enabled adaptive optics (AO)-assisted (Do et al. 2015) and wider field (Feldmeier-Krause et al. 2017) studies of fainter red giants in the inner parsec (Do et al. 2015) or near the Galactic center, at spectral resolutions of ~4000–5000. The medium-resolution studies have found evidence for a metal-poor population that comprises roughly 10% of the stellar population. The metal-poor, alpha-enhanced nature of one kinematically confirmed Galactic center red giant has been determined by our team using high-resolution spectroscopy (Ryde et al. 2016a), but the metallicity distribution of the metal-rich stellar component in the Galactic center remains a subject of debate. Rich et al. (2012) examined high-resolution ($R = 23,000$) H-band spectra of 58 red giants ranging from 140 to 400 pc from the nucleus, finding no abundance gradient and $\langle[\mathrm{Fe/H}]\rangle = -0.2$. The AO-aided investigation of the central parsec by Do et al. (2015) found the majority of stars with suprasolar metallicities, including one star with $[\mathrm{Fe/H}] = +0.96$. Feldmeier-Krause et al. (2017) used a Bayesian approach to derive stellar parameters and abundances similar to those of Do et al. (2015) and found $\langle[\mathrm{Fe/H}]\rangle = +0.26$ with stars reaching nearly 10 times solar as well. While the inferred surface gravities of

1

Table 1
Stellar Coordinates, Position, and Exposure Times

Star	Observation Date	R.A. (h:m:s)	Decl. (d:m:s)	(l, b) (°, °)	Exposure Time (s)
GC 10812	2015 Apr 27	17:45:37.229	−29:00:16.62	(359.942, −0.036)	1200
GC 11473	2015 Apr 27	17:45:42.642	−29:00:10.23	(359.953, −0.052)	1600
GC 13282	2015 Apr 27	17:45:39.492	−28:59:58.74	(359.950, −0.040)	960
GC 14024	2015 Apr 27	17:45:42.026	−28:59:54.97	(359.956, −0.047)	960
GC 16887	2015 Apr 27	17:45:44.041	−28:59:27.66	(359.966, −0.050)	2000
GC 6227	2015 Apr 27	17:45:38.855	−29:01:08.71	(359.932, −0.048)	2000
GC 7688	2015 Apr 27	17:45:42.173	−29:00:54.99	(359.942, −0.057)	960
GC 15540	2015 Apr 28	17:45:41.931	−28:59:23.39	(359.963, −0.043)	500
GC 10195	2016 Apr 18	17:45:43.103	−29:00:25.45	(359.951, −0.055)	2000
GC 11532	2016 Apr 18	17:45:42.898	−29:00:09.60	(359.954, −0.052)	2000
GC 13882	2016 Apr 18	17:45:38.701	−28:59:55.15	(359.949, −0.037)	3000
GC 14724	2016 Apr 18	17:45:37.310	−28:59:49.43	(359.948, −0.032)	2000
GC 16763	2016 Apr 18	17:45:37.288	−29:01:12.67	(359.928, −0.044)	2000
GC 7104	2016 Apr 19	17:45:38.943	−29:00:58.44	(359.935, −0.047)	2000
GC 11025	2016 Apr 19	17:45:37.126	−29:00:14.39	(359.942, −0.035)	2000
GC 16867	2016 Apr 19	17:45:36.021	−29:00:09.20	(359.941, −0.031)	2000
GC 16895	2016 Apr 19	17:45:35.640	−29:00:47.00	(359.931, −0.035)	2000
GC 8631	2016 Apr 19	17:45:43.016	−29:00:46.02	(359.946, −0.058)	3000

Do et al. (2015) were of concern, sometimes reaching $\log g \approx 4$ for red giants, those of Feldmeier-Krause et al. (2017) are more in line with stellar parameters expected for an old stellar population at 8 kpc. Nonetheless, it is a truly daunting task to undertake abundance analysis including derivation of stellar parameters, for relatively low S/N spectra at $R \sim 4$–5000, especially for metal-rich, cool stars. The ubiquitous blending and lack of continuum points legitimately raise the question as to whether any analysis at such low resolution is even possible. When strong lines can be identified in the spectra, they are certain to be so strongly saturated and blended that no trustworthy derivation of abundance by traditional means is possible. In general, abundance determinations at different resolutions are a complex interplay of accuracy, metallicity, effective temperature, spectral band and coverage, as well as S/N.

The need to establish the metallicity distribution with precision has heightened as new studies of the Galactic center question the origin of the population. Minniti et al. (2016) report RR Lyrae in the "nuclear" bulge region, within 1° of the Galactic center. They propose that the presence of RR Lyrae imply that the nucleus was built from the debris of globular clusters and therefore from an old metal-poor population. The confirmation of RR Lyrae near Sgr A* potentially extends Minniti's model of globular cluster accretion to the nucleus itself; our measurement of the abundance distribution can test this hypothesis.

Here we report [Fe/H] for giants in the Galactic center from high-resolution ($R \sim 24000$) spectra in the 2.4 μm K band, obtained using NIRSPEC at the W.M. Keck Observatory. We have spectra covering most of the K band for stars with $12 < K < 10.5$. We have analyzed our spectra using a high-resolution detailed abundance analysis, with the benefit of a new linelist (B. Thorsbro et al. 2018, in preparation). The current paper is the first in a series, in which forthcoming papers will deal with specific elemental abundances, such as those of the α elements and that of Sc, and V, as well as comparative studies to other bulge fields.

2. Observations

We have obtained high-resolution ($R \sim 24,000$) infrared K-band spectra for 18 M-giants belonging to the Nuclear Star Cluster (NSC) of the Milky Way, using NIRSPEC (McLean et al. 1998; McLean 2005) at Keck II. The observations were made during four half-nights on 2015 April 27–28 and 2016 April 18–19. In Table 1 their coordinates and total exposure times are given. The Galactic coordinates in the table are seemingly offset from Sgr A*, because the center of the Galactic coordinate system was defined in 1958 (Blaauw et al. 1960) and is offset relative to the actual center. Instead of using (l, b) one can use $(l*, b*)$, where the center is shifted to Sgr A*; see e.g., Fritz et al. (2016).

In Figure 1 the stars are shown on a UKIDSS finding chart (Lawrence et al. 2013), with all of them lying within 90″ angular distance from the Galactic center. This corresponds to a projected galactocentric distance of $R_c < 3.6$ pc, adopting the distance to the Galactic center of 8.3 kpc (Chatzopoulos et al. 2015a; Bland-Hawthorn & Gerhard 2016). The stellar population of the NSC has a half-light radius of approximately 3′ (Fritz et al. 2016), exceeding by a factor of two the image shown in Figure 1.

Our stars were selected from a sample of Galactic center giants observed at low spectral resolution ($R = 4000$ or $R = 1500$) with the integral field spectrometer SINFONI (Bonnet et al. 2003; Eisenhauer et al. 2003) on the VLT.[6] We chose candidates with measurable CO bandheads in order to derive the stellar temperature, excluding candidates with neighbors too close for seeing-limited spectroscopy. The orange circle in Figure 1 shows a circle of a radius of 30″, enclosing a region excluded from targeting due to extreme crowding. We also used the catalogs of Blum et al. (2003) and Matsunaga et al. (2009) to exclude some known AGB/LPV stars like Miras, and known red supergiants. The aim of this sample is to collect a relatively unbiased, large sample of old Galactic center stars, which can be used in our studies of the

---

[6] The SINFONI spectra are from the programs 077.B-0503, 183.B-0100 and 087.B-0117.
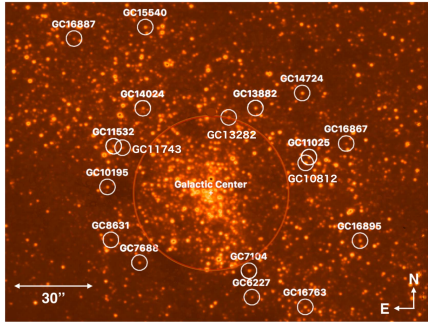
Figure 1. UKIDSS finding chart of the Galactic center region (Lawrence et al. 2013). The image captures the inner part of the Nuclear Star Cluster, which has a diameter of 6′. Our target stars are marked with white circles and are summarized in Table 1. The orange circle surrounding the Galactic center denotes an angular radius of 30″ and marks the region where we have avoided stars due to problems with crowding in seeing-limited observations. 30″ corresponds to a projected galactocentric distance of $R_c = 1.2$ pc, adopting the distance to the Galactic center of 8.3 kpc (Chatzopoulos et al. 2015a; Bland-Hawthorn & Gerhard 2016). The white cross marks the location of the Galactic center.

Figure 2. K_s magnitude vs. $H - K_s$ color for stars toward the NSC. Our target stars are marked with colored dots scaled with metallicity. The extinction vector is shown with the arrow. The most metal-poor star is the same as in Ryde et al. (2016b).

metallicity distribution. Since we have to avoid very cool stars ($T < 3300$ K) due to the difficulty of analyzing such stars, we might be slightly underestimating the mean metallicity, since these cool giants would sample the more metal-rich end. Our final sample should be relatively unbiased in color, covering the full $H - K_s$ range, see Figure 2. It is also encouraging that the metallicity distribution is not very sensitive to the selection function, as shown by Nandakumar et al. (2017) when investigating its influence on different spectroscopic surveys, such as APOGEE, *Gaia*-ESO, Lamost, and Rave. In order to avoid an additional layer of complexity in target selection, we did not add proper motion as an additional constraint. Table 2 gives the absolute K magnitude (M_K[7], with uncertainties of ~0.09, except δM_K[GC 7688] ~ 0.8), apparent K_s magnitudes (with uncertainties of ~0.05), and $H - K_s$ colors (with uncertainties of ~0.08). NIRSPEC spectra of giants in the K band as faint as $K_s < 12$ are possible to acquire with the Keck telescope, for reasonable exposure times (see Table 1).

Using the $0\rlap{.}''432 \times 12''$ slit and the NIRSPEC-7 filter, a spectral resolution of $R \sim 24{,}000$ was achieved. The analyzed spectra cover the wavelength region from 21,100 to 24,000 Å, distributed over five spectral orders with gaps in between, see Figure 3. To achieve proper background and dark subtraction, we observed with an ABBA scheme with a nod throw of 6″ along the slit. Total exposure times were in the range 960–3000 s.

The data were reduced with the NIRSPEC software red-spec (Kim et al. 2015) providing final 1D wavelength-calibrated spectra. Special care was taken to ensure the tracing of the correct target star on the slit, since several stars were inevitably observed at the same time in these crowded fields. IRAF (Tody 1993) was subsequently used to normalize the
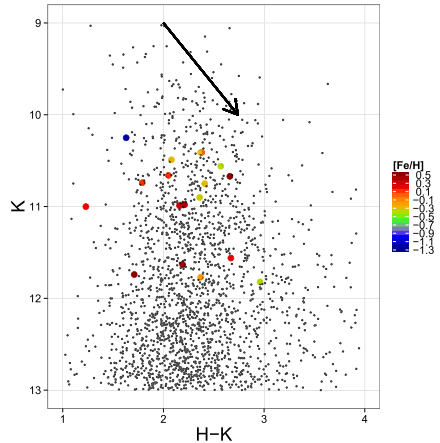
continuum, eliminate obvious cosmic ray hits, and correct for telluric lines. For the last, we observed a few bright telluric standard stars using the same setup as the target stars, twice per night. The star finally chosen for the telluric line division was the rapidly rotating O6.5V star HIP 89584, a star with a K magnitude of 7.3 and a $v(\sin i) \sim 140$ km s^{-1} (Simón-Díaz & Herrero 2014). The broad Brackett $n = 4$–7 hydrogen line at 21655 Å was smoothed out and rectified. The telluric star spectrum, observed to be used for the final night's targets, had to be filtered for a fringing pattern, using standard tools in redspec.

Since the telluric absorption spectrum consists of different molecular species, and their scaling to the time of observations is not always the same for all species, a final check of the performance of the telluric line reduction was done by overplotting the telluric spectrum on the target. This is important in order to explain possible spurious features arising from the reduction. Also, knowledge of whether a telluric line affects the Fe lines under study is crucial. Special care was also taken, if needed, to eliminate the portions of the spectrum where the sky emission lines of OH were present, as they cannot always be corrected.

In order to benchmark the performance of our analysis method (see Section 3), we have also analyzed the KPNO high-resolution spectrum of the metal-poor giant α Boo (Arcturus Hinkle et al. 1995), with the fundamental parameters $T_{\rm eff} = 4286$ K, $\log g = 1.64$, [Fe/H] $= -0.57$, and $\xi_{\rm micro} = 1.58$ km s^{-1} (Jönsson et al. 2017).

3. Analysis

In this first paper of the series, we investigate the Fe abundances of stars in the NSC, in order to measure its metallicity distribution. In forthcoming papers, we will also investigate other elements; most significantly we will

---

[7] These are based on the apparent K_s magnitudes, derived metallicities, and 10 Gyr isochrones (Bressan et al. 2012). The uncertainty of GC 7688, which is a foreground star (see Section 5.2), is larger due to the uncertainty in distance (1σ range from 4 to 8.3 kpc).

3

Table 2
Stellar Photometry and Parameters

Star	M_K	K_S	$H - K_S$	T_{eff} (K)	Photometry			Isochrones			ξ_{mac} (km s^{-1})
					$\log g$ (dex)	[Fe/H] (dex)	ξ_{mic} (km s^{-1})	$\log g$ (dex)	[Fe/H] (dex)	ξ_{mic} (km s^{-1})	
GC 10812	−6.38	10.25	1.63	3800	0.47	−1.18	2.4	0.34	−1.15	2.5	14.0
GC 11473	−4.81	11.74	1.71	3550	0.97	+0.48	2.1	1.13	+0.64	2.0	12.0
GC 13282	−6.24	10.99	2.16	3700	0.45	−0.11	2.4	0.97	−0.05	2.1	14.0
GC 14024	−6.13	10.98	2.21	3650	0.42	+0.02	2.4	1.23	+0.42	2.0	14.0
GC 16887	−5.52	11.63	2.19	3500	0.67	+0.24	2.3	0.96	+0.41	2.1	13.0
GC 6227	−6.43	11.82	2.96	3800	0.75	−0.64	2.2	0.95	−0.38	2.1	14.0
GC 7688	−4.34	11.00	1.23	4150	1.02	−0.26	2.1	1.78	−0.08	1.8	13.5
GC 15540	−6.46	10.49	2.08	3600	0.28	−0.19	2.5	0.72	−0.16	2.2	14.0
GC 10195	−7.15	10.67	2.66	3500	0.19	−0.03	2.6	0.68	+0.04	2.3	13.0
GC 11532	−6.59	10.90	2.36	3500	0.29	−0.47	2.5	0.35	−0.56	2.5	14.0
GC 13882	−7.02	10.41	2.37	3300	0.15	−0.31	2.6	0.15	−0.31	2.6	15.5
GC 14724	−7.18	10.56	2.57	3600	0.16	−0.44	2.6	0.55	−0.49	2.3	14.0
GC 16763	−6.35	10.66	2.05	3600	0.29	−0.23	2.5	0.65	−0.29	2.3	14.0
GC 7104	−5.96	10.74	1.79	3750	0.53	−0.31	2.4	0.92	−0.28	2.1	14.0
GC 11025	−6.88	10.41	2.38	3400	0.21	+0.34	2.6	0.69	+0.27	2.3	14.3
GC 16867	−5.73	11.77	2.37	3650	0.66	−0.33	2.3	0.74	−0.29	2.2	13.0
GC 16895	−6.69	10.75	2.41	3450	0.23	−0.16	2.6	0.51	−0.10	2.4	14.0
GC 8631	−6.18	11.56	2.67	3900	0.61	+0.18	2.3	1.63	+0.36	1.9	13.5
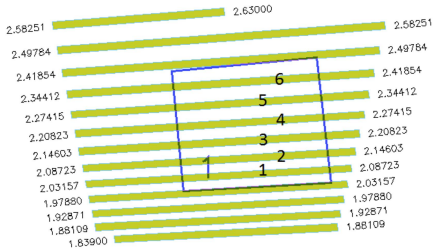
Figure 3. Outline of the spectral orders is shown by yellow bands. The detector array is marked with the blue square, which shows the spectral coverage obtained with the NIRSPEC settings used during our observations. The six spectral orders captured by the array are marked. Only orders 2–5 were used in our analysis.

Table 3
Stellar Kinematics

Star	v_{rad}^{LSR} (km s^{-1})	μ_l (mas yr^{-1})	μ_b (mas yr^{-1})	r ($''$)
GC 10812	−44	2.31 ± 0.27	−3.12 ± 0.27	39
GC 11473	206			39
GC 13282	128	−2.85 ± 1.95	−2.12 ± 1.95	30
GC 14024	−16	2.08 ± 0.21	1.90 ± 0.21	42
GC 16887	60			80
GC 6227	−102	−2.83 ± 0.58	1.02 ± 0.58	43
GC 7688	−22	0.40 ± 0.71	0.85 ± 0.71	38
GC 15540	−54	−2.07 ± 0.09	0.27 ± 0.09	69
GC 10195	63	0.44 ± 0.70	0.75 ± 0.70	40
GC 11532	−28	2.08 ± 0.74	1.18 ± 0.74	42
GC 13882	195	−1.66 ± 0.81	−1.78 ± 0.81	37
GC 14724	−3	−3.46 ± 0.82	1.13 ± 0.82	53
GC 16763	−44			57
GC 7104	−58	1.76 ± 0.23	0.19 ± 0.23	34
GC 11025	67	⋯	⋯	41
GC 16867	38	⋯	⋯	56
GC 16895	−95	⋯	⋯	61
GC 8631	−20	⋯	⋯	43

investigate the diagnostically important α-element abundance trends with metallicity. Several α elements are represented in the wavelength region we have observed (namely Mg, Si, Ca, and Ti). However, with respect to the number of lines, line strengths, and available non-local thermodynamic equilibrium (LTE) corrections, our ongoing work indicates that the Si abundance is the best proxy for the general α-element trends. The other elements might be more challenging. Furthermore, the very strong Sc lines detected in our stars are of great interest to investigate whether or not their strengths actually reflect a higher-than-normal Sc abundance. These issues will be addressed in forthcoming papers in the series.

In all our investigations, we have analyzed (and will analyze) our red-giant spectra with tailored synthetic spectra, based on spherical model atmospheres. Due to the extreme extinction and its patchy nature toward the Galactic center, the effective temperatures and surface gravities cannot be determined photometrically without unacceptably high uncertainty. Therefore, we have to resort to other methods, described in the following subsections. With the stellar parameters determined,

we determine the metallicity from seven individual Fe lines in the K band, by minimizing the χ^2 between the observed and synthetic spectra.

3.1. Stellar Dynamics

The angular distance from Sgr* and the LSR radial velocities (v_{rad}^{LSR}) of all our stars are listed in Table 3. We also provide proper motions (μ_l and μ_b) for those stars for which we were able to retrieve proper motions (see the discussion in Section 5.2).

3.2. Spectral Synthesis

The main input for tailoring the synthetic spectra are the stellar parameters and an accurate line list, in this case of Fe lines. The accurate determination of the stellar parameters of

the target stars is of large importance for the final result and its uncertainties. The four fundamental parameters (or stellar parameters) are the effective temperature ($T_{\rm eff}$), surface gravity (log g), metallicity ([Fe/H]), and microturbulence ($\xi_{\rm mic}$). Occasionally, [α/Fe] (especially [Mg/Fe]) is also considered a fundamental parameter, due to its influence on the continuous opacity. In the following subsections we will discuss these parameters and the line list we use, before discussing the abundance determination itself.

3.2.1. Effective Temperatures

The effective temperatures, $T_{\rm eff}$, of the target stars, are determined by integrating the strength of the 2.3 μm ($v = 2{-}0$) CO band in the integral field SINFONI spectra (at spectral resolution of $R = 4000$ and $R = 1500$) and using the relation between the CO-band strength and the $T_{\rm eff}$ given in Schultheis et al. (2016). These authors have shown that this relation works very well in the temperature and metallicity ranges we are interested in. It is valid between 3200 and 4500 K and $-1.2 <$ [Fe/H] < 0.5, with a typical dispersion of about 150 K. Indeed, we find no correlation between $T_{\rm eff}$ and [Fe/H]. Our derived effective temperatures are given in the fifth column of Table 2.

3.2.2. Surface Gravities

The surface gravity, log g, is important to set the pressure structure of the model atmospheres. Also, in the calculation of the synthetic spectra, the continuous opacity as well as the ionization states of atoms are sensitive to it. There are several methods that can be applied to determine the surface gravity for giants. Unfortunately, these usually require high-resolution optical spectra and employ the ionization balance between Fe I and Fe II lines or the strengths of pressure-broadened wings of strong lines; these are not available for the K band.

Instead, we initially constrain the surface gravities photometrically. Since we assume that our target stars are members of the NSC (see Section 5.2), the distance is in principle very well determined. The distances can otherwise be a large source of uncertainty for photometrically determined log g (see for example Schultheis et al. 2017). On the other hand, the interstellar extinction toward the Galactic center region is both high and variable (Schödel et al. 2015) which plagues the photometric log g determination, overwhelming the other uncertainties in the stellar masses, bolometric corrections, and effective temperatures. We determined the extinction, star by star, using the $H - K$ color excess and assuming an intrinsic $(H - K)_0 = 0.18$. The color excess $E(H - K)$ was converted to A_K using the extinction law of Fritz et al. (2011) with $A_K = 1.351 \times E(H - K)$. However, as shown in Schultheis et al. (2014), this method overestimates the extinction for high A_K values and also shows some dependence on stellar parameters such as $T_{\rm eff}$, log g, and [Fe/H]. A rough estimate of a general uncertainty in the photometric log g is $\sim$0.3 dex, taking into account the uncertainties in the extinction determination as well as in the extinction law. The uncertainties could, however, easily exceed that value due to the large uncertainties in the extinction, A_K. The gravities determined photometrically are given in the sixth column of Table 2.

These photometric gravities and the spectroscopically determined effective temperatures of our target stars are plotted in the H-R diagram in Figure 4 as crosses, color-coded with the
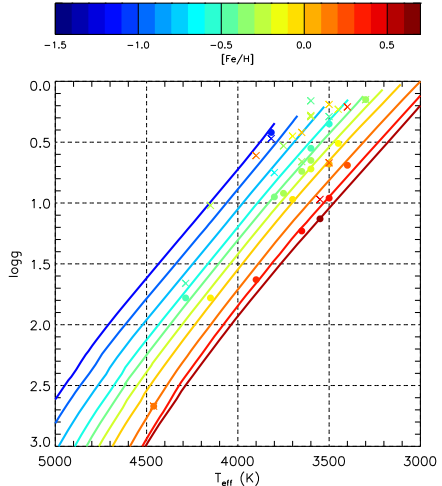

Figure 4. H-R diagram Yonsei–Yale isochrones (Demarque et al. 2004) with an appropriate [α/Fe] enhancement for metal-poor stars. The metallicities of the isochrones are from [Fe/H] = -1.2 to 0.6, in steps of 0.2 dex. The log g of the stars are determined given the $T_{\rm eff}$ determined from low-resolution spectra and the metallicity from the high-resolution spectra, assuming an old age of 3–10 Gyr. The two warmest giants are the standard stars α Boo (Arcturus) and μ Leo.

metallicities we derive for these stellar parameters (see Section 3.3 for details). Since calculated isochrones tell us that not all combinations of $T_{\rm eff}$, log g, and [Fe/H] are possible, we have also plotted Yonsei–Yale 10 Gyr isochrones (Demarque et al. 2004) appropriate for bulge stars in the figure. This will show where our stars with given $T_{\rm eff}$ are expected to lie, for given metallicities. Our photometrically determined log g do not obviously fall on the corresponding isochrones. Some stars are off by as much as a factor of 10, which corresponds to overestimating the extinction by $A_K \sim 0.8$ mag, an acceptable error in this region. Since the uncertainties are expected to be large and spurious, we have also resorted to another method for determining the surface gravities of our target stars, using the information buried in the isochrones.

Assuming that our Galactic center stars are all older than at least $\sim$5 Gyr (Blum et al. 2003; Clarkson et al. 2008; Pfuhl et al. 2011) and thanks to the fact that isochrones for stars of ages 5–13 Gyr are quite insensitive to the age on the giant branch, we can constrain the surface gravities, given a derived $T_{\rm eff}$ from our low-resolution spectra and [Fe/H] from our high-resolution spectra. This is done in an iterative manner, in the sense that log g is assumed when determining a first guess of the metallicity. The star is then plotted in an H-R diagram and if the star falls far away from the isochrone with the relevant metallicity, log g is changed accordingly, and a new iteration is made. We have interpolated in a grid of Yonsei–Yale isochrones for giants of 10 Gyr (Demarque et al. 2004). The isochrones are α enhanced, such that [α/Fe] = 0.3 for [Fe/H] < -0.5, and for higher metallicities the [α/Fe] linearly decreases with metallicity up to solar metallicity, above which
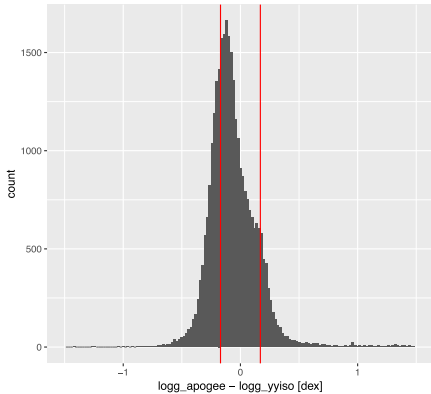
Figure 5. Histogram of the difference between $\log g$ determined by the APOGEE consortium for 30,000 giant stars in the APOGEE DR13 sample and $\log g$ determined by our isochrone-fitting method. The vertical lines represent the $\pm 2\sigma$ interval using the uncertainties reported by APOGEE, with $\sigma = 0.08$.

Figure 6. Difference between the determination of $\log g$ by the APOGEE consortium for 30,000 giants and that by our isochrone-fitting method plotted vs. APOGEE's $\log g$. The red line is the 0.50 quantile for the data.

it is zero. For a given set of $(T_{eff}, [Fe/H])$ we can then get the corresponding $\log g$ by interpolating in the grid. These isochrones are shown in Figure 4, where we also have color-coded them with their metallicities.

The $\log g$ determination is quite sensitive to the location in the H-R diagram. If a star has a determined metallicity which is, for example, too low compared to its location on the isochrone, $\log g$ has to be lowered for a given temperature. Decreasing the surface gravity will tend to decrease the pressures, including the electron pressure in the atmospheres, which leads, in general, to stronger lines, since the continuous opacity decreases. The metallicity determined from the observed spectra for a lower $\log g$ will therefore decrease even more. After a few iterations a consistent set of T_{eff}, $\log g$, and $[Fe/H]$ (given an age of 5–13 Gyr) can be found.

We have tested this purely spectroscopic method on 30,000 giant stars from the DR13 APOGEE sample (Majewski et al. 2017). Using the effective temperatures and metallicities derived by APOGEE, we determine the surface gravities through our isochrone-fitting method (assuming 10 Gyr isochrones) and compare these to those derived by APOGEE. No independently derived distances are required to apply this method. We find a median difference of -0.1 ± 0.1 dex between $\log g$ determined by APOGEE and predicted by our isochrone-fitting method, see Figure 5. APOGEE reports a general uncertainty of 0.08 for all of their $\log g$ determinations, as plotted in Figure 5; consequently the derived differences cannot be significant. In the histogram, there is a shoulder or maybe a bi-modality. This might, however, be expected since among the APOGEE stars in the solar neighborhood there are also young stars, whereas our method assumes an old age. Allowing for younger isochrones, our isochrone-determined $\log g$ would decrease by as much as 0.15 dex. Although we do not have any information on the ages of the APOGEE stars, we might assume that the large peak in the bi-modality in Figure 5 is the young, thin disk. If correct, using young isochrones would move that peak to the right, resulting in a more uniform
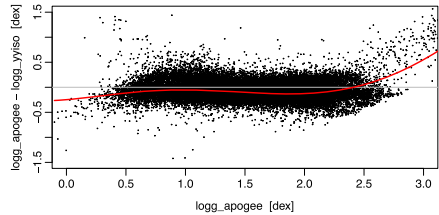
distribution. In Figure 6 we plot this difference versus $\log g$ to show that there is no trend with $\log g$.

In Jönsson et al. (2017) carefully and spectroscopically determined stellar parameters of K giants are compared to the Bressan et al. (2012) isochrones for different ages. The overall agreement is excellent, which again is very reassuring for our method. Comparing the Yonsei–Yale isochrones (Demarque et al. 2004) to those of Bressan et al. (2012), we find an agreement of better than 0.1 dex for the full metallicity range for our type of giants.

The final surface gravities derived from isochrones are given in the ninth column of Table 2. Our stars are also plotted in an H-R diagram in Figure 4 as large dots, color-coded with their metallicities derived in Section 3.3.

3.2.3. Microturbulence

The microturbulence, ξ_{micro}, is introduced in stellar atmosphere modeling and spectral synthesis in order to capture non-thermal motions in the stellar atmosphere, which occur on scales smaller than a mean-free path of the photons, and therefore affects the line formation process and the radiative transfer, analogously to thermal motions (see e.g., Gray 2005). Only the equivalent widths of strong lines are affected by microturbulence, which is why it can observationally be set by the requirement that the abundances determined from, for example, Fe lines of a large range of line strengths, produce no trend. Since there are not enough Fe line of different strengths in our spectra, we have used a relation with $\log g$ based on ξ_{micro} values derived from analysing spectra of five red giant stars ($0.5 < \log g < 2.5$) in this way by Smith et al. (2013), in which we interpolate. The lines we use for the metallicity determination are affected by the microturbulence. Our estimated microturbulences are given in the eighth and eleventh columns of Table 2, for $\log g$ photometrically determined, and fitted from isochrones, respectively.

3.2.4. α-element Over-abundance

Since the line strengths will depend on the number density of free electrons in the stellar atmosphere, the Mg abundance in particular might be important. We have assumed a general α-element enhancement typical for bulge giants such that for metallicities lower than $[Fe/H] = -0.5$ the overabundance of the α elements is $[\alpha/Fe] = 0.3$. For higher metallicities up to solar, the $[\alpha/Fe]$ linearly decreases with metallicity. Above solar it is assumed to be zero.

6

Table 4
Fe Line List

Wavelength in air, λ_{air} (Å)	E_{exc} (eV)	$\log gf$ (dex)
21779.651	3.640	−4.30
21894.983	6.145	−0.14
22380.835	5.033	−0.41
22392.915	5.100	−1.21
22419.976	6.218	−0.23
22473.263	6.119	+0.48
22619.873	4.991	−0.36

3.2.5. Line List

The Fe lines used are taken from a carefully compiled and tested line list for use in the K band (B. Thorsbro et al. 2018, in preparation). This atomic line list is based on an extraction from the VALD3 database (Piskunov et al. 1995; Ryabchikova et al. 1997, 2015; Kupka et al. 1999, 2000). Wavelengths and line-strengths (astrophysical $\log gf$-values) are updated using the solar center intensity atlas (Livingston & Wallace 1991). We have also made use of recent laboratory measurements of atomic line strengths of Mg, and Sc (Pehlivan Rhodin et al. 2015; Pehlivan Rhodin et al. 2017), as well as of Si (A. Pehlivan Rhodin et al. 2018, in preparation) in the K band. Of approximately 700 identified, interesting spectral lines for cool stars, about 570 lines have been assigned new values. A subset of Fe lines from this line list, used in the present investigation, is given in Table 4.

We also observed ten benchmark stars of similar stellar parameters in the same fashion as our target stars, in order to test the performance of this line list. We find an excellent agreement, to within 0.05 dex, between the abundances we determined with this list and the reference values for these stars. In the abundance analysis, we also include molecular line lists of CN (Sneden et al. 2014).

3.3. Abundance Determination

In the spectral synthesis, the radiative transfer and line formation is calculated for a given model atmosphere defined by the fundamental stellar parameters. We have chosen to use the code Spectroscopy Made Easy, SME (Valenti & Piskunov 1996, 2012) for this. SME uses a grid of model atmospheres in which the code interpolates for a given set of fundamental parameters of the analyzed star. We use one-dimensional (1D) MARCS models, which are hydrostatic model photospheres in spherical geometry, computed assuming LTE, chemical equilibrium, homogeneity, and conservation of the total flux (radiative plus convective, the convective flux being computed using the mixing-length recipe) (Gustafsson et al. 2008). The program then iteratively synthesizes spectra, calculated in spherical symmetry, for the searched abundances, under a scheme to minimize the χ^2 when comparing with the observed spectra. The spectral lines, which are used for the abundance analysis, are marked with masks in the pre-normalized observed spectra.

As in all spectral analyses, it is the contrast between the continuum and line depth that provides the abundance. Therefore, the continuum in the observed spectrum has to be well defined. The observed continuum levels depend on the S/N of the spectra and possible residuals from the telluric line

reduction. Therefore, special care needs to be taken to scrutinize and to define local continua around the spectral lines used for the abundance determination. Furthermore, the continuous opacity in the spectral synthesis has to be correct. In the atmosphere of a cool star, the continuous opacity is due to H^- free–free opacity, which is affected by the electron density. The abundances of the species that are the major electron donors in the continuum-forming regions need to be determined as well. For a typical star in our sample, the major electron donors are magnesium (1/2 of all electrons), iron (1/3 of electrons), and silicon (1/10); this is why the α-element abundance is important as an input parameter.

Due to the way SME works, by minimizing the χ^2 when comparing observed spectra with synthesized spectra at every sampling point, the line profiles need to be accurately characterized and the broadening of the line must be well determined. At the resolution of the instrument, the broadening is mainly due to the spectrometer's resolution, which we can determine from narrow, unsaturated telluric lines to be $R \sim 24,000$. The intrinsic broadening of the stellar lines is, however, also important. Of the stellar-line broadening mechanisms, the macroturbulence ($\xi_{macro}^{stellar}$), due to large-scale motions in the stellar atmosphere which reshape the lines, is unknown but can be determined by fitting stellar lines. The total Gaussian broadening needed to broaden the synthetic lines (ξ_{macro}^{total}), which includes the instrumental profile, is estimated from well-formed, medium-strong lines. The final values are given in Table 2 as ξ_{macro} for short.

Molecular lines are ubiquitous in spectra of cool stars of the type we are investigating. CN is the most dominant molecule apart from the CO bandhead region. We have fitted these lines in order to fit the overall spectrum but also to take care of possible minor blends in the Fe lines.

Assumptions that LTE is valid are made when synthesizing the spectra of Fe lines. Bergemann et al. (2012) show that this is a good approximation for cool, low-gravity stars, where the photoionization, which is the main cause for departure of LTE, is unimportant for the statistical equilibrium of neutral iron.

A remaining question is whether 1D model atmospheres are still appropriate. Černiauskas et al. (2017) show for their red giants, which are slightly warmer than ours, that abundance corrections when using a full 3D hydrodynamical line modeling are small compared to using a traditional 1D approach, which means that the influence of convection should be small.

In Table 2 we present the metallicities derived for our stars for both sets of $\log g$.

3.4. Uncertainties in the Derived Abundances

The uncertainties in the derived metallicities are allocated in part between the fitting procedure of the observed to the synthetic spectrum, and the uncertainties in the determined stellar parameters.

Noise in the spectra, telluric residuals, and level of molecular contamination in the continuum make the continuum levels uncertain. Also, at $R = 24,000$ the sensitivity of the lines to a change in abundance (see Figure 9[8]) is naturally less than at higher resolution. We estimate these systematic uncertainties to be of the order of ±0.15 dex in the [Fe/H] abundance.

---

[8] In Figure 9 a change in metallicity by ±0.2 dex is shown and is clearly detectable.

7

Table 5
Uncertainties in the Derived Metallicities, [Fe/H], Due to Uncertainties in Parameters for a Typical Giant in Our Sample (GC 16763): $T_{eff} = 3600$ K, $\log g = 0.65$, [Fe/H] $= -0.3$, $\xi_{micro} = 2.3$ km s^{-1}, and [α/Fe] $= 0.2$

Parameter	Change	Δ[Fe/H] (dex)
ΔT_{eff}	-150 K	$+0.04$
	$+150$ K	-0.02
$\Delta \log g$	-0.3 dex	-0.04
	$+0.3$ dex	$+0.19$
$\Delta \xi_{micro}$	-0.3 km s^{-1}	$+0.11$
	$+0.3$ km s^{-1}	-0.10
Δ[α/Fe]	-0.2 dex	-0.09
	$+0.2$ dex	$+0.14$
3450 K/$\log g = 0.42$/$\xi_{micro} = 2.4$ km s^{-1}		-0.03
3750 K/$\log g = 0.91$/$\xi_{micro} = 2.1$ km s^{-1}		$+0.17$

We present the uncertainties in the metallicity determination caused by a typical uncertainty change for one stellar parameter at a time in Table 5.

The uncertainty for the temperature determination from the CO band-head indices is ± 150 K (Schultheis et al. 2016).

The uncertainties in the surface gravity, $\log g$, determined from isochrone fitting can be estimated by propagating the uncertainty in temperature through our procedure. For a typical giant in our sample, GC 16763, this leads to $\log g = 0.42$ (for $T_{eff} = 3450$ K) and $\log g = 0.91$ (for $T_{eff} = 3750$ K). Including the uncertainties in the metallicity determination, we estimate the uncertainty in our $\log g$ determination to $\Delta \log g = 0.3$ dex.

The uncertainties in the microturbulence is difficult to assess, since it is an ad hoc parameter. The values are within 0.6 km s^{-1} of each other, according to the prescription we use. We therefore set the uncertainty to $\Delta \xi_{micro} = 0.3$ km s^{-1}.

The uncertainty in [α/Fe] is estimated to be well under 0.2 dex with the typical range $-0.1 <$ [α/Fe] $< +0.4$. We see from Table 5 that the uncertainties in $\log g$, microturbulence, but also the [α/Fe] abundance, all contribute at a 0.1–0.2 dex level. The uncertainties are certainly correlated. One way of assessing the total uncertainty is the perform our $\log g$ determination for the spread in temperature. The last two rows in the table presents these results. The uncertainty is within 0.2 dex.

The total uncertainty in [Fe/H] is thus of the order of ± 0.2 dex.

4. Results

Figures 7 and 8 show spectra of all of the 18 giants. It shows a portion of the observed wavelength region where four Fe lines are indicated. The observations, shifted to the laboratory frame (with radial velocities, v_{rad}^{LSR}, values given in Table 3), are shown by the black underlying spectra and the synthetic spectra are overlaid in red. The stellar parameters are indicated above each spectrum. We have also plotted the telluric spectrum in green, shifted with the same velocity as the target star. This shows how well the telluric division has performed. In other regions where the telluric contamination is more severe, this overlaid telluric spectrum shows where to trust the spectrum the most and where spurious features can be explained by residuals from the division. Figure 9 shows the change in the synthetic spectra due to an abundance change of ± 0.2 dex, which shows the sensitivity of the lines to this type of change.

Our derived stellar parameters including the metallicity, [Fe/H], are given in Table 2. Typical estimated uncertainties in the derived metallicities are Δ[Fe/H] $= 0.2$ dex.

The distributions of our derived metallicities are shown in Figures 10 and 11, both as histograms and as kernel density estimations (KDEs), smoothed with a Gaussian kernel using Silverman's rule-of-thumb bandwidth (Feigelson & Babu 2012). The latter is preferred over histograms due to the problems with the choice of bin size for a histogram and choice of bin positions (see Feigelson & Babu 2012). Figure 10 shows the metallicity distribution for the analysis in which the surface gravities are derived from placing the star on isochrones, given the effective temperatures and metallicities of the stars (see Section 3.2.2). Figure 11 shows the metallicity distribution for the analysis in which the surface gravities are determined from photometry.

5. Discussion

5.1. General Remarks

Our goal is to determine the distribution of metallicities of the stars in the NSC of the Milky Way with the ultimate goal of exploring the trend of [α/Fe] versus [Fe/H]. In order to achieve this goal, with as high precision and accuracy as possible, high-resolution spectra ($R \gtrsim 20,000$) with good S/Ns are needed. The decreased sensitivity to the metallicity, severe atomic and molecular blending of cool stars, and increased difficulties to deal with telluric lines can otherwise be a large source of uncertainty. At low spectral resolution, when neighboring lines start to blend, unknown or missing blends are likely to compromise the abundance determination, not to mention the additional strong line issue. In wavelength regions with severe telluric contamination, as high spectral resolution as possible is needed to disentangle the telluric spectrum.

Furthermore, the target stars have to be observed in the K band (2.2–2.4 μm) due to the extreme optical extinction toward the center of the Galaxy. However, the strong telluric lines represent a complicating factor. This means that new methodology needs to be developed since traditional ones using optical spectroscopy and photometry are unusable. High-resolution spectroscopy in the K band has been used infrequently for abundance analyses, which means that properties of the spectral lines in this wavelength region are not as well studied as, for example, in the optical region. We have developed our K-band line list (B. Thorsbro et al 2018, in preparation) that is the source of our Fe lines used in this analysis. Similarly, the APOGEE project (Majewski et al. 2017) had to develop their own proper line list to be able to perform their own spectral analysis of H-band spectra (Smith et al. 2013; Shetrone et al. 2015).

Spectroscopic observations of Galactic center stars are challenging, especially for metal-rich, cool giants. Compromising with spectral resolution and/or the signal-to-noise level is tempting and yields a larger number of stars that can be investigated, but will inevitably lead to large uncertainties. In these types of spectra the abundance analysis tends to be biased toward the strongest lines in the spectrum, lines that should not be used for an abundance determination because they are quite sensitive to the microturbulence and only weakly sensitive to abundance, the parameter we wish to measure. In the worst case the abundance is totally drowned in the uncertainty of the microturbulence. These lines are often saturated and lie on the
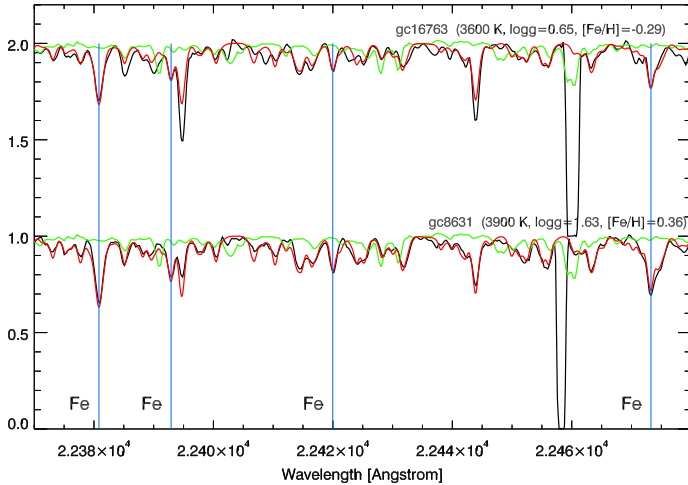
8

Figure 7. Two normalized, high-resolution spectra of giants in the NSC, one metal-poor and one metal-rich. The metal-poor spectrum is shifted up for clarity. Four Fe lines are marked with the blue lines. Synthetic spectra are shown in red and the green spectrum shows where the telluric lines hit the spectrum. Apart from the strong Sc line redward of the second Fe line and a Ti line at 22444 Å the other spectral features are mainly due to CN lines.

flat part of the curve-of-growth (see, for example, Gray 2005). A change in the microturbulence of 0.5 km s^{-1} for, e.g., a weak Sc line with an equivalent width of $W = 50$ mÅ leads to an imperceptible change in the abundance of $\delta[\mathrm{Sc/Fe}] = 0.01$, whereas a saturated line with $W = 350$ mÅ would change by as much as 0.4 dex. Weak lines are therefore the preferred diagnostics for the determination of elemental abundances. It should, at the same time, be noted that the lower the S/N, the more uncertain these weak lines' abundance will become. That is why spectra of high resolution *and* high S/N are necessary for a precise abundance determination.

In the K band, lines in a typical M giant start to saturate at an equivalent width of $W \sim 300$ mÅ, which corresponds to a typical line depth in the core of lines of 0.75 of the continuum, at a resolution of $R = 24{,}000$. A very strong line, with small pressure broadening, reaches down to 0.55 of the continuum. Lines stronger than this should be avoided. A massively strong line can reach 0.35, and no line can get deeper than this in the near-IR if formed in LTE. Note that this is different for lines formed in the UV. In that wavelength region the lines can get much deeper, since the gradient of the Planck function with respect to the temperature in the atmosphere is greater.

If an IR spectral line is not formed in LTE and scattering plays a large role for the line source function, the line might be expected to be stronger. This may be the reason for the strong Sc lines at 22395 Å (see Figures 7 and 8), which are much stronger than any reasonable Sc abundance can result in, for a line formed in LTE. This type of line should obviously not be used to measure the overall metallicity of a star at any spectral resolution, and will disturb global spectral-fitting routines in LTE.

We have chosen the spectral resolution and S/Ns (or exposure times) such that we can obtain spectra of such high

quality that we can optimize for a detailed abundance analysis while keeping the uncertainties to a minimum.

5.2. Membership of Our Targets of the NSC

Direct distance measurements cannot determine whether the stars are in the nuclear region, since this has a radius of about 230 pc (Launhardt et al. 2002), which is small compared to the distance to the Galactic center of about 8.3 kpc (Chatzopoulos et al. 2015a). Thus, a direct distance precision of less than 2% would be necessary to be useful. That is far from possible for giants. There is, however, high extinction within the Galactic center (Chatzopoulos et al. 2015b), a fact can be used to determine distances relative to the very center.

The concept, which is very similar to that of Ryde et al. (2016a), is the following. We determine the fraction of the comparison stars (f) bluer than the target star and then use the nuclear component model of Chatzopoulos et al. (2015a) to determine at which distance, z, from the very center the star would need to be placed, so that f of all stars in the model are in front of z. The 3D model of Chatzopoulos et al. (2015b), which we use, is obtained by fitting Galactic center data, accounting for flattening. Although it does not include bulge-bar and disk components, it is preferable for stars close to the center, since the nuclear components are not modeled at all in other models. Combining the model of Chatzopoulos et al. (2015b) with bulge models does not work, because in the latter the nuclear region is included in the bulge fit.

The comparison stars are stars with an extinction-corrected $K_s < 9$ from Nishiyama et al. (2009). With this magnitude limit, we avoid very red stars that are too faint to be in the sample. Usually we use stars within 100″ of Sgr A* to limit the influence of extinction variations in the plane of the sky, but we also use a second sample out to 500″ for

9

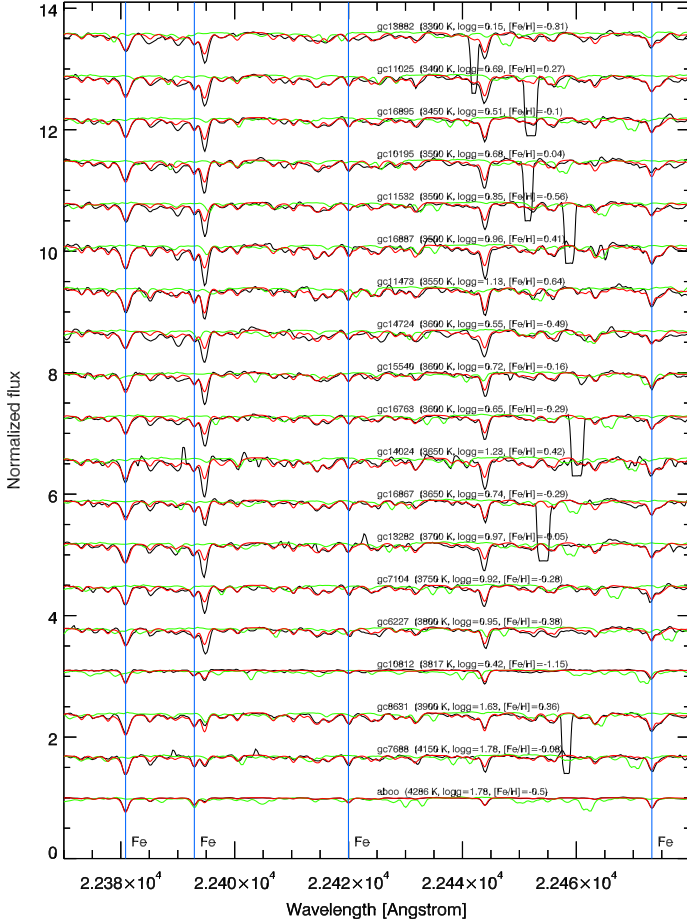**Figure 8.** Seventeen high-resolution spectra of giants in the NSC as well as that of GC 7688, and the reference stars Arcturus (α Boo). Names and stellar parameters are indicated above every spectrum. Four Fe lines are marked with the blue lines. Synthetic spectra are shown in red and the green spectrum shows where the telluric lines hit the spectrum. The missing parts of a few of the spectra are wavelength regions where telluric emission lines of OH lie. Sometimes these are not possible to divide out. Apart from the strong Sc line redward of the second Fe line and a Ti line at 22444 Å the other spectral features are mainly due to CN lines.

very blue stars because the other sample contains too few very blue stars. We add 0.22 in quadrature to the general uncertainties of the measured color $H - K_s$. This number follows from the variation of A_{K_s} extinction in the plane of the sky (Schödel et al. 2010) and the extinction law of Fritz et al. (2011), which we use. Due to the patchy nature of the extinction, larger uncertainties are not excluded. We do not account for intrinsic color variations, as these are small for luminous giants in $H - K_s$ compared to the extinction variation.

In Figure 12, we compare the colors of our targets with the mentioned comparison sample of Nishiyama et al. (2009). Most stars have typical colors. Four stars are bluer than 90% of the stars, which therefore might place them in the foreground. Two of these stars (GC 11473 and GC 7104), are redder than GC 10812, for which we made a detailed orbit calculation in Ryde et al. (2016a) placing it in the nuclear disk or cluster. These two stars are thus likely to be located there. We note though that GC 10812 is of lower metallicity, [Fe/H] < −1.0, than the other stars in our sample. The most likely distances from the
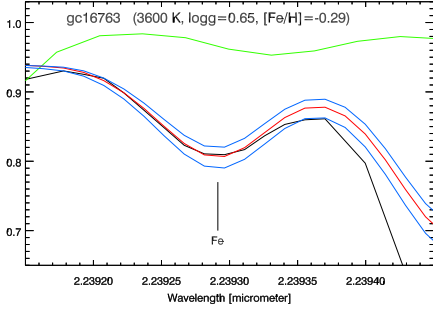
Figure 9. Zoom-in of the GC 16763 spectrum, also shown in Figures 7 and 8. The observed spectrum of one of the iron lines used in the metallicity determination is shown in black and the best synthetic spectrum in red, for the stellar parameters given above the spectrum. Overlaid are two synthetic spectra in blue, one with $\Delta[Fe/H] = +0.2$ and one with $\Delta[Fe/H] = -0.2$. This shows the sensitivity of the spectral lines to a change of this magnitude. The green spectrum is the telluric spectrum.
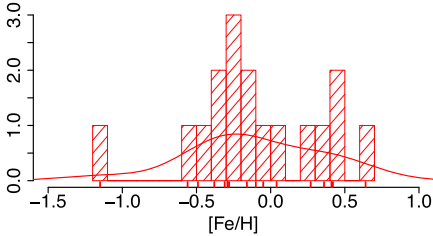
Figure 10. Histogram of the derived metallicities of stars in the NSC. The actual metallicity values are shown by the red tick marks below the histogram. The full line is a kernel density estimation using Silverman's rule-of-thumb bandwidth (Feigelson & Babu 2012) of the metallicities, shown to visualize the data. Here we have excluded the star GC 7688 since we will find that it probably is not a star in the NSC, see Section 5.2.
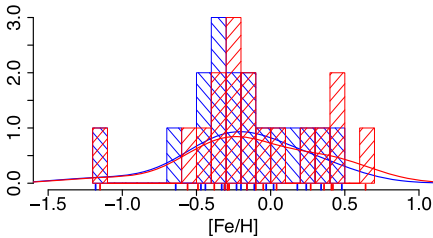
Figure 11. Histogram in blue of metallicities of stars in the NSC, derived using photometrically determined $\log g$. The red histogram is identical to that presented in Figure 10. The full lines are KDEs of the metallicities to guide the eye.

Galactic center of these two stars are (including 1σ limits): $D(GC\,11473) = -36^{+29}_{-109}$ pc and $D(GC\,7104) = -12^{+8}_{-84}$ pc, thus putting them well within the nuclear disk. In Figure 13 we give the most probable distances for the other 15 stars of the
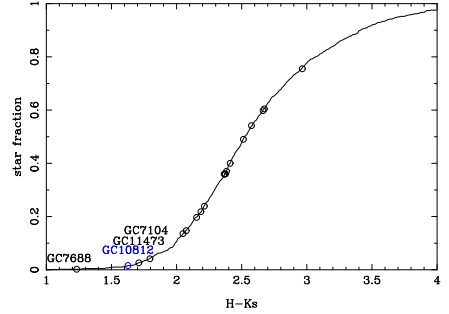

Figure 12. Cumulative plot of $H - K_s$ colors of stars in the Galactic center region. Our targets are marked with circles and the four bluest stars are indicated. The metal-poor giant, GC 10812, discussed in Ryde et al. (2016b) is indicated in blue.
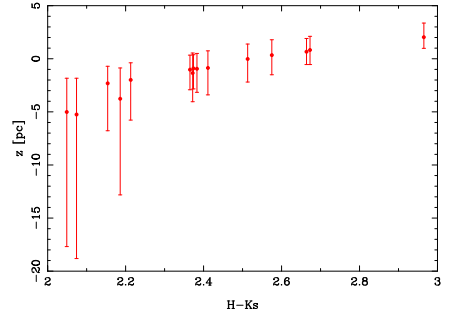

Figure 13. From the extinction-derived distance of the targets relative to the Galactic center. Negative z values are in front of the center. Three stars at small $H - K$ and z are off the scales of this plot; their z are given in the text.

sample. All these stars are redder than the discussed stars and are possible or likely members of the NSC, which has a half-light radius of about 4–9 pc (Schödel et al. 2014; Fritz et al. 2016).

GC 7688 is by far the bluest star in our sample but is not metal-rich and appears to have high T_{eff} (Table 2). Its distance to the Galactic center, estimated by our model, is $D(GC\,7688) = -282^{+125}_{-241}$ pc. While this range overlaps with the nuclear disk size of Launhardt et al. (2002), we think that for this star the omission of the bulge and disk in our model leads to a relevant distance underestimate. Therefore, the star is probably a bulge member.

We now examine the dynamics of our stars in order to test their membership in the nuclear region during their entire orbit. For the kinematics, we mainly use the radial velocities published in Fritz et al. (2016). For most of our stars, proper motions were obtained in that effort, but were not used in that analysis and catalog because their precision was too low to derive reliable masses from the dispersions. For our purpose, however, of comparing a few stars with a known population, a lower precision is sufficient. We use all stars with an uncertainty < 2 mas yr^{-1}. For four stars, we obtain new proper
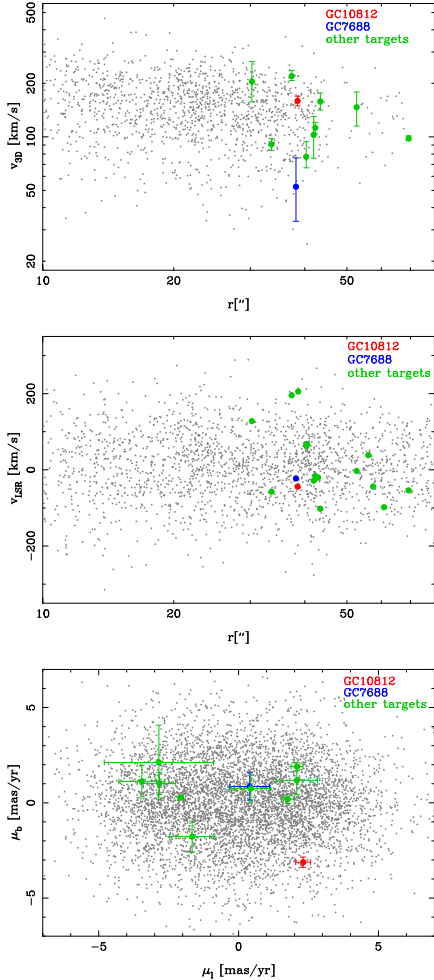
11

Figure 14. Kinematics of the targets. The plots show the space velocity velocity (upper panel), line-of-sight velocities (middle panel), and proper motions of the targets (colored; lower panel) in comparison with other stars in the Galactic center (gray). In the top panel we assume a distance of 8.3 kpc for the conversion of proper motions to velocities. Since some stars do not have a proper motion measurement, they are not shown in the space velocity and proper motion plots. In the bottom plot we only show only comparison stars which have $r > 20''$, since the velocities of stars are larger in the center and our stars are also outside the central $20''$.

motions using data obtained in the ESO programs 087-B-0182 and 091-B-0172, providing us with a baseline of about two years. The proper motions are obtained in a similar way as in

Fritz et al. (2011); the distortion is corrected by applying the radially symmetric formalism first used in Trippe et al. (2008). It was shown in Fritz et al. (2010) that the distortion is stable between instrument interventions during the epochs of observations, thus it is acceptable that the adopted parameters for the distortion correction were obtained in other observations within the same intervention cycle. The uncertainty consists of the scatter between different images and of, as a dominating component, a conservative uncertainty floor of 1 mas per epoch. For a few of our stars, it was not possible to derive proper motions, because too few good images were available.

Our radial velocities are measured from NIRSPEC, since they have a better precision than the SINFONI velocities. Considering their uncertainties, the two are consistent. The uncertainty in the velocities is about 1 km s^{-1} with about equal contributions from wavelength calibration, S/N and LSR uncertainties. All velocities are listed in Table 3 and are shown in Figure 14.

We find that the motions of our stars are similar to typical stars in the region. Thus, it strengthens our conclusions that most stars are members of a nuclear component. In particular, the relative blue star GC 7104 has a 3D motion, which is smaller than that of star GC 10812. Since we have shown in Ryde et al. (2016b) that the star GC 10812 does not leave the nuclear environment, GC 7104 is certainly a nuclear star. The other medium-blue star (GC 11473) has, unfortunately, no proper motions determined and a $v_{\rm rad}^{\rm LSR} = 206$ km s^{-1}. This star could be member of a nuclear component, since the other stars have similar velocities. Since most of the other stars stay in the nucleus, this star probably stays there as well. However, we cannot be certain without determined proper motions. The bluest star, GC 7688, has one of the smallest space velocities of all stars. Its proper motion is within nearly 1σ of zero and $v_{\rm rad}^{\rm LSR} = -22$ km s^{-1} is rather small. From that follows that the star is currently close to its apocenter and we conclude it is like that over most of its eccentric orbit; it will be closer to the center compared to its current location. Nevertheless, even if it enters the nuclear region, it is still clearly different from the typical nuclear stars since most are not on such eccentric orbits.

Overall, we find that all but three of our target stars are likely or possibly members of the NSC, see Table 6. From the remaining three, one (GC 7104) is almost certainly a member of the nuclear disk and GC 11473 is probably also a member. One star, GC 7688, is likely not a member of a nuclear component. We have therefore excluded this star from the the sample of NSC giants, and omit it from the histogram in Figures 10 and 11.

5.3. Metallicity Distribution

The distributions in Figures 10 and 11 actually only show the 17 stars located in the NSC. We derive a metallicity distribution that is broad, spanning $-0.5 <$ [Fe/H] $< +0.5$ (see Figure 10). In finding no stars with [Fe/H] $> +0.6$, the extremely high metallicities of Do et al. (2015) would not appear to be confirmed, and we find very few stars with [Fe/H] < -0.7 (less than $\sim$6%). We recall that the uncertainties in the metallicities are of the order of 0.2 dex. Also, the width and form of the metallicity distribution is not significantly different between the distributions based on the two different methods for the determination of the surface gravity, log g.

Table 6
Spectroscopic Stellar Parameters and the Probable Locations of the Stars in the Nuclear Components (Nuclear Star Cluster (NSC), Nuclear Disk (ND), or Foreground Bulge (FB))

Star	T_{eff} (K)	$\log g$ (dex)	[Fe/H] (dex)	ξ_{mic} (km s^{-1})	Location
GC 10812	3800	0.34	−1.15	2.5	NSC
GC 11473	3550	1.13	+0.64	2.0	ND
GC 13282	3700	0.97	−0.05	2.1	NSC
GC 14024	3650	1.23	+0.42	2.0	NSC
GC 16887	3500	0.96	+0.41	2.1	NSC
GC 6227	3800	0.95	−0.38	2.1	NSC
GC 7688	4150	1.78	−0.08	1.8	FB
GC 15540	3600	0.72	−0.16	2.2	NSC
GC 10195	3500	0.68	+0.04	2.3	NSC
GC 11532	3500	0.35	−0.56	2.5	NSC
GC 13882	3300	0.15	−0.31	2.6	NSC
GC 14724	3600	0.55	−0.49	2.3	NSC
GC 16763	3600	0.65	−0.29	2.3	NSC
GC 7104	3750	0.92	−0.28	2.1	ND
GC 11025	3400	0.69	+0.27	2.3	NSC
GC 16867	3650	0.74	−0.29	2.2	NSC
GC 16895	3450	0.51	−0.10	2.4	NSC
GC 8631	3900	1.63	+0.36	1.9	NSC

Table 7
Uncertainties in the Derived Metallicities, [Fe/H], of Our Most Metal-rich star (GC 11473): T_{eff} = 3550 K, $\log g$ = 1.13, [Fe/H] = +0.6, ξ_{micro} = 2.0 km s^{-1}, and [α/Fe] = 0.0

Model	Parameters $T_{eff}/\log g/\xi_{micro}$ (K)/(dex)/(km s^{-1})	[Fe/H] (dex)
isochrone	3550/1.13/2.0	0.6
photometric	3550/0.97/2.1	0.4
isochrone: ΔT_{eff} = −150 K	3400/0.84/2.2	0.4
isochrone: ΔT_{eff} −150 K; $\Delta\xi$ = 0.3 km s^{-1}	3400/0.84/2.5	0.3

However, it will be valuable to make careful differential measurements between ever fainter giants and the "manifest" supergiant population; such differential measurements may be the most valuable as we consider how the present-day starburst differs in chemistry from the foundational old stellar population.

5.4. How Metal-rich are the Metal-rich Stars?

The Galactic center is a unique region where one might expect to find the most metal-rich stars in the Galaxy. The reason is due to the presumed early, strong burst of star formation with high star formation efficiency that this region must have experienced according to chemical-evolution models (see e.g., Grieco et al. 2015). The question is then whether, and how many, super metal-rich stars can be formed. One might worry about the spectral analysis of these very metal-rich stars since lines become increasingly saturated and therefore less abundance sensitive.

We have derived higher-than-normal metallicities ([Fe/H] > +0.5 dex) for one star in our sample. Even though other authors have also found stars of such high metallicities (see, for example, APOGEE, Majewski et al. 2017, *Gaia*-ESO, Rojas-Arriagada et al. 2017, and Do et al. 2015), the difficulties in an abundance analysis increase for higher metallicities, with line crowding and lines getting stronger and more saturated, which means an increased sensitivity to microturbulence. The question is how much we can trust the highest metallicities.

In Table 7 we present the metallicities derived for the metal-rich star GC 11473 for a few models with varying stellar parameters. The first two rows give the metallicities derived from models with surface gravities based on isochrones and on photometry, respectively. The high metallicity derived is very sensitive to $\log g$ and microturbulence. In order to investigate what the lower uncertainty limit is for the metallicity determination, we decrease T_{eff} within the uncertainty range and change $\log g$ (based on isochrones, see Section 3.2.2) and the microturbulence, accordingly. We then derive a metallicity of [Fe/H] = 0.4. Furthermore, allowing for a reasonable increase of the microturbulence of 0.3 km s^{-1}, the metallicity will decrease an additional 0.1 dex. Thus, due to the uncertainties affecting the most metal-rich stars, our highest metallicity star has such uncertainties that a more normal metallicity of [Fe/H] = +0.3 to +0.4 dex is still consistent with our observed spectrum.

Our determined velocities and derived proper motions of our stars are given in Table 3. In order to determine the velocity dispersion, we divided our sample of NSC stars (i.e., excluding GC 7688) in two groups in metallicity with a division at solar metallicity. Using only radial velocities (which we have for all 17 stars) we get σ = 94 $\pm$ 24 km s^{-1} for the metal-poor group and σ = 87 $\pm$ 20 km s^{-1} for the metal-rich group. If we determine the velocity dispersion using also the proper motions, and treat all dimensions the same, we arrive at σ = 79 $\pm$ 14 km s^{-1} and σ = 111 $\pm$ 18 km s^{-1}, respectively. Thus, we see no kinematic difference between the groups. Our stars are, on average, about 41″ from Sgr* in projection, where the dispersion is about 83 km s^{-1}. Our values are thus consistent with this value.

At first glance, our abundance distribution appears similar to that of the Galactic bulge/bar and, most significantly, is not populated with stars at the extremes of the abundance distribution; nor did we exclude from our sample any such candidates. It is also noteworthy that the abundance distribution is inconsistent with being a solar metallicity disk population or consistent with an inward extension of the metal-poor halo.

Our metallicity distribution, based on high-resolution spectroscopy of the old population, can be contrasted with high-resolution studies by Carr et al. (2000), Ramírez et al. (2000), Cunha et al. (2007), and Davies et al. (2009), probing the present-day compositions by observing young (<1 Gyr), luminous cool cluster giants within 30 pc of the Galactic center. They find a narrow, near-solar iron abundance distribution. Compared to these earlier efforts, our distribution is more broad, and indeed other studies that address the fainter population of red giants are finding more complex abundance distributions. Earlier work by Ryde & Schultheis (2015) suggested that the alpha abundances are also similar to the Galactic bulge; we may therefore acknowledge a growing picture in which the central cluster includes an older, > few, perhaps 10 Gyr population that resembles the bulge/bar more than other stellar populations. Based on existing sample sizes, it is quite premature to even discuss chemical evolution models.

6. Conclusions

We have analyzed high signal-to-noise and high-resolution K-band spectra of 18 M giants with $10.5 < K_s < 12$, projected $\sim$1–2 pc near the Galactic center. These are among the faintest Galactic center giants studied at high resolution, and their stellar parameters place them as intermediate-age to old red giants. This work provides a window into the nature of what is likely the ancient foundational population of the Galactic nuclear cluster. Using additional proper motion measurements and radial velocities, we conclude that 17 of them are members of the nuclear cluster. We find a broad metallicity distribution ranging from [Fe/H] $\sim$ −0.5 to [Fe/H] $\sim$ +0.5 dex and no evidence that the kinematics depends on [Fe/H]. We find no additional stars near [Fe/H] = −1, and even the most metal-rich stars in our sample can be analyzed and fall within the range of +0.5 dex, the upper limit for the bulge as found by previous studies. The most metal-rich star, GC 1143, is found to have [Fe/H] = +0.64. However, uncertainties in the stellar parameters might in principle bring this down to [Fe/H] $\sim$ 0.3–0.4 dex. Given our small sample, we can state that the Metallicity Distribution Function (MDF) is broadly similar to other fields in the Galactic bulge, but appears not to be as narrow as that found for the supergiants (Cunha et al. 2007). A larger sample is necessary to explore hints of substructure in the abundance distribution and to confirm whether any correlation between abundance and kinematics is present. If the substructure in the [Fe/H] distribution strengthens with increasing sample size, it may either reflect a globular cluster-like origin for the central cluster (similar to Terzan 5 and its complex abundance distribution e.g., Origlia et al. 2011) or multiple populations of a different origin. Our next steps will be to explore the alpha elements in these stars, noting that Cunha et al. (2007) found some enhanced alpha elements in the supergiant population, while Ryde & Schultheis (2015) found scaled solar abundances at the metal-rich end. As the nuclear star cluster is likely to be a superposition of stellar populations of different ages, and likely enrichment histories, it will be of great importance to measure the trends of [α/Fe] versus [Fe/H], which may shed light on the history of the nuclear cluster.

Facility: KECK:II (NIRSPEC).

ORCID iDs

R. M. Rich ● https://orcid.org/0000-0003-0427-8387
N. Ryde ● https://orcid.org/0000-0001-6294-3790
M. Schultheis ● https://orcid.org/0000-0002-6590-1657
L. Origlia ● https://orcid.org/0000-0002-6040-5849
H. Jönsson ● https://orcid.org/0000-0002-4912-8609

References

Bensby, T., Feltzing, S., Gould, A., et al. 2017, A&A, 605, A89
Bensby, T., Yee, J. C., Feltzing, S., et al. 2013, A&A, 549, A147
Bergemann, M., Kudritzki, R.-P., Plez, B., et al. 2012, ApJ, 751, 156
Blaauw, A., Gum, C. S., Pawsey, J. L., & Westerhout, G. 1960, MNRAS, 121, 123
Bland-Hawthorn, J., & Gerhard, O. 2016, ARA&A, 54, 529
Blum, R. D., Ramírez, S. V., Sellgren, K., & Olsen, K. 2003, ApJ, 597, 323
Bonnet, H., Ströbele, S., Biancat-Marchet, F., et al. 2003, Proc. SPIE, 4839, 329
Bressan, A., Marigo, P., Girardi, L., et al. 2012, MNRAS, 427, 127
Carr, J. S., Sellgren, K., & Balachandran, S. C. 2000, ApJ, 530, 307
Černiauskas, A., Kučinskas, A., Klevas, J., et al. 2017, A&A, 604, A35
Chatzopoulos, S., Fritz, T. K., Gerhard, O., et al. 2015a, MNRAS, 447, 948
Chatzopoulos, S., Gerhard, O., Fritz, T. K., et al. 2015b, MNRAS, 453, 939
Clarkson, W., Sahu, K., Anderson, J., et al. 2008, ApJ, 684, 1110
Cunha, K., Sellgren, K., Smith, V. V., et al. 2007, ApJ, 669, 1011
Davies, B., Origlia, L., Kudritzki, R.-P., et al. 2009, ApJ, 694, 46
Demarque, P., Woo, J.-H., Kim, Y.-C., & Yi, S. K. 2004, ApJS, 155, 667
Do, T., Kerzendorf, W., Winsor, N., et al. 2015, ApJ, 809, 143
Dong, H., Schödel, R., Williams, B. F., et al. 2017, MNRAS, 471, 3617
Eisenhauer, F., Abuter, R., Bickert, K., et al. 2003, Proc. SPIE, 4841, 1548
Feigelson, E. D., & Babu, G. J. 2012, Modern Statistical Methods for Astronomy (Cambridge: Cambridge Univ. Press)
Feldmeier-Krause, A., Kerzendorf, W., Neumayer, N., et al. 2017, MNRAS, 464, 194
Feldmeier-Krause, A., Neumayer, N., Schödel, R., et al. 2015, A&A, 584, A2
Figer, D. F., Rich, R. M., Kim, S. S., Morris, M., & Serabyn, E. 2004, ApJ, 601, 319
Fritz, T., Gillessen, S., Trippe, S., et al. 2010, MNRAS, 401, 1177
Fritz, T. K., Chatzopoulos, S., Gerhard, O., et al. 2016, ApJ, 821, 44
Fritz, T. K., Gillessen, S., Dodds-Eden, K., et al. 2011, ApJ, 737, 73
Gray, D. F. 2005, The Observation and Analysis of Stellar Photospheres (3rd ed.; Cambridge: Cambridge Univ. Press)
Grieco, V., Matteucci, F., Ryde, N., Schultheis, M., & Uttenthaler, S. 2015, MNRAS, 450, 2094
Gustafsson, B., Edvardsson, B., Eriksson, K., et al. 2008, A&A, 486, 951
Hinkle, K., Wallace, L., & Livingston, W. C. 1995, Infrared atlas of the Arcturus spectrum 0.9-5.3 microns (San Francisco, CA: ASP)
Jönsson, H., Ryde, N., Nordlander, T., et al. 2017, A&A, 598, A100
Kim, S., Prato, L., & McLean, I. 2015, REDSPEC: NIRSPEC data reduction, Astrophysics Source Code Library, ascl:1507.017
Kuijken, K., & Rich, R. M. 2002, AJ, 124, 2054
Kupka, F., Piskunov, N., Ryabchikova, T. A., Stempels, H. C., & Weiss, W. W. 1999, A&AS, 138, 119
Kupka, F. G., Ryabchikova, T. A., Piskunov, N. E., Stempels, H. C., & Weiss, W. W. 2000, BaltA, 9, 590
Launhardt, R., Zylka, R., & Mezger, P. G. 2002, A&A, 384, 112
Lawrence, A., Warren, S. J., Almaini, O., et al. 2012, yCat, 2319, 0
Livingston, W., & Wallace, L. 1991, An atlas of the solar spectrum in the infrared from 1850 to 9000 cm⁻¹ (1.1 to 5.4 micrometer), NSO Technical Report (Tucson, AZ: National Solar Observatory)
Majewski, S. R., Schiavon, R. P., Frinchaboy, P. M., et al. 2017, AJ, 154, 94
Matsunaga, N., Kawadu, T., Nishiyama, S., et al. 2009, MNRAS, 399, 1709
McLean, I. S. 2005, in Proc. ESO Workshop, High Resolution Infrared Spectroscopy in Astronomy, ed. H. U. Käufl, R. Siebenmorgen, & A. F. M. Moorwood (Garching: ESO), 25
McLean, I. S., Becklin, E. E., Bendiksen, O., et al. 1998, Proc. SPIE, 3354, 566
Minniti, D., Contreras Ramos, R., Zoccali, M., et al. 2016, ApJL, 830, L14
Nandakumar, G., Schultheis, M., Hayden, M., et al. 2017, A&A, 606, A97
Nishiyama, S., Tamura, M., Hatano, H., et al. 2009, ApJ, 696, 1407
Paumard, T., Genzel, R., Martins, F., et al. 2006, ApJ, 643, 1011
Pehlivan Rhodin, A., Nilsson, H., & Hartman, H. 2015, A&A, 582, A98
Pehlivan Rhodin, A., Hartman, H., Nilsson, H., & Jönsson, P. 2017, A&A, 598, A102
Pfuhl, O., Fritz, T. K., Zilka, M., et al. 2011, ApJ, 741, 108
Piskunov, N. E., Kupka, F., Ryabchikova, T. A., Weiss, W. W., & Jeffery, C. S. 1995, A&AS, 112, 525
Ramírez, S. V., Sellgren, K., Carr, J. S., et al. 2000, ApJ, 537, 205
Rich, R. M., Origlia, L., & Valenti, E. 2012, ApJ, 746, 59
Rojas-Arriagada, A., Recio-Blanco, A., de Laverny, P., et al. 2017, A&A, 601, A140
Ryabchikova, T., Piskunov, N., Kurucz, R. L., et al. 2015, PhyS, 90, 054005
Ryabchikova, T. A., Piskunov, N. E., Kupka, F., & Weiss, W. W. 1997, BaltA, 6, 244

14

Ryde, N., Fritz, T. K., Rich, R. M., et al. 2016a, ApJ, 831, 40
Ryde, N., & Schultheis, M. 2015, A&A, 573, A14
Ryde, N., Schultheis, M., Grieco, V., et al. 2016b, AJ, 151, 1
Schödel, R., Feldmeier, A., Kunneriath, D., et al. 2014, A&A, 566, A47
Schödel, R., Feldmeier, A., Kunneriath, D., et al. 2015, A&A, 577, C1
Schödel, R., Najarro, F., Muzic, K., & Eckart, A. 2010, A&A, 511, A18
Schultheis, M., Chen, B. Q., Jiang, B. W., et al. 2014, A&A, 566, A120
Schultheis, M., Rojas-Arriagada, A., García Pérez, A. E., et al. 2017, A&A, 600, A14
Schultheis, M., Ryde, N., & Nandakumar, G. 2016, A&A, 590, A6
Shetrone, M., Bizyaev, D., Lawler, J., et al. 2015, ApJS, 221, 24
Simón-Díaz, S., & Herrero, A. 2014, A&A, 562, A135
Smith, V. V., Cunha, K., Shetrone, M. D., et al. 2013, ApJ, 765, 16
Sneden, C., Lucatello, S., Ram, R. S., Brooke, J. S. A., & Bernath, P. 2014, ApJS, 214, 26
Tody, D. 1993, in ASP Conf. Ser. 52, Astronomical Data Analysis Software and Systems II, ed. R. J. Hanisch, R. J. V. Brissenden, & J. Barnes (San Francisco, CA: ASP), 173
Trippe, S., Gillessen, S., Gerhard, O. E., et al. 2008, A&A, 492, 419
Valenti, J. A., & Piskunov, N. 1996, A&AS, 118, 595
Valenti, J. A., & Piskunov, N. 2012, SME: Spectroscopy Made Easy, Astrophysics Source Code Library, ascl:1202.013

15

59

Paper III

Evidence against Anomalous Compositions for Giants in the Galactic Nuclear Star Cluster

B. Thorsbro[1] , N. Ryde[1] , M. Schultheis[2] , H. Hartman[1,3] , R. M. Rich[4] , M. Lomaeva[1] , L. Origlia[5] , and H. Jönsson[1]
[1] Lund Observatory, Department of Astronomy and Theoretical Physics, Lund University, Box 43, SE-22100 Lund, Sweden; thorsbro@astro.lu.se
[2] Observatoire de la Côte d'Azur, CNRS UMR 7293, BP4229, Laboratoire Lagrange, F-06304 Nice Cedex 4, France
[3] Malmö University, Materials Science and Applied Mathematics, SE-20506 Malmö, Sweden
[4] Department of Physics and Astronomy, UCLA, 430 Portola Plaza, Box 951547, Los Angeles, CA 90095-1547, USA
[5] INAF—Osservatorio Astronomico di Bologna, via Gobetti 93/3, I-40129 Bologna, Italy

Abstract

Very strong Sc I lines have recently been found in cool M giants in the Nuclear Star Cluster (NSC) in the Galactic center. Interpreting these as anomalously high scandium abundances in the Galactic center would imply a unique enhancement signature and chemical evolution history for NSCs, and a potential test for models of chemical enrichment in these objects. We present high resolution K-band spectra (NIRSPEC/Keck II) of cool M giants situated in the solar neighborhood and compare them with spectra of M giants in the NSC. We clearly identify strong Sc I lines in our solar neighborhood sample as well as in the NSC sample. The strong Sc I lines in M giants are therefore not unique to stars in the NSC and we argue that the strong lines are a property of the line formation process that currently escapes accurate theoretical modeling. We further conclude that for giant stars with effective temperatures below approximately 3800 K these Sc I lines should not be used for deriving the scandium abundances in any astrophysical environment until we better understand how these lines are formed. We also discuss the lines of vanadium, titanium, and yttrium identified in the spectra, which demonstrate a similar striking increase in strength below 3500 K effective temperature.

Key words: Galaxy: center – stars: abundances – stars: late-type

1. Introduction

With the advent of high resolution infrared spectroscopy, it has become possible to explore the spectra and composition of stars in the nuclear star cluster (NSC) just a few parsecs from the Galactic center. Several chemical abundance studies have addressed the giants in the Galactic center region and the NSC (see, e.g., Ryde & Schultheis 2015; Rich et al. 2017; Do et al. 2018). Spectroscopy in the Galactic center poses a special challenge, as the high extinction generally at present restricts investigations to the infrared K band. Although there is considerable heritage in the 1.6 μm H band from, e.g., APOGEE and earlier studies using NIRSPEC/Keck II (e.g., Origlia et al. 2011), one is challenged by the paucity of weak lines suitable for abundance analysis, as well as the presence of molecular bands that cause blends. The cool, luminous, giants of the NSC are easiest to observe, but pose the greatest perils for analysis.

Low resolution studies have advanced a scenario in which the NSC and nuclear disk have abundant metal-rich stars, reaching to [Fe/H] = +1 (Do et al. 2015; Feldmeier-Krause et al. 2017). Rich et al. (2017) challenges this picture with new high resolution NIRSPEC spectra in the Galactic center, and finds no stars above [Fe/H] = +0.6. Do et al. (2018) reports high resolution spectra of NSC stars behind AO correction, arguing for extreme enhancements of scandium, vanadium, and yttrium; in some cases, the analysis finds 10 times solar abundance for these elements.

Especially interesting are the strong Sc I lines found in M giants that are discussed in Rich et al. (2017). They suggest non-LTE effects as the cause for them, while Do et al. (2018) argue for extreme overabundance (as much as a factor of 10 compared to iron) of scandium in the NSC. If confirmed, this latter interpretation would be a chemical signature of the

special environment in the Galactic center and potentially very important. There are good reasons to assume that the enrichment and star formation histories might be different in the Galactic center, especially if the NSC has a unique formation history. Large magnetic fields, suppressed star formation, high turbulence, tidal forces, and the deep Galactic center potential well might lead to a very different chemical history for the stellar populations in the Galactic center. Furthermore, one might expect inhomogeneities in the trends with a larger scatter, including outliers due to a possible mixture of populations that in principle might include the disk, inner halo, NSC, nuclear disk, and bulge. A unique scandium abundance trend for the NSC would suggest that the Galactic center and similar environments is a site for a new channel of nucleosynthesis of scandium and possibly other elements. Such a trend might also provide a powerful chemical tag for stars formed in nuclear environments.

Scandium resides between the α-elements calcium and titanium in the periodic table and is considered an iron-group element. Even titanium is sometimes considered an iron-group element, such as in the discussion of the metal-poor star HD 84937 (Sneden et al. 2016); therefore, scandium can be seen as an intermediate element between the α elements and the iron-peak group. The precise origin of scandium and its only stable isotope, ^{45}Sc, seems to be complex and is still a matter of debate. Scandium is produced in the innermost ejected layers of core-collapse SNe (type II) during neon burning and explosive silicon and oxygen burning via the radioactive progenitor ^{45}Ti, as reviewed by Woosley & Weaver (1995) and Romano et al. (2010), while the contribution from type Ia SNe seems to be negligible (Iwamoto et al. 1999; Clayton 2003). However, the predicted trends of scandium with [Fe/H] disagree even when taking into account metallicity- and mass-dependent yields,

which might be important (Woosley & Weaver 1995; Chieffi & Limongi 2002; Nomoto et al. 2013). Chemical evolution models predict too little scandium production. This could be due to the problems in the stellar yield calculations (see also Romano et al. 2010). It should be noted, however, that although extreme enhancements of individual elements are known in stars of low metallicity, for stars with [Fe/H] > 0, the total metal production is so high that no single supernova event can affect the abundance of a given species, save perhaps for an r-process production event that might result from a neutron star merger. These factors raise the bar significantly for any purported enhancements of metals in stars of high metallicity.

From an observational point of view, scandium seems to behave like a typical α-element, e.g., enhanced in the thick disk and the Galactic bulge (Battistini & Bensby 2015; Lomaeva 2018). Nissen et al. (2000) and Howes et al. (2016) also find [Sc/Fe] ≈ +0.3 abundances for halo stars and metal-poor stars toward the bulge; however, their studies have no stars more metal-rich than [Fe/H] ∼ −1.5. It is noteworthy that Gratton & Sneden (1991), Prochaska & McWilliam (2000), and Ernandes et al. (2018) report a constant [Sc/Fe] ∼ 0 (and as well for V) for Galactic bulge globular clusters spanning −1.5 < [Fe/H] < 0.0. Smith et al. (2002) report a solar mean scandium abundance for 12 red giants all having subsolar metallicity in the Large Magellanic Cloud (LMC)—an investigation carried out in the K-band.

In the Galactic center, the picture is more complicated. Carr et al. (2000) measured scandium abundance for the cool supergiant star IRS7 located in the Galactic center and found extremely strong Sc I lines as well as V I and Ti I lines. An abundance of [Sc/Fe] ∼ 0.9 dex is required to fit the strength of the Sc I lines. However, supergiant stars are affected by large velocity fields, depth-dependent turbulence, temperature inhomogeneities, etc., and it is known that fully realistic atmospheres for supergiants remain a challenge.

We have employed high resolution K band spectroscopy to overcome the high and variable extinction toward the NSC (see, e.g., Ryde et al. 2016a; Rich et al. 2017). High resolution, K-band spectroscopy was pioneered in the late 80s by Smith & Lambert (1985, 1986, 1990). With the largest telescopes we can now push further to observe cool M giants, and thus avoid the supergiant stars. However, as we emphasized earlier, even the interpretation of the M giant spectra is challenging. Our aim here is to test whether the strong scandium lines in cool M giants in the NSC are due to either physical effects in the line formation process (Rich et al. 2017) or due to intrinsically high scandium abundances (Do et al. 2018). Toward this aim, we have acquired spectra for a range of solar neighborhood stars, similar to those we have observed in the NSC in Rich et al. (2017), using the same instrument and telescope configuration (NIRSPEC on KECK II). These are used as a benchmark to compare with and we discuss different possible reasons for the strong Sc I lines in the K-band spectra of M giants.

2. Observations

The high resolution, K-band spectra have been obtained using the NIRSPEC (McLean 2005; McLean et al. 2007) facility at Keck II, using the 0″432 × 12″ slit and the NIRSPEC-7 filter, giving the resolving power of $R \sim 23{,}000$ needed for accurate abundance determination. Five spectral orders are recorded, covering the wavelength range of

21,000–24,000 Å. However, the wavelength coverage is not complete; there are gaps between the orders.

Apart from the 18 stars observed in the Galactic center, which are presented in Ryde et al. (2016b) and Rich et al. (2017), seven M giants in the solar neighborhood vicinity have been observed using nirspec on Keck II using the configuration described above, on 2017 July 28–29, under program U103NS (PI: Rich). These stars are selected to be of the same spectral type as the stars observed in the NSC. Table 1 provides the basic data for the new observations including the apparent K_s band magnitudes. For details about the data reduction process, we refer to Rich et al. (2017).

Spectra of three observed solar neighborhood stars are plotted in Figure 1 together with three Galactic center stars from Rich et al. (2017). The stars have been ordered by temperature to illustrate the change in line strengths for scandium, vanadium, and yttrium, which decrease dramatically from 3400 to 3800 K. For scandium, we can illuminate this behavior by investigating the atomic physics in greater depth, something that we cannot yet do for the other features.

3. Analysis

3.1. The Atomic Structure of Sc I

In addition to the abundance of an element, there are other parameters affecting the line strengths of absorption lines. One is the oscillator strength and another is the population of the lower level. The latter depends strongly on the excitation energy. For most elements, the near-IR transitions appear at high excitation energies, making the level populations lower. This is the case for most iron-group elements such as Fe I, where the lower excitation levels, such as the 4s levels, do not have near-IR transitions. For Sc I, the structure is different, with low excitation transitions 3d²4s–3d4s4p appearing in the K-band.

Figure 2 shows the energy level diagrams for Sc I and Fe I, respectively, plotted with the same vertical energy scale. The dashed line shows the ionization energy for each atom. As can be seen, there is a significant difference in the excitation of the near-IR lines, where Sc I originates at much lower energies, around 1.5 eV, compared to Fe I at 3.6 and 6.1 eV. At temperatures of 3500–4500 K in the line-forming atmospheric depths, as for the stars in the current study, the Boltzmann factor, $e^{-\Delta E/k_b T}$, gives a difference of 3 orders of magnitudes comparing the two different excitation energies and in this case the different atoms, which means a difference of 3 orders of magnitude for relative level population. Note, however, that the abundance difference between iron and scandium in a solar mixture of gas is more than 4 orders of magnitude. A further implication is, as noted early by Smith & Lambert (1985, 1990), that non-LTE effects should be smaller for high excitation lines, which are formed in deeper, warmer layers of the stellar atmosphere and lines from the dominant stage of ionization. Non-LTE effects could thus affect low excitation lines from neutral species in M giants. It would, therefore, not be unexpected if non-LTE effects should plague the Sc abundances derived from our low excitation Sc I lines.

3.2. Atomic Data of Sc I Lines

In general, there is a lack of experimental atomic data for near-IR transitions.[6] In response to this need, we have initiated

---

[6] https://www.nature.com/news/nailing-fingerprints-in-the-stars-1.14239

Star	Obs. Date	K_s	R.A. [h:m:s]	Decl. [d:m:s]	$T_{\rm eff}$ [K]	log g	[Fe/H]	$\xi_{\rm micro}$ [km s^{-1}]	[Sc/Fe]
2M17584888−2351011	2017 Jul 30	6.49	17:58:48.89	−23:51:01.17	3652	1.44	0.27	2.0	0.80
2M18103303−1626220	2017 Jul 29	6.51	18:10:33.04	−16:26:22.06	3436	0.79	0.27	2.2	0.77
2M18191551−1726223	2017 Jul 29	6.56	18:19:15.51	−17:26:22.35	3596	1.16	0.21	2.0	0.54
2M18550791+4754062	2017 Jul 30	7.63	18:55:07.92	47:54:06.22	3915	1.40	−0.27	2.0	0.37
2M19122965+2753128	2017 Jul 29	6.60	19:12:29.66	27:53:12.83	3263	0.25	0.27	2.4	0.58
2M19411424+4601483	2017 Jul 30	7.69	19:41:14.25	46:01:48.14	3935	1.41	−0.37	2.0	0.43
2M21533239+5804499	2017 Jul 29	6.58	21:53:32.40	58:04:49.94	3708	1.17	0.29	2.0	0.16
α Boo	⋯	−2.91	14:15:39.67	19:10:56.67	4286	1.66	−0.52	1.7	0.16
GC 7688	⋯	11.00	17:45:42.17	−29:00:54.99	4150	1.78	−0.08	1.8	0.13
GC 11025	⋯	10.41	17:45:37.13	−29:00:14.39	3400	0.69	0.27	2.3	1.27
GC 11473	⋯	11.74	17:45:42.64	−29:00:10.23	3550	1.13	0.64	2.0	0.37

Note. We assume solar abundances of $A(\rm Fe) = 7.45$ (Grevesse et al. 2007) and $A(\rm Sc) = 3.04$ (Pehlivan Rhodin et al. 2017).

a program to provide accurate and vetted near-IR atomic data for stellar spectroscopy. Scandium is one of the elements covered. Being an odd element, scandium has a nonzero nuclear spin of $I = 5/2$ allowing for hyperfine structure (HFS). In recent works, we have measured the oscillator strengths and HFS of Sc I (Pehlivan et al. 2015; van Deelen 2017). The oscillator strengths are derived using the radiative and lifetime method, and the uncertainties are 0.03 dex for the lines used in the present study. Since the HFS is a result of the interaction between the nuclear and electronic angular momenta, the effect is larger for electrons close to the nucleus. Unpaired s-electrons are thus expected to show the largest HFS.

The states responsible for the transitions used in the present study, 3d²4s–3d4s4p, involve an unpaired 4s-electron, making the HFS of the lines used large. This is indeed what is observed in the laboratory measurements. The HFS-data used in the present study are derived from fitting Fourier Transform Spectroscopy measurements (van Deelen 2017).

3.3. Analyzing the Effect of Temperature and HFS

We model theoretical line formation of spectral Sc I lines to explore the effects of both temperature and HFS, using the BSYN and EQWIDTH codes based on routines from the MARCS model atmosphere code (Gustafsson et al. 2008). We use one-dimensional (1D) MARCS atmosphere models, which are hydrostatic model photospheres in spherical geometry, computed assuming LTE, chemical equilibrium, homogeneity, and conservation of the total flux (radiative plus convective, the convective flux being computed using the mixing-length recipe). The resulting line strength measured in equivalent width is plotted against temperature in Figure 3. For the spectral line based on a single atomic level transition, we use the measured oscillator strength from Pehlivan et al. (2015). For the HFS-based spectral line, we use the combined work of Pehlivan et al. (2015) and van Deelen (2017). The fact that the HFS spectral line is a combination of many weak lines means that the spectral line does not saturate in the classical sense of a spectral line based on a single atomic transition, and thus can form a much stronger line.

Using the same code and model assumptions, we further derive scandium abundances for a given spectral Sc I line having an equivalent width of 300 mÅ, which is presented in Figure 4.

3.4. Accurate Stellar Parameters

The stellar parameters of the seven solar neighborhood stars presented here are obtained from the APOGEE Data Release 14 (Blanton et al. 2017; Majewski et al. 2017; Abolfathi et al. 2018). The stellar parameters have been determined using the APOGEE stellar parameters and chemical abundance pipeline (ASPCAP; García Pérez et al. 2016) and then calibrated using photometric effective temperatures, asteroseismic surface gravities, as well as stellar clusters (Holtzman et al. 2018). Jönsson et al. (2018) evaluate the performance of ASPCAP by comparing the stellar parameters and abundances derived to those of high resolution optical studies of giants. The typical uncertainties found in $T_{\rm eff}$, log g and [Fe/H] are in the order of ∼100 K, ∼0.2 dex, and ∼0.1 dex, respectively. Similar uncertainties are found in Schultheis et al. (2017) by comparing to other spectroscopic results for bulge giants in Baade's Window. However, since both comparisons were made for mainly stars with $T_{\rm eff} > 3800\,\rm K$ (Schultheis et al. 2017 have two cooler comparison stars), these results cannot strictly be extrapolated to our much cooler M giants.

Since $T_{\rm eff}$ is the parameter with the greatest influence on the derived Sc abundance (see Section 3.1 and Figures 3, 5, and 6), we go on evaluating the ASPCAP accuracy of this parameter further. Table 2 shows a comparison of the effective temperature measured by APOGEE and the photometric $T_{\rm eff}$ based on the $J - K_S$ versus $T_{\rm eff}$ relation from Houdashelt et al. (2000). In addition, we queried the Gaia DR2 database and found Gaia temperature estimates for seven of our objects. The temperatures from Gaia DR2 were determined by using the $G_{\rm BP} - G$ and $G_{\rm RP} - G$ colors as inputs together with a training set of different labels from different spectroscopic surveys such as APOGEE, RAVE, LAMOST, and the Kepler Input Catalog. For a more detailed description of the Gaia DR2 temperatures, we refer to Andrae et al. (2018). The mean difference between the spectroscopic and photometric temperatures from Houdashelt et al. (2000) is ∼50 K with a standard deviation of 240 K. The mean difference between APOGEE and Gaia is ∼90 K with a standard deviation of 185 K. We can conclude that the spectroscopic temperatures of our cool M giants derived from APOGEE are consistent with those of photometric measurements and Gaia's estimated temperatures, and hence are expected not to show any large systematic uncertainties that in turn would skew our abundance analysis.
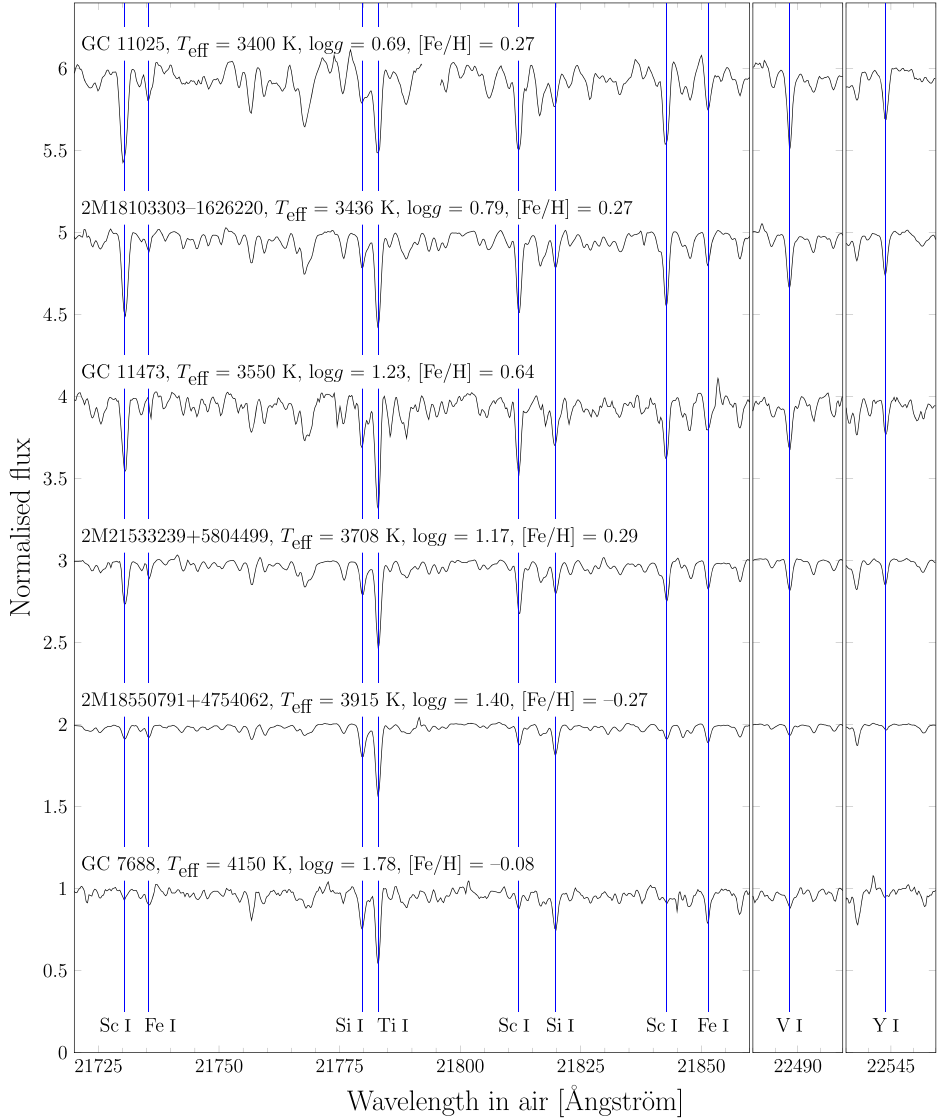
3

Figure 1. Six M giant stars plotted together with increasing temperature from top to bottom with blue vertical lines identifying lines of interest. The normalized fluxes have been translated upward with integer values for presentation. The stars are a mix of three Galactic center stars (GC 7688, GC 11025, and GC 11473) and three solar neighborhood stars (2M18103303−1626220, 2M18550791+4754062, and 2M21533239+5804499). The spectra show striking strong scandium, vanadium, and yttrium lines in the cooler stars, even though the stars are located in widely different environments. As temperatures increase to 3900 K and beyond, the neutral lines of scandium, vanadium, and yttrium begin to vanish, presumably due to ionization.
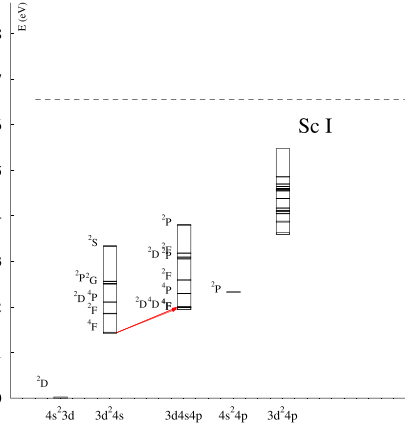
Figure 2. Energy level diagrams for Sc I and Fe I, respectively. The vertical energy scale is the same, and the dashed line shows the ionization energy. The observed lines are marked with red arrows. Note that the near-IR Sc I lines are located at significantly lower excitation energies compared to the near-IR Fe I lines.
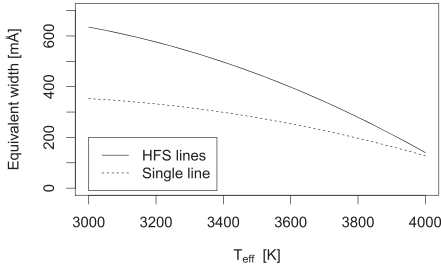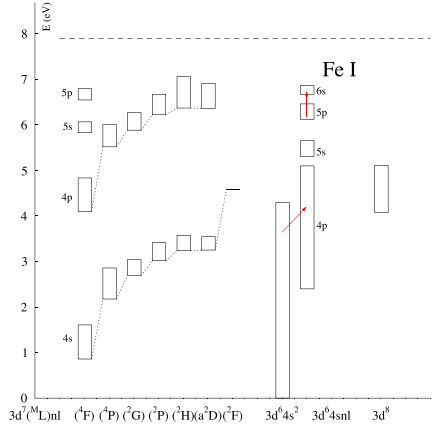
Figure 3. Equivalent width of a Sc I line as a function of temperature depends on whether the Sc I line is considered to be a combination of many small lines due to hyperfine structure (HFS) or if the line is considered to be a singular atomic level transition. Notice how at high temperature the two analyses converge, but at cooler temperatures the HFS of the line enables the spectral line feature to become considerably stronger compared to basing the analysis on a singular atomic level transition. The metallicity and scandium abundance is assumed to be solar, and the surface gravity is assumed to follow isochrone relations with changing temperatures. Non-LTE and 3D effects are not considered.
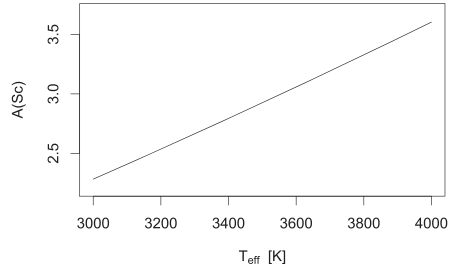
Figure 4. This plot assumes a Sc I line with a fixed equivalent width of 300 mÅ, as might be the situation when analyzing an observed spectrum. Plotted is the number density abundance of scandium as a function of temperature derived from this Sc I line. The plot shows how cooler temperatures counteract higher abundances when modeling such a feature. Note that a temperature difference of 100 K corresponds to an abundance difference of more than 0.1 dex. The metallicity is assumed to be solar, and the surface gravity is assumed to follow isochrone relations with varying temperature. Non-LTE and 3D effects are not considered.

For α Boo the *Gaia* FGK benchmark stars parameters are used (Jofré et al. 2014, 2015; Heiter et al. 2015) with uncertainties in $T_{\rm eff}$, $\log g$ and [Fe/H] being 35 K, 0.09 dex and 0.08 dex, respectively.

The stellar parameters of the three Galactic center stars have been determined by Rich et al. (2017). The $T_{\rm eff}$ is determined from the strength of the CO bandhead in low resolution, K-band spectra (Schultheis et al. 2016). The uncertainties in $T_{\rm eff}$, $\log g$, and [Fe/H] are in the order of $\sim$150 K, $\sim$0.3 dex, and $\sim$0.2 dex, respectively.

For determination of microturbulence, we look to the abundance investigations of M giants in the solar neighborhood based on high resolution near-IR spectra (Smith & Lambert 1985; Smith et al. 1989; Smith & Lambert 1990), and for red

giants in the LMC (Smith et al. 2002). The microturbulence was found by demanding that abundances from lines from a few atomic species be independent of strength, with values from 2 to 3 km s^{-1} for M giants. A more recent detailed analysis of spectra of five red giant stars by Smith et al. (2013) is used to provide an empirical relation described by Rich et al. (2017) for estimating microturbulence for our stars. The microturbulence values used are listed in Table 1.

3.5. Scandium Abundance Determination

To determine the scandium abundance of the analyzed stars, we find best fitting synthetic spectra based on radiative transfer and line formation calculated for a given model atmosphere (MARCS atmosphere models in spherical geometry; Gustafsson
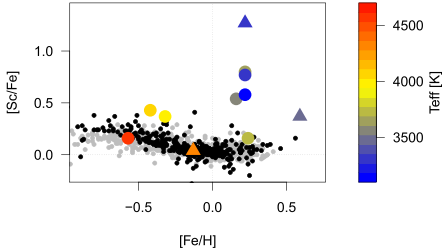
5

Figure 5. [Sc/Fe] vs. [Fe/H] for stars in the solar neighborhood (disks) and Galactic center (triangles), colored by their effective temperature. Shown also are the scandium abundances derived from local disk giants from Lomaeva (Lomaeva 2018) as black dots and the scandium abundances derived from disk dwarfs by Battistini & Bensby (2015) as gray dots. Note how the derived [Sc/Fe] abundance ratio increases drastically as the stars becomes cooler, while the stars near 4000 K and above are more in agreement with both Lomaeva (Lomaeva 2018) and Battistini & Bensby (2015).
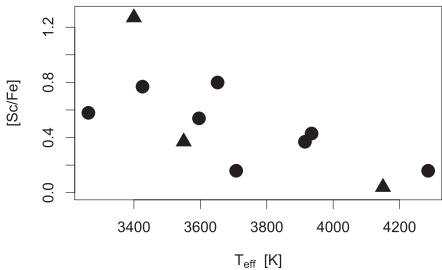
Figure 6. [Sc/Fe] vs. $T_{\rm eff}$ for stars in the solar neighborhood (disks) and Galactic center (triangles). Notice that both populations follow approximately the same trend. This plot shows that the derived scandium abundance simply increases with lower temperatures, suggesting that the derived "abundances" are spurious, being systemically in error, perhaps due to an incomplete model of the line formation.

Table 2
Comparison of Effective Temperatures between APOGEE, Photometric Temperature, and Those of the *Gaia* DR2 Release

Star	$T_{\rm eff}^{\rm APOGEE}$	$T_{\rm eff}^{\rm photometric}$	$T_{\rm eff}^{Gaia}$
2M17584888−2351011	3652	3673	⋯
2M18103303−1626220	3436	3350	3282
2M18191551−1726223	3596	3191	3297
2M18550791+4754062	3915	3870	4000
2M19122965+2753128	3263	3402	3286
2M19411424+4601483	3935	4238	4048
2M21533239+5804499	3708	3451	3423

et al. 2008), assuming the fundamental stellar parameters shown in Table 1. We use the code Spectroscopy Made Easy (SME) for synthesizing model spectra and finding the best fit to the observed spectra using χ^2 minimization (Valenti & Piskunov 1996, 2012).

We use four neutral scandium (Sc I) features seen in the spectra of the analyzed stars for determining scandium abundances. The approximate wavelength in air of these features are 21730, 21812, 21842, and 22394 Å, where the first

three are visible in the spectra plotted in Figure 1. Due to hyperfine splitting of neutral scandium, the four spectral features consist of a total of 59 scandium lines, making the analysis robust against saturation effects that could otherwise be suspected due to the strength of the spectral features.

The determined scandium abundances are shown in Table 1 and plotted in Figure 5 as a function of [Fe/H] and in Figure 6 as a function of temperature. The uncertainties in [Sc/Fe] are on the order of ∼0.1 dex, assuming that the model assumptions hold.

4. Results and Discussion

4.1. Observed Spectra

Our central result is given in Figure 1, which shows an array of our NSC K band spectra interleaved with our identically observed local giants of similar spectral type (i.e., very similar stellar parameters). It is clear from this figure that the M giant spectra are overall quite similar, even taking into account the small differences in stellar parameters. This similarity extends to many of the atomic lines as well. At first glance, the plot suggests that the scandium abundance simply increases with lower temperature; this begins to point toward an explanation other than a true enhancement in scandium abundance, such as being unable to accurately model the line formation. Similar enhancements for vanadium and yttrium are also clear; both of these lines strengthen dramatically below 3600 K. We can conclude based only on empirical grounds that there is room for only very small differences in the abundances of these elements between stars in the Nuclear Cluster Stars and stars in the solar neighborhood. In particular, the scandium abundance is very unlikely to be anomalously elevated in the Galactic center NSC, as asserted in Do et al. (2018).

4.2. Derived Scandium Abundances

Figure 5 shows our derived scandium abundances in the form of the [Sc/Fe] trend versus metallicity, i.e., the [Fe/H] abundances. We show our seven M giants in the solar neighborhood together with α-Boo and three M giants in the NSC (from Rich et al. 2017), colored as a function of effective temperature. As a background trend, we also plot the [Sc/Fe] abundance trends found for the solar neighborhood, determined from optical Sc II lines from Jönsson et al. (2017) and Lomaeva (2018) for K giant spectra and from Battistini & Bensby (2015) for dwarf star spectra; these trends follow approximately that of a typical α-like element in the solar neighborhood, with elevated [Sc/Fe] at [Fe/H] < −0.5 and a gentle decline toward Solar [Sc/Fe]. It is evident that these well-established trends are very different from our derived [Sc/Fe] values based on Sc I lines in our M giant spectra. Our derived abundance ratio determined for α-Boo do agree with the general trend. It is evident that two giants with the highest temperature (from both the NSC and Local giants) fall exactly on the general trend even though their abundances are 0.5 dex apart. All of the cooler stars fall above the trend, and it is evident that the coolest stars are 0.5–1.3 dex above the trend, with the coolest stars showing the most extreme derived [Sc/Fe] "abundance" values.

Indeed, the most striking feature seen in Figure 6 is how our derived [Sc/Fe] "abundance" ratios increase dramatically with decreasing $T_{\rm eff}$ leading to anomalously high scandium abundances of up to 1.3 dex for the cooler stars ($T_{\rm eff} < 3800$ K), while

6

the warmer stars show more normal [Sc/Fe]. There is no astrophysical basis for the scandium abundance to depend on the *temperatures* of the stars, and therefore we can safely conclude that the derived abundances for the cooler stars are either plagued with very large systematic uncertainties or based on assumptions in the abundance determination that are not valid. This calls for a discussion of the physical processes involved.

We note that Smith et al. (2002) did not derive any anomalously high scandium abundances from their high resolution, near-IR spectra of 12 M giants in the LMC with effective temperatures in the range of 3600–4000 K and metallicities between −1.1 and −0.3 dex. The Sc I line they used at 23404.8 Å, which is not included in our wavelength range, is measured to have equivalent widths in the range of 70–650 mÅ. This is comparable to the equivalent widths of similar lines we find for our stars in the same temperature range. Apart from scandium, Smith et al. (2002) also derived the abundances of sodium, titanium, and iron, all from neutral lines. The [Na/Fe] and [Ti/Fe] abundance trends decrease with iron slightly below the disk trends, which is to be expected for the LMC. However, their [Sc/Fe] trend does not show such a depletion, possibly indicating higher-than-expected scandium abundances derived. Finally, Smith et al. (2002) find that the scandium abundance determination is very temperature sensitive with an uncertainty of almost 0.2 dex for a shift in 100 K in the effective temperature, which agrees with the modeled temperature sensitivity that we find to be above 0.1 dex, as discussed earlier in Section 3.3.

4.3. Understanding the Strong Scandium Lines

As already noted in the discussion of spectral lines in M giants in the NSC (Rich et al. 2017), the Sc I lines observed in the K-band are indeed stronger than expected from an LTE spectral synthesis analysis for a reasonable scandium abundance. In this context, it is therefore of interest to consider possible processes and properties of these spectral lines that might be responsible for these anomalously high line strengths.

In LTE and for unblended, weak lines, i.e., lines that are not saturated, the observed line strengths are directly proportional to the atomic line strengths (Einstein A coefficients or $\log gf$-values) and the number density abundance ($A_{\text{element}} = \log N_{\text{element}} [\text{cm}^{-3}]$) of the element causing the spectral line. In order to derive the abundance, it is therefore vital with a well determined $\log gf$-value. We therefore use the recent laboratory measurements of Pehlivan et al. (2015) for all our lines. This ensures a minimum uncertainty due to the intrinsic line strengths of the Sc I lines.

The strength of saturated lines can, on the other hand, also be very sensitive to the assumed microturbulence (see, e.g., Gray 2005), leading to large uncertainties in the derived abundances. However, having an odd nuclear spin, the scandium lines are subdivided into many components due to the HFS. In the case of our Sc I lines, the HFS has the effect of delaying the onset of saturation (since the strong line feature consists of many weak lines), but also to change the appearance of the line. Furthermore, the pressure broadening effect should be smaller on the components compared to an equally strong single line. We have, therefore, taken into account the HFS in our synthesis, successfully reproducing the line profile. Furthermore, our modeled lines are indeed relatively insensitive to microturbulence, even though the components have a relatively large summed equivalent width.

A further concern when working with spectral lines that yield anomalously high abundances, but also with lines in metal-rich and especially cool stars in general, is the contribution of unaccounted blends from molecular and atomic species. The accurate wavelength of molecular lines blending is a concern, but if the wavelengths are known precisely enough, these lines may be properly accounted for. The CN line list we use (Sneden et al. 2014) is very precise, so such blends can be accurately taken into account. Blended atomic lines might make an abundance analysis impossible; the existence of such blends might be known, but their atomic data are not accurately known, or there might be unknown blending lines that are not taken into account at all. However, in our spectra, all four Sc I lines are stronger than modeled by approximately the same amount. Therefore, it is very unlikely that all four lines would be blended at the same time. We therefore conclude that the Sc I lines are not significantly affected by blends.

Sc I lines are known to be temperature sensitive, and one concern would be that the anomalously strong Sc I lines are caused by a systematically incorrect temperature scale. To assess this possibility, we have determined the [Sc/Fe] abundances and the equivalent widths from a grid of stellar models. We have focused on the temperature range of M giants ($3000 < T_{\text{eff}} [\text{K}] < 4000$) since these are optimal objects to be observed in the NSC. A surface gravity is determined for a given (T_{eff}, $\log g$) combination from the Yale–Yonsei (YY) isochrones (Demarque et al. 2004). Figure 4 shows the derived Sc number density abundances from a line of a typical equivalent width of 300 mÅ. A decrease of 100 K in T_{eff} increases the derived Sc abundances by more than 0.1 dex. The scandium lines are indeed temperature sensitive, but this alone cannot explain the systematically stronger lines for our cooler stars. There is no reason to believe that the cooler solar neighborhood stars have T_{eff} systematically too high by up to 800 K.

We conclude that our derived abundances, based on an *LTE* abundance analysis, are precise and accurate to within at least 0.2 dex, with the temperature sensitivity being the largest source of uncertainty. However, we can also conclude that stars below approximately $T_{\text{eff}} < 3800$ K should not be used for deriving stellar scandium abundances from these lines based on a traditional LTE analysis. We have demonstrated the strong temperature dependence but we cannot specify which model assumptions are invalidated, complicating any abundance analysis. However, with its low ionization potential, Sc I is a minority ionization stage throughout the photosphere, and any departures from LTE (and 3D effects) will affect Sc I lines more than ionized lines (Asplund 2005). Changes in the ionization rates, and therefore the ionization balance, change the relative population of the minority species more that that of the majority species.

No non-LTE investigations of scandium have been made for cool giants (to our knowledge), but Zhang et al. (2008) investigated the formation of *optical* scandium lines in the Sun and found large departures from LTE for Sc I lines and none for ionized lines. The Sc I lines in the Sun are weaker than expected from LTE, whereas we see the opposite for M giants. Whereas for metal-poor, cool stars, photoionization is a major process that can under-populate neutral atoms (Gehren et al. 2001), leading to weaker lines in non-LTE, for collision-dominated ions (Gehren et al. 2001), photon suction and over-recombination tend to strengthen the lines instead. An

7

over-recombination can be caused by the smaller mean-intensity-field compared to the Planck function, which is the case in the near-IR (Asplund 2005). These are processes that could cause stronger lines than expected from an LTE treatment.

The treatment of convection when using a full 3D hydrodynamical modeling instead of using a traditional 1D approach could also significantly affect the line formation. For neutral lines in the near-IR formed in red giants discussed in Kučinskas et al. (2013), Černiauskas et al. (2017), which are slightly warmer than ours, the abundance corrections are shown, however, to be small.

A strong suspicion is thus that Sc I lines formed in cool M giant atmospheres also are affected by non-LTE effects. In their non-LTE study of titanium lines, with a similarly low ionization potential as for scandium, Bergemann et al. (2012) show that the J-band lines in supergiants are indeed strengthened in non-LTE. The effect increases for increasing metallicities and decreasing temperatures, from a negligible effect at 4200 K to 0.4 dex at 3400 K, their lowest temperature point. Above 4200 K, the opposite effect is in play. If the same processes are important for scandium, these trends could explain also the strengthening of the scandium lines for cool, metal-rich stars. A detailed non-LTE study is, however, required to find the dominant process in play for the scandium lines in the K-band for M giants. However, in general, it is difficult to isolate the dominant process causing a departure of a Boltzmann–Saha level population for a transition in a complex atomic structure (Bergemann et al. 2012).

4.4. Vanadium and Yttrium Lines in the K-band

In the K-band, there are a number of very strong vanadium and yttrium lines, see, for example, the spectra plotted in Figure 1. Do et al. (2018) suggest these elements to be significantly enhanced at the Galactic center, also with a potentially very different chemical enrichment history there. Based on the similarity of the solar neighborhood stars we present here, one might suspect that the V I and Y I lines might suffer from the same line strengthening effects as the scandium lines do.

Yttrium is homologous to scandium, residing just below scandium in the periodic table. It has the same atomic structure but with principle quantum numbers one unit larger and thus 4d and 5s instead of 3d and 4s for Sc I, which makes Y I lines of the configurations $4d^25s$–$4d5s5p$ appear at low excitation energies. The strength of the Y I line should therefore react in the same way to the line formation process, and is thus expected to be stronger in the same way as in the case of Sc I. In addition, lanthanum residing in the period below yttrium, would show a similar effect for the lines $5d^26s$–$5d6s6p$, had there been lines detected in the K-band. Only the relative abundance differs. Laboratory studies of Y I and La I are ongoing.

Vanadium is the next odd element after scandium, lying after titanium in the periodic table. Its structure more closely resembles that of the iron-group elements, such as Fe I with the majority of the strong transitions appearing at high excitation. There are exceptions, such as the transition at $3d^5$ a^6S–$3d^5(^5D)4p$ z^6P at 22493 Å. A non-LTE strengthening of vanadium cannot be excluded. We infer that non-LTE strengthening is the best option to explain the odd behavior of vanadium, given the arguments advanced here for scandium.

5. Conclusions

Our question in this paper is whether the abundance of scandium in stars observed in the NSC is really unusual. An unusual abundance would have a profound effect on our understanding of the formation of the NSC and its stellar population. There are several physical reasons for a spectral line to be strong, and by going through all of these, we conclude that the strong Sc I lines in the NSC are most likely due to line formation effects and certainly not due to an anomalous high scandium abundance. These Sc I lines in the K-band are not good abundance diagnostics for the elements in cool M giants. Our conclusion is based on the fact that similar stars in the solar neighborhood, where the scandium abundances are known, show similarly strong Sc I lines, much stronger than can be modeled with traditional synthetic spectroscopy. We conclude that the Sc I lines in cool stars are strong everywhere in the Galaxy and this is an inherent property of the line formation process, and should not be used to derive the scandium abundance of the stars. Lines of ionized scandium should be used instead or studies should use warmer stars. Non-LTE calculations for scandium, and perhaps other physical phenomena needing theoretical modeling, are needed before we can use the Sc I lines at all.

Our findings emphasize the perils of attempting to infer composition from a small number of lines that are far too strong for any conventional application of abundance analysis. Although high resolution infrared spectroscopy makes it possible to study the composition of stars in highly obscured regions, the relative paucity of weak lines requires that work in the infrared be approached with great caution. In the case where anomalies are suspected, it is important to turn to general established trends derived from optical measurements in the disk and bulge, as an additional essential check before claiming to discover unusual composition. We also note that at high metallicities, it would be quite surprising to see large enhancements of any species, that would imply extreme productions of individual elements in a metal-rich environment.

The cool giants we have analyzed are almost certainly on the asymptotic giant branch (AGB) and, as such, they are likely to be the most luminous stars in their stellar population, contributing a substantial fraction of the K band integrated light. We know that the NSC is a complex stellar population with a wide range of age and we might expect many extragalactic NSCs to also have wide age ranges and possibly host very substantial populations of cool, luminous AGB stars. Individual supergiants can also contribute a substantial portion of the integrated light in the K band. There is a growing trend to attempt to infer detailed abundances (e.g., abundances of individual atomic species) from the integrated light of stellar populations. The temptation is strong for the extragalactic NSCs of low luminosity spirals, which have relatively low broadening due to the stellar velocity dispersion, making them very attractive targets for spectrum synthesis. We emphasize that if such a practice is carried out for the integrated light in the K band, it should be done using actual spectra of solar neighborhood giants and a full population synthesis code. The numbers of cool AGB stars are small, and their contribution to the stellar population is stochastic (Frogel et al. 1990). Even then, our understanding of line formation for cool giants is far from complete and therefore, we suggest that integrated light studies using only the K band be avoided.

8

High resolution spectroscopy in the near-infrared is a relatively new subject area. The advent of very high resolution spectrographs on the current generation of 8–10 m telescopes and future plans for ELTs give the subject great promise. It is important to support this endeavor with an equally serious investment in laboratory measurements, so that full advantage can be taken of the expected bounty of high quality data.

Facility: Keck II (NIRSPEC).

Software: SME (Valenti & Piskunov 1996, 2012), BSYN & EQWIDTH (Gustafsson et al. 2008).

ORCID iDs

B. Thorsbro ⬛ https://orcid.org/0000-0002-5633-4400
N. Ryde ⬛ https://orcid.org/0000-0001-6294-3790
M. Schultheis ⬛ https://orcid.org/0000-0002-6590-1657
H. Hartman ⬛ https://orcid.org/0000-0001-9853-2555
R. M. Rich ⬛ https://orcid.org/0000-0003-0427-8387
M. Lomaeva ⬛ https://orcid.org/0000-0001-8161-1732
L. Origlia ⬛ https://orcid.org/0000-0002-6040-5849
H. Jönsson ⬛ https://orcid.org/0000-0002-4912-8609

References

Abolfathi, B., Aguado, D. S., Aguilar, G., et al. 2018, ApJS, 235, 42
Andrae, R., Fouesneau, M., Creevey, O., et al. 2018, A&A, 616, A8
Asplund, M. 2005, ARA&A, 43, 481
Battistini, C., & Bensby, T. 2015, A&A, 577, A9
Bergemann, M., Kudritzki, R.-P., Plez, B., et al. 2012, ApJ, 751, 156
Blanton, M. R., Bershady, M. A., Abolfathi, B., et al. 2017, AJ, 154, 28
Carr, J. S., Sellgren, K., & Balachandran, S. C. 2000, ApJ, 530, 307
Černiauskas, A., Kučinskas, A., Klevas, J., et al. 2017, A&A, 604, A35
Chieffi, A., & Limongi, M. 2002, ApJ, 577, 281
Clayton, D. 2003, Handbook of Isotopes in the Cosmos (Cambridge: Cambridge Univ. Press)
Demarque, P., Woo, J.-H., Kim, Y.-C., & Yi, S. K. 2004, ApJS, 155, 667
Do, T., Kerzendorf, W., Konopacky, Q., et al. 2018, ApJL, 855, L5
Do, T., Kerzendorf, W., Winsor, N., et al. 2015, ApJ, 809, 143
Ernandes, H., Barbuy, B., Alves-Brito, A., et al. 2018, A&A, 616, A18
Feldmeier-Krause, A., Kerzendorf, W., Neumayer, N., et al. 2017, MNRAS, 464, 194
Frogel, J. A., Mould, J., & Blanco, V. M. 1990, ApJ, 352, 96
García Pérez, A. E., Allende Prieto, C., Holtzman, J. A., et al. 2016, AJ, 151, 144
Gehren, T., Butler, K., Mashonkina, L., Reetz, J., & Shi, J. 2001, A&A, 366, 981
Gratton, R. G., & Sneden, C. 1991, A&A, 241, 501
Gray, D. F. 2005, The Observation and Analysis of Stellar Photospheres (3rd ed.; Cambridge: Cambridge Univ. Press)
Grevesse, N., Asplund, M., & Sauval, A. J. 2007, SSRv, 130, 105
Gustafsson, B., Edvardsson, B., Eriksson, K., et al. 2008, A&A, 486, 951
Heiter, U., Jofré, P., Gustafsson, B., et al. 2015, A&A, 582, A49
Holtzman, J. A., Hasselquist, S., Shetrone, M., et al. 2018, AJ, 156, 125
Houdashelt, M. L., Bell, R. A., & Sweigart, A. V. 2000, AJ, 119, 1448
Howes, L. M., Asplund, M., Keller, S. C., et al. 2016, MNRAS, 460, 884
Iwamoto, K., Brachwitz, F., Nomoto, K., et al. 1999, ApJS, 125, 439
Jofré, P., Heiter, U., Soubiran, C., et al. 2014, A&A, 564, A133
Jofré, P., Heiter, U., Soubiran, C., et al. 2015, A&A, 582, A81
Jönsson, H., Allende Prieto, C., Holtzman, J. A., et al. 2018, AJ, 156, 126
Jönsson, H., Ryde, N., Nordlander, T., et al. 2017, A&A, 598, A100
Kučinskas, A., Steffen, M., Ludwig, H.-G., et al. 2013, A&A, 549, A14
Lomaeva, M. 2018, A&A, submitted
Majewski, S. R., Schiavon, R. P., Frinchaboy, P. M., et al. 2017, AJ, 154, 94
McLean, I. S. 2005, in High Resolution Infrared Spectroscopy in Astronomy, ed. H. U. Käufl, R. Siebenmorgen, & A. F. M. Moorwood (Berlin: Springer), 25
McLean, I. S., Prato, L., McGovern, M. R., et al. 2007, ApJ, 658, 1217
Nissen, P. E., Chen, Y. Q., Schuster, W. J., & Zhao, G. 2000, A&A, 353, 722
Nomoto, K., Kobayashi, C., & Tominaga, N. 2013, ARA&A, 51, 457
Origlia, L., Rich, R. M., Ferraro, F. R., et al. 2011, ApJL, 726, L20
Pehlivan, A., Nilsson, H., & Hartman, H. 2015, A&A, 582, A98
Pehlivan Rhodin, A., Belmonte, M. T., Engström, L., et al. 2017, MNRAS, 472, 3337
Prochaska, J. X., & McWilliam, A. 2000, ApJL, 537, L57
Rich, R. M., Ryde, N., Thorsbro, B., et al. 2017, AJ, 154, 239
Romano, D., Karakas, A. I, Tosi, M., & Matteucci, F. 2010, A&A, 522, A32
Ryde, N., Fritz, T. K., Rich, R. M., et al. 2016a, ApJ, 831, 40
Ryde, N., & Schultheis, M. 2015, A&A, 573, A14
Ryde, N., Schultheis, M., Grieco, V., et al. 2016b, AJ, 151, 1
Schultheis, M., Rojas-Arriagada, A., García Pérez, A. E., et al. 2017, A&A, 600, A14
Schultheis, M., Ryde, N., & Nandakumar, G. 2016, A&A, 590, A6
Smith, M. A., Patten, B. M., & Goldberg, L. 1989, AJ, 98, 2233
Smith, V. V., Cunha, K., Shetrone, M. D., et al. 2013, ApJ, 765, 16
Smith, V. V., Hinkle, K. H., Cunha, K., et al. 2002, AJ, 124, 3241
Smith, V. V., & Lambert, D. L. 1985, ApJ, 294, 326
Smith, V. V., & Lambert, D. L. 1986, ApJ, 311, 843
Smith, V. V., & Lambert, D. L. 1990, ApJS, 72, 387
Sneden, C., Cowan, J. J., Kobayashi, C., et al. 2016, ApJ, 817, 53
Sneden, C., Lucatello, S., Ram, R. S., Brooke, J. S. A., & Bernath, P. 2014, ApJS, 214, 26
Valenti, J. A., & Piskunov, N. 1996, A&AS, 118, 595
Valenti, J. A., & Piskunov, N. 2012, SME: Spectroscopy Made Easy, Astrophysics Source Code Library, ascl:1202.013
van Deelen, F. 2017, Master's thesis, Lund Univ., http://lup.lub.lu.se/student-papers/record/8912010
Woosley, S. E., & Weaver, T. A. 1995, ApJS, 101, 181
Zhang, H. W., Gehren, T., & Zhao, G. 2008, A&A, 481, 489

Paper IV
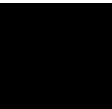
Atomic Data Needs in Astrophysics: The Galactic Center "Scandium Mystery"

Brian Thorsbro

Department of Astronomy and Theoretical Physics, Lund University, Box 43, 221 00 Lund, Sweden;
thorsbro@astro.lu.se

Abstract: Investigating the Galactic center offers unique insights into the buildup and history of our Galaxy and is a stepping stone to understand galaxies in a larger context. It is reasonable to expect that the stars found in the Galactic center might have a different composition compared to stars found in the local neighborhood around the Sun. It is therefore quite exciting when recently there were reports of unusual neutral scandium, yttrium, and vanadium abundances found in the Galactic center stars, compared to local neighborhood stars. To explain the scandium abundances in the Galactic center, we turn to recent laboratory measurements and theoretical calculations done on the atomic oscillator strengths of neutral scandium lines in the near infrared. We combine these with measurements of the hyper fine splitting of neutral scandium. We show how these results can be used to explain the reported unusual scandium abundances and conclude that in this respect, the environment of the Galactic center is not that different from the environment in the local neighborhood around the sun.

Keywords: Galactic center; stellar abundances; scandium; hyper fine splitting

---

1. Introduction

Understanding the formation and evolution of galaxies is one of the important questions in astrophysics today [1]. The Milky Way, our own Galaxy, is central as it is the galaxy we can observe in the greatest detail, both because we want to explore the world we live in and because we can use it to understand galaxies at large, assuming the mediocrity principle, i.e., that we are not special.

Our Galaxy is currently seen as a barred spiral galaxy with multiple stellar populations, often roughly classified as the halo, the thin and thick disks, the bulge, and the Galactic center [1].

Key components to understanding the formation and evolution of the Galaxy are understanding the star formation rate and the mass distribution of the formed stars [2]. The constituents of the Galaxy that are easiest to observe are its stars, and the Galactic evolution can be decoded from its stars by understanding stellar structure and evolution. Fortunately, stellar structure and evolution theories are well developed, and they allow us to model how stars evolve and eventually perish [3]. In particular, we can model what kind of chemical species are synthesized in stars and consequently distributed to the surrounding environment, from which new stars are born.

Combining galactic and stellar evolution models thus demands the study of chemical evolution models that predict the abundances of chemical species in stars at different times and locations [4]. The chemical composition of the photosphere of a star, which is the region of the star from which light escapes, changes during the life of the star as heavier elements settle. However, as the star turns into a red giant towards the end of its life, convection inside the star remixes the material, undoing the settling of the heavy elements. A few light element species produced by the fusion processes in the center of the star are transported up to the photosphere with this convection as well. Apart from that, however, one can approximately assume to observe the composition of the environment in which the star was born by observing the composition of its current photosphere. These observations are done

with stellar spectroscopy, and the abundance of chemical species in the photosphere is determined using abundance analysis, which thus enables comparisons between models and observations.

In our study, we focus on the Galactic center, which is interesting as it is an environment that is unique to the Galaxy, particularly because of the presence of the super massive black hole. This could lead to a different evolution of stars compared to the environment in the vicinity of our Sun. In order to be able to observe stars in the Galactic center, one has to turn to very bright giant stars and observe them in the infrared wavelength regions. More energetic light is absorbed and scattered away by the dust lying between the center and the Sun, and thus, it is not possible to observe the Galactic center in the visible light wavelength range.

One chemical species that is of concern here is neutral scandium. In early 2018, it was reported that unusually high amounts of scandium, together with yttrium and vanadium, might be present in the Galactic center stars [5]. A unique scandium abundance in the Galactic center would suggest that the center is a site for a new channel of nucleosynthesis of neutral scandium and possibly other elements. Such a trend is important to understand, especially when observing the centers of far away galaxies, which would be a natural choice to observe first, as the center is the most luminous part of a galaxy.

In this work, we summarize our findings first reported in Thorsbro et al. [6] and discuss the atomic data needs in astrophysics on the basis of this.

2. Results

2.1. Observations

We observed 18 stars in the Galactic center and eight stars located in the solar neighborhood. The exact information about the observations of these stars, as well as how they were analyzed were detailed by Thorsbro et al. [6], Ryde et al. [7], Rich et al. [8]. All of the stars were of similar stellar classification, denominated M giants, which means that they had an effective temperature[1] between 3000 and 4000 K. The solar neighborhood stars were observed as a control group to compare the Galactic center stars. The stars were observed with the Keck II telescope (10 m class telescope), mounted with the NIRSPECspectrograph [9]. The spectra of the stars were recorded in the near infrared wavelength region around 2 microns ($\sim$5000 cm^{-1}) with a resolving power R $= \frac{\lambda}{\Delta\lambda} \simeq$ 23,000.

In the spring of 2018, Do et al. [5] reported to have found evidence for unusual high scandium abundances in stars in the Galactic center located within a few parsecs from the super massive black hole of our Galaxy. Their observed stars displayed unusually strong scandium line features in their spectra. They argued that modeling the observed spectra with synthetic spectra from first principles was impossible unless one assumed an unusually high scandium abundance. They further compared their observed stars to a star found in a globular cluster, which was a high stellar density environment, and showed that the comparison star did not show the same unusually high abundances. It is worth noting that the comparison star had an effective temperature that was about 800 to 1000 K warmer compared to the their observed Galactic center stars.

In Figure 1, the spectra from our observations are shown as we published them in Thorsbro et al. [6]. Here, it is worth noticing that the scandium line features were strong for stars located in both the Galactic center and in the solar neighborhood. Further, for both environments, the strength of the scandium line features diminished as the temperature increased. We could thus immediately conclude that the environment of the star did not seem to be connected to the strength of the line features. To improve our understanding, we therefore investigated if there could be assumptions in the modeling from first principles that needed to be revisited.

---

[1]　effective temperature is defined by the corresponding black-body radiation curve with an equal amount of radiation to the radiation coming from the star.
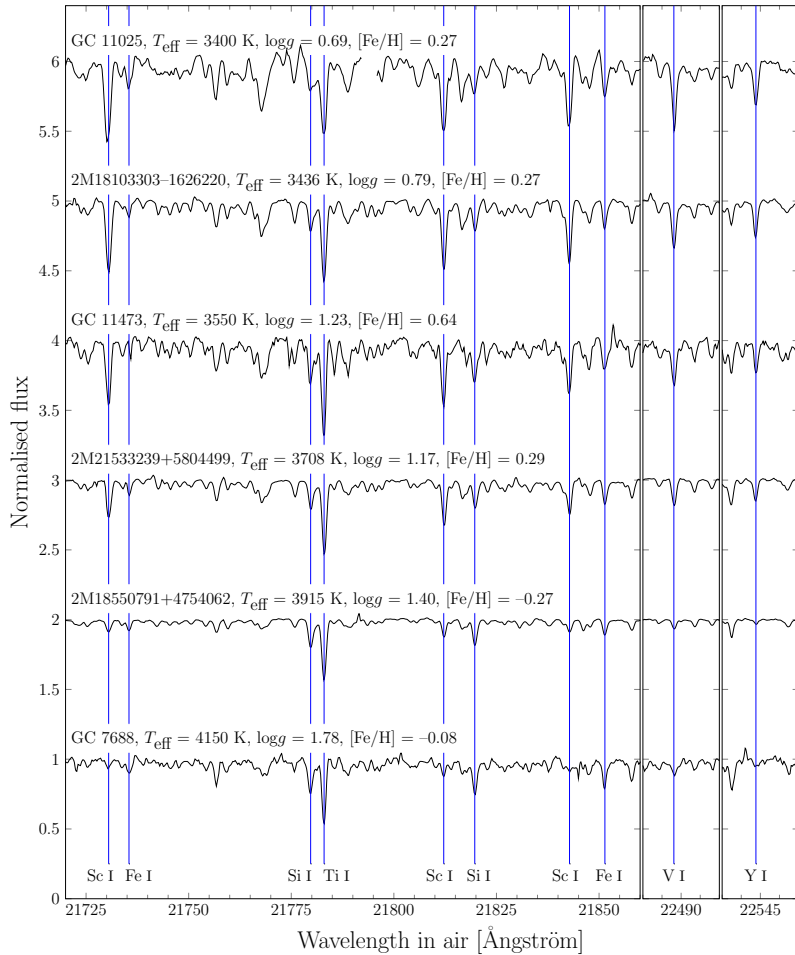
Figure 1. This figure from Thorsbro et al. [6] (their Figure 1) shows that the strong scandium feature seems to be connected to the effective temperature of the star. Six stellar spectra are plotted together with increasing temperature from top to bottom with blue vertical lines identifying lines of interest. The normalized fluxes are translated upward with integer values for presentation. The stars are a mix of three Galactic center stars (GC 7688, GC 11025, and GC 11473) and three solar neighborhood stars (2M18103303–1626220, 2M18550791+4754062, and 2M21533239+5804499). The spectra show strikingly strong scandium, vanadium, and yttrium lines in the cooler stars, even though the stars are located in widely different environments. As temperatures increase to 3900 K and beyond, the neutral lines of scandium, vanadium, and yttrium begin to vanish, presumably due to ionization.

2.2. *Analyzing the Hyperfine Structure*

The line transition in neutral scandium that is shown in Figure 1 is the $3d^24s$—$3d4s4p$ transition. Neutral scandium has a nuclear spin of $I = 7/2$, and since this transition involves an unpaired 4s-election, the hyperfine splitting is expected to be strong.

In general, there is a lack of experimental atomic data for near-IR transitions [10]. In response to this need, a program was initiated to provide accurate and vetted near-IR atomic data for stellar spectroscopy. This program was lead by Henrik Hartman and Per Jönsson at Malmö University in Sweden using the Edlén laboratory, a joint effort of Malmö and Lund universities.

Recent works measured the oscillator strengths and hyperfine structure of neutral scandium [11,12]. Both of these works utilized the Fourier transform spectrometer in the Edlén laboratory examining neutral scandium energized in a hollow cathode lamp.

In the work of Pehlivan et al. [11] intensity calibrated spectra of Sc I are used to experimentally determine branching fractions, which are then combined with radiative lifetimes from the literature [13–15] to derive accurate oscillator strengths for Sc I.

In the work of van Deelen [12], synthetic model spectra of Sc I hyperfine structure (HFS) multiplets were constructed and fitted to experimentally measured spectra. The results were compared to similar results from the literature [16–23], and investigations were initiated to examine the significant differences more closely. The work of van Deelen [12] can be considered the most recent and accurate compilation of Sc I HFS data for the near infrared wavelength region.

In the work of Thorsbro et al. [6], the theoretical line formation of a spectral Sc I line was modeled to explore the effects of both temperature and HFS, using the BSYNand EQWIDTHcodes based on routines from the MARCSmodel atmosphere code [24]. One-dimensional (1D) MARCS atmosphere models were used. These models were hydrostatic model photospheres in spherical geometry, computed assuming local thermodynamic equilibrium (LTE), chemical equilibrium, homogeneity, and conservation of the total flux (radiative plus convective, the convective flux being computed using the mixing length recipe [25]). The resulting line strength measured in equivalent width is plotted against temperature in Figure 2. For the spectral line based on a single atomic level transition, we used the measured oscillator strength from Pehlivan et al. [11]. For the HFS based spectral line, we used the combined work of Pehlivan et al. [11], van Deelen [12].

From Figure 2, it is clear that for the cooler stars, it was crucial to have the correctly modeled HFS to explain the stronger Sc I lines. That a Sc I line has an HFS means that in reality, it consists of many weaker lines. That the many weak lines appear as a single line is due to the fact that the resolution of the spectrometer is not high enough to resolve all the details and also due to different line broadening effects caused by temperature, pressure, and other conditions in the observed star that make the weak lines blend together. The onset of saturation is delayed as the many weaker lines individually saturate later compared to that of a singular strong line.
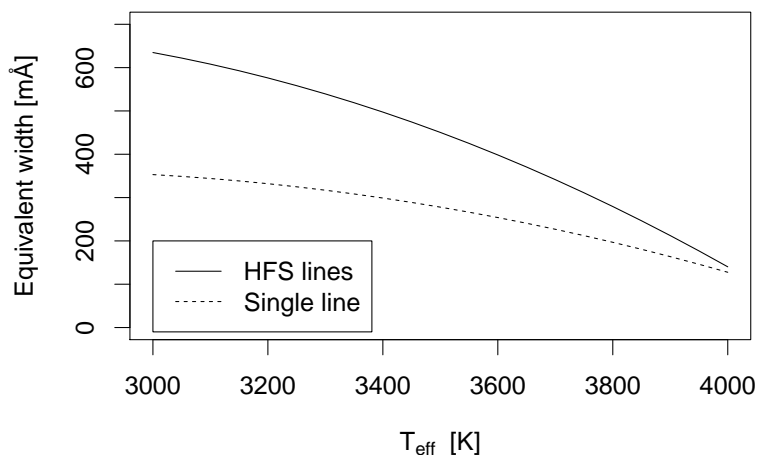
Figure 2. Figure from Thorsbro et al. [6] (their Figure 3). The equivalent width of a Sc I line as a function of temperature depends on whether the Sc I line is considered to be a combination of many small lines due to the hyperfine structure (HFS) or if the line is considered to be a singular atomic level transition. Notice how at high temperature, the two analyses converge, but at cooler temperatures, the HFS of the line enables the spectral line feature to become considerably stronger compared to basing the analysis on a singular atomic level transition. The metallicity and scandium abundance is assumed to be solar, and the surface gravity is assumed to follow isochrone relations with changing temperatures. Non-LTE and 3D effects are not considered.

2.3. Other Important Physical Effects

When it comes to accurate abundance analysis, having the correct atomic physics data is not always enough. Other effects need to be considered, like the 3D structure of the stellar atmosphere and its dynamics [26], as well as departure from local thermodynamic equilibrium [27,28]. This work recognizes that these effects are likely to be important for good abundance analysis of scandium in cool stars and therefore encourages this to be investigated further.

3. Conclusions

As shown in Figure 1, the strong scandium features found in stellar spectra dd not seem to be connected to the location of the observed star, as otherwise suggested by Do et al. [5]. Rather, it was shown by Thorsbro et al. [6] that an atomic physics approach was needed to explain the formation of strong lines, as shown in Figure 2. In particular, it was shown that the works of Pehlivan et al. [11], van Deelen [12] were needed to understand this line formation, showing that even today, there is still a need to investigate the atomic physics properties of many chemical species. The galactic center therefore did not seem to be that different from the solar neighborhood in this respect.

Abbreviations

The following abbreviations are used in this manuscript:

HFS   Hyperfine structure
LTE   Local thermodynamic equilibrium

References

1. Bland-Hawthorn, J.; Gerhard, O. The Galaxy in Context: Structural, Kinematic, and Integrated Properties. *Annu. Rev. Astron. Astrophys.* **2016**, *54*, 529–596. [CrossRef]

2. Madau, P.; Dickinson, M. Cosmic Star-Formation History. *Annu. Rev. Astron. Astrophys.* **2014**, *52*, 415–486. [CrossRef]

3. Prialnik, D. *An Introduction to the Theory of Stellar Structure and Evolution*; Cambridge University Press: Cambridge, UK, 2000.

4. McWilliam, A. Abundance Ratios and Galactic Chemical Evolution. *Annu. Rev. Astron. Astrophys.* **1997**, *35*, 503–556. [CrossRef]

5. Do, T.; Kerzendorf, W.; Konopacky, Q.; Marcinik, J.M.; Ghez, A.; Lu, J.R.; Morris, M.R. Super-solar Metallicity Stars in the Galactic Center Nuclear Star Cluster: Unusual Sc, V, and Y Abundances. *Astrophys. J. Lett.* **2018**, *855*, L5. [CrossRef]

6. Thorsbro, B.; Ryde, N.; Schultheis, M.; Hartman, H.; Rich, R.M.; Lomaeva, M.; Origlia, L.; Jönsson, H. Evidence against Anomalous Compositions for Giants in the Galactic Nuclear Star Cluster. *Astrophys. J. Lett.* **2018**, *866*, 52. [CrossRef]

7. Ryde, N.; Fritz, T.K.; Rich, R.M.; Thorsbro, B.; Schultheis, M.; Origlia, L.; Chatzopoulos, S. Detailed Abundance Analysis of a Metal-poor Giant in the Galactic Center. *Astrophys. J. Lett.* **2016**, *831*, 40. [CrossRef]

8. Rich, R.M.; Ryde, N.; Thorsbro, B.; Fritz, T.K.; Schultheis, M.; Origlia, L.; Jönsson, H. Detailed Abundances for the Old Population near the Galactic Center. I. Metallicity Distribution of the Nuclear Star Cluster. *arXiv* **2017**, arXiv:1710.0847.

9. McLean, I.S. Science Highlights from 4 Years of NIRSPEC on the Keck II Telescope. In *High Resolution Infrared Spectroscopy in Astronomy*; Käufl, H.U., Siebenmorgen, R., Moorwood, A.F.M., Eds.; Springer: Berlin/Heidelberg, Germany, 2005; p. 25.

10. Nature, E. Nailing fingerprints in the stars. *Nature* **2013**, *503*, 437. [CrossRef]

11. Pehlivan, A.; Nilsson, H.; Hartman, H. Laboratory oscillator strengths of Sc i in the near-infrared region for astrophysical applications. *Astron. Astrophys.* **2015**, *582*, A98. [CrossRef]

12. Van Deelen, F. *Hyperfine Structure Measurements in Scandium for IR Spectroscopy*; Lund University Student Paper; Lund University: Lund, Sweden, 2017.

13. Marsden, G.C.; den Hartog, E.A.; Lawler, J.E.; Dakin, J.T.; Roberts, V.D. Radiative lifetimes of even- and odd-parity levels in Sc I and Sc II. *J. Opt. Soc. Am. B Opt. Phys.* **1988**, *5*, 606–613. [CrossRef]

14. Lawler, J.E.; Dakin, J.T. Absolute transition probabilities in Sc i and Sc ii. *J. Opt. Soc. Am. B Opt. Phys.* **1989**, *6*, 1457–1466. [CrossRef]

15. Öztürk, İ.K.; Çelik, G.; Gökçe, Y.; Atalay, B.; Güzelçimen, F.; Er, A.; Basar, G.; Kröger, S. Transition probabilities of neutral scandium. *Can. J. Phys.* **2014**, *92*, 1425–1429. [CrossRef]

16. Childs, W.J. Off-Diagonal Hyperfine Structure in Sc^{45}. *Phys. Rev. A Gen. Phys.* **1971**, *4*, 1767–1774. [CrossRef]

17. Zeiske, W.; Meisel, G.; Gebauer, H.; Hofer, B.; Ertmer, W. Hyperfine structure of CW dye laser populated high lying levels of ^{45}Sc by atomic-beam magnetic-resonance. *Phys. Lett. A* **1976**, *55*, 405–406. [CrossRef]

18. Ertmer, W.; Hofer, B. Zero-field hyperfine structure measurements of the metastable states 3 d ^{2} 4 s ^{4} F $_{3/2,9/2}$ of ^{45}Sc using laser-fluorescence atomic-beam-magnetic-resonance technique. *Z. Fur Phys. A Hadron. Nucl.* **1976**, *276*, 9–14. [CrossRef]

19. Siefart, E. Calculation of the Hyperfinestructure and gJ-Values of the 3d 4s 4p-Configuration of Scandium. *Ann. Der Phys.* **1977**, *489*, 286–294. [CrossRef]

20. Singh, R.; Rao, G.N.; Thareja, R.K. Laser optogalvanic spectroscopy of ScI: Hyperfine-structure studies. *J. Opt. Soc. Am. B Opt. Phys.* **1991**, *8*, 12–16. [CrossRef]

21. Aboussaïd, A.; Carleer, M.; Hurtmans, D.; Biémont, E.; Godefroid, M.R. Hyperfine structure of Sc I by infrared Fourier transform spectroscopy. *Phys. Scr.* **1996**, *53*, 28–32. [CrossRef]

22. Krzykowski, A.; Stefańska, D. Hyperfine structure measurements of the even electron levels in scandium atom. *J. Phys. B At. Mol. Phys.* **2008**, *41*, 055001. [CrossRef]

23. Basar, G.; Basar, G.; Günay, F.; Öztürk, İ.K.; Kröger, S. Experimental Investigation of the Hyperfine Structure and Theoretical Studies of the Even Configurations of Sc I. *Phys. Scr.* **2004**, *69*, 189. [CrossRef]

24. Gustafsson, B.; Edvardsson, B.; Eriksson, K.; Jørgensen, U.G.; Nordlund, Å.; Plez, B. A grid of MARCS model atmospheres for late-type stars. I. Methods and general properties. *Astron. Astrophys.* **2008**, *486*, 951–970. [CrossRef]

25. Henyey, L.; Vardya, M.S.; Bodenheimer, P. Studies in Stellar Evolution. III. The Calculation of Model Envelopes. *Astrophys. J.* **1965**, *142*, 841. [CrossRef]

26. Scott, P.; Asplund, M.; Grevesse, N.; Bergemann, M.; Sauval, A.J. The elemental composition of the Sun. II. The iron group elements Sc to Ni. *Astron. Astrophys.* **2015**, *573*, A26. [CrossRef]

27. Zhang, H.W.; Gehren, T.; Zhao, G. A non-local thermodynamic equilibrum study of scandium in the Sun. *Astron. Astrophys.* **2008**, *481*, 489–497. [CrossRef]

28. Bergemann, M.; Nordlander, T., NLTE Radiative Transfer in Cool Stars. In *Determination of Atmospheric Parameters of B-, A-, F- and G-Type Stars*; GeoPlanet: Earth and Planetary Sciences Series; Niemczura, E., Smalley, B., Pych, W., Eds.; Springer International Publishing: Cham, Switzerland, 2014; pp. 169–185. ISBN 978-3-319-06955-5. [CrossRef]

Paper V

Detailed Abundances in the Galactic Center: Evidence of a Metal-rich Alpha-enhanced Stellar Population

B. Thorsbro[1] , N. Ryde[1] , R. M. Rich[2] , M. Schultheis[3] , F. Renaud[1] , E. Spitoni[4] , T. K. Fritz[5,6] ,
A. Mastrobuono-Battisti[1] , L. Origlia[7] , F. Matteucci[8,9,10] , and R. Schödel[11]

[1] Lund Observatory, Department of Astronomy and Theoretical Physics, Lund University, Box 43, SE-22100 Lund, Sweden; thorsbro@astro.lu.se
[2] Department of Physics and Astronomy, UCLA, 430 Portola Plaza, Box 951547, Los Angeles, CA 90095-1547, USA
[3] Observatoire de la Côte d'Azur, CNRS UMR 7293, BP4229, Laboratoire Lagrange, F-06304 Nice Cedex 4, France
[4] Stellar Astrophysics Centre, Department of Physics and Astronomy, Aarhus University, Ny Munkegade 120, DK-8000 Aarhus C, Denmark
[5] Instituto de Astrofísica de Canarias, Calle Via Láctea s/n, E-38206 La Laguna, Tenerife, Spain
[6] Universidad de La Laguna. Avda. Astrofísico Fco. Sánchez, La Laguna, Tenerife, Spain
[7] INAF—OAS Osservatorio di Astrofisica e Scienza dello Spazio di Bologna, Via Gobetti 93/3, I-40129 Bologna, Italy
[8] Dipartimento di Fisica, Sezione di Astronomia, Università di Trieste, via G.B. Tiepolo 11, I-34131, Trieste, Italy
[9] I.N.A.F. Osservatorio Astronomico di Trieste, via G.B. Tiepolo 11, I-34131, Trieste, Italy
[10] I.N.F.N. Sezione di Trieste, via Valerio 2, I-34134 Trieste, Italy
[11] Instituto de Astrofísica de Andalucía (CSIC), Glorieta de la Astronomía s/n, E-18008 Granada, Spain

Abstract

We present a detailed study of the composition of 20 M giants in the Galactic center with 15 of them confirmed to be in the nuclear star cluster. As a control sample we have also observed 7 M giants in the Milky Way disk with similar stellar parameters. All 27 stars are observed using the NIRSPEC spectrograph on the KECK II telescope in the K-band at a resolving power of $R = 23{,}000$. We report the first silicon abundance trends versus [Fe/H] for stars in the Galactic center. While finding a disk/bulge-like trend at subsolar metallicities, we find that [Si/Fe] is enhanced at supersolar metallicities. We speculate on possible enrichment scenarios to explain such a trend. However, the sample size is modest and the result needs to be confirmed by additional measurements of silicon and other α-elements. We also derive a new distribution of [Fe/H] and find the most metal-rich stars at [Fe/H] $= +0.5$ dex, confirming our earlier conclusions that the Galactic center hosts no stars with extreme chemical compositions.

Unified Astronomy Thesaurus concepts: Chemical abundances (224); Late-type stars (909); Star clusters (1567); Galactic center (565); Galaxy chemical evolution (580); Chemical enrichment (225)

1. Introduction

Nuclear star clusters are ubiquitous in galaxies: they are present in $\gtrsim$70% of early- and late-type galaxies with stellar masses above 10^8–10^{10} $M_\odot$. At greater stellar masses, their frequency decreases in early-type galaxies, but stays high in late types. Nuclear star clusters have been found to coexist with supermassive black holes (SMBH), especially at the low-mass range for SMBH. However, there are numerous cases of nuclear star clusters, where a central black hole could not be detected, i.e., has a tight upper mass limit. The masses of nuclear star clusters display scaling relationships with the masses of their host galaxies. This supports the idea that the nuclei of galaxies may have coevolved with their hosts. Reviews by Neumayer et al. (2020), Böker (2010), Neumayer (2017), and Seth et al. (2019) consider nuclear star clusters, their formation history, and their role in the evolution of galaxies.

The nuclear star cluster at the center of the Milky Way (NSC) has a half-light radius of about 5 pc (corresponding to about $2''$ at the distance of the GC), a mass of $2.5 \pm 0.4 \times 10^7 M_\odot$, is flattened along the Galactic north–south direction, and rotates parallel to the Galactic disk. The Milky Way's central black hole, Sagittarius A* (Sgr A*), is located at the precise center of the NSC. The NSC appears to be very similar to extragalactic NSCs. It is currently the only one where we can observationally resolve individual stars and it therefore plays a key role as a template for its extragalactic

counterparts (Schödel et al. 2014; Fritz et al. 2016; Neumayer et al. 2020).

The NSC is not well isolated, but lies embedded in the so-called nuclear stellar disk (NSD), a dense stellar region that has a radius of 100–200 pc and a scale height of about 45 pc (Launhardt et al. 2002). In spite of massive young clusters and other signs of ongoing massive star formation, 80%–90% of the stars in the NSD appear to have formed more than 8 Gyr ago (Nogueras-Lara et al. 2018b, 2019a).

Due to the copenetration and overlap of different stellar components along the line of sight to the GC (disk, bulge/bar, nuclear disk, and nuclear cluster) assigning membership of any given star to the NSC is a complex issue. As members of the NSC have orbits that linger at the apocenter, it is not necessary to observe stars very near the black hole to gain insights into the physical properties of the NSC. But contamination of any target sample by stars that are not in the NSC increases as a function of distance from from Sgr A*.

Two channels have been proposed to account for the presence of NSCs in galaxies (see, e.g., Neumayer 2017; Neumayer et al. 2020). (1) Inspiral via dynamical friction and subsequent merger of globular cluster like systems into the nucleus (Tremaine et al. 1975; Capuzzo-Dolcetta 1993; Antonini et al. 2012). (2) In situ formation of stars, that might result from an extended star formation history, including sharing some history with the formation of the bulge/bar population (Loose et al. 1982; Milosavljević 2004; Mapelli et al. 2012; Mastrobuono-Battisti et al. 2019). (3) Finally, a

1

channel worthy of consideration would be the capture of Galactic bulge stars on ergodic orbits; these stars might plausibly originate in nuclear disks or spirals or in bars.

In the case of the NSC we can test these scenarios by studying its stars. Very young massive stars detected in the central parsec of the Galaxy provide unambiguous evidence for current in situ star formation (Genzel et al. 2010; Feldmeier-Krause et al. 2015). Using galaxy simulations, Guillard et al. (2016) proposed a hybrid formation scenario in which clusters bring some gas with them to form a fraction of NSC stars in situ. If drawn from the Milky Way globular cluster system—even that of the bulge—such stars would be expected to contribute stars of predominantly subsolar metallicity. However, young and more metal-rich star clusters formed close to the Galactic center may also have contributed to its build up (Arca-Sedda et al. 2015).

The compositions of stars can strongly constrain which of these scenarios is dominant. Early investigations in the Galactic center, ∼tens of parsecs from Sgr A*, focused on the brightest star in the region, the M2 supergiant IRS 7 (Carr et al. 2000; Davies et al. 2009), and later extended to include other bright targets (Ramírez et al. 2000; Cunha et al. 2007). These studies commonly found $-0.2 < $ [Fe/H] $ < +0.4$ and an α-abundance in the range between about 0.0 and 0.5 dex, both in reference to solar values by Grevesse et al. (2007). Analyzing fainter red giants, most likely located more distant in the NSD, Ryde & Schultheis (2015) and Ryde et al. (2016b) find similar results, but with lower alphas.

Do et al. (2015) used medium resolution, adaptive optics-fed spectroscopy to probe the central parsec, and found some metal-poor star candidates and an extremely metal-rich abundance distribution reaching up to 10 times solar in [Fe/H]. Metal poor giants were confirmed; the high resolution abundance analysis of a metal-poor, alpha-enhanced M giant 58 pc from SgrA* was conducted by Ryde et al. (2016a). Rich et al. (2017) reported the first high resolution abundance analysis for members of the NSC, finding a wide abundance distribution with mean [Fe/H] $= -0.16$ dex extending up to $+0.6$ dex. Feldmeier-Krause et al. (2017) used medium resolution KMOS spectroscopy to derive metallicities for 700 stars in the central 4 pc². They find a significantly more metal-rich distribution (median 0.29 dex; extended to $+1$ dex). High resolution spectroscopy of two stars in the central parsec resulted in a claim by Do et al. (2018) for extreme abundances of scandium, vanadium, and yttrium in the NSC, along with iron abundances too high to measure with current atmosphere models. While our work does not have access to the central parsec, we did confirm that the lines of scandium, vanadium, and yttrium are strong in cool NSC giants (Thorsbro et al. 2018a). However, from our local disk control sample, we find these lines are also strong in cool local disk giants. Thus, the strong lines are a property of cool stars, and we attribute this strength not to an abundance increase but rather to hyperfine splitting (that delays saturation) and temperature sensitive non-LTE strengthening of the line (for more details, see Thorsbro et al. 2018a). Najarro et al. (2009) investigated two luminous blue variables in the Quintuplet cluster and find solar metallicity with enhanced α-abundances.

Investigations into variable stars are also relevant for the study of the Galactic center as RR Lyrae stars can be tracers of very old stellar populations (Minniti et al. 2016; Dong et al. 2017) and classical Cepheids can be tracers of young stellar populations Matsunaga et al. (2015) and Kovtyukh et al. (2019). At present, a handful of RR ab variables are found near the NSC from the Dong et al. (2017) study but their actual membership in the NSC remains a matter of debate.

In general α-element abundance trends have not been investigated, which would help constrain different models for the formation and evolution of the inner Galaxy (e.g., Matteucci 2012; Di Matteo 2016). Here we report a new, interesting abundance trend in [Si/Fe], from the observations of 20 M giants in the NSC and vicinity and 7 M giants observed in the Milky Way disk (MWD). This is a continuation of the work started by Ryde et al. (2016a), Rich et al. (2017), and Thorsbro et al. (2018a).

2. Observations

27 M giants have been observed at medium/high spectral resolution in the K-band using the NIRSPEC (McLean 2005; McLean et al. 2007) facility at Keck II, and are summarized in Table 1. We used the 0″432 × 12″ slit and the NIRSPEC-7 filter, giving the resolving power of $R \sim 23,000$, which is a minimum for determining accurate abundances from spectra of such cool stars. Five spectral orders are recorded, covering the wavelength range of 21000–24000 Å. However, the wavelength coverage is not complete; there are gaps between the orders.

Seven of these observed stars are located in the MWD with similar temperature ranges as the observed Galactic center stars, thus enabling them to be used as a control sample having similar systematic uncertainties. The MWD stars are presented in Thorsbro et al. (2018a), where they are important for the discussion on the strong, K-band Sc I lines detected in Galactic center stars. The other 20 stars are located in the Galactic center, of which 17 are observed under the programs U87NS (2015 April, PI: Rich) and U103NS (2016 April, PI: Rich) and presented in Ryde et al. (2016b) and Rich et al. (2017). Figure 1 shows a JHKs RGB image from the GALACTICNU-CLEUS survey (Nogueras-Lara et al. 2018a, 2019b) of the observed stars. Figure 2 shows a color–magnitude diagram (CMD) with our Galactic center M giants, color-coded with the derived metallicities (see Section 3.4), superimposed on the 2MASS sample of the Galactic center field. Our target stars have been selected over the full width of the CMD in order to avoid any selection bias. Note that the star listed as GC 7688 in Rich et al. (2017) is not included as it has been identified as a foreground bulge star. Three stars have been added to the sample, all of them observed on 2017 July 28–29, under program U103NS (PI: Rich). These are selected in the same way as the 17 original stars from low-resolution SINFONI spectra (see Rich et al. 2017). Similarly, these are observed with an ABBA scheme with a nod throw of 6″ along the slit, in order to achieve proper background and dark subtraction. The three added stars have each been exposed for 2000 s. These stars are also reduced with the NIRSPEC software redspec (Kim et al. 2015), and thereafter with IRAF (Tody 1993) to normalize the continuum, eliminate cosmic-ray hits, and correct for telluric lines. The latter has been done with a high signal-to-noise spectrum of the rapidly rotating O6.5V star HIP89584. For more details about the data reduction process, refer to Rich et al. (2017).

2

Table 1
Compiled Data for the Observed Stars Discussed in This Paper

Star Uncertainties:	K_s	R.A. (h:m:s)	Decl. (d:m:s)	T_{eff} ±150 (K)	$\log g$ ±0.3	[Fe/H] ±0.15 (dex)	ξ_{micro} ±0.15 (km s^{-1})	[Si/Fe] ±0.15 (dex)	Location
2M17584888 − 2351011	6.49	17:58:48.89	−23:51:01.17	3652	1.30	0.55	2.0	0.06	MWD
2M18103303 − 1626220	6.51	18:10:33.04	−16:26:22.06	3436	0.61	0.06	2.3	0.02	MWD
2M18191551 − 1726223	6.56	18:19:15.51	−17:26:22.35	3596	0.84	−0.02	2.2	0.00	MWD
2M18550791 + 4754062	7.63	18:55:07.92	47:54:06.22	3915	1.24	−0.20	2.0	0.07	MWD
2M19122965 + 2753128	6.60	19:12:29.66	27:53:12.83	3263	0.48	0.29	2.4	0.12	MWD
2M19411424 + 4601483	7.69	19:41:14.25	46:01:48.14	3935	1.13	−0.41	2.0	0.21	MWD
2M21533239 + 5804499	6.58	21:53:32.40	58:04:49.94	3708	1.28	0.35	2.0	−0.01	MWD
GC 25[a]	10.44	17:45:40.93	−29:00:24.39	3383	0.38	−0.08	2.5	0.08	NSC
GC 6227	11.82	17:45:38.86	−29:01:08.71	3681	0.92	−0.27	2.1	0.11	NSC[b]
GC 7104	10.74	17:45:38.94	−29:00:58.44	3657	1.09	0.30	2.0	0.20	NSD
GC 8623	10.53	17:45:41.83	−29:00:46.15	3433	0.38	−0.12	2.5	0.07	NSC
GC 8631	11.56	17:45:43.02	−29:00:46.02	3899	1.41	0.27	1.9	0.23	NSC
GC 10195	10.67	17:45:43.10	−29:00:25.45	3414	0.55	−0.01	2.4	0.03	NSC[b]
GC 10812	10.25	17:45:37.23	−29:00:16.62	3895	0.60	−1.02	2.3	0.41	NSD
GC 11025	10.41	17:45:37.13	−29:00:14.39	3359	0.64	0.25	2.3	0.25	NSC
GC 11473	11.74	17:45:42.64	−29:00:10.23	3520	1.06	0.38	2.0	0.26	NSD
GC 11532	10.90	17:45:42.90	−29:00:09.60	3450	0.48	−0.23	2.4	0.09	NSC
GC 13282	10.99	17:45:39.49	−28:59:58.74	3543	0.77	−0.04	2.2	−0.02	NSC
GC 13727	10.82	17:45:39.59	−28:59:56.21	3382	0.31	−0.28	2.5	0.15	NSC
GC 13882	10.56	17:45:38.70	−28:59:55.15	3344	0.35	−0.17	2.5	0.01	NSC
GC 14024	10.99	17:45:42.03	−28:59:54.97	3450	0.96	0.49	2.1	0.15	NSC
GC 14724	10.56	17:45:37.31	−28:59:49.43	3482	0.45	−0.32	2.4	0.14	NSC
GC 15540	10.49	17:45:41.93	−28:59:23.39	3496	0.61	0.01	2.3	0.04	NSC
GC 16763	10.66	17:45:37.29	−29:01:12.67	3510	0.58	−0.15	2.3	−0.03	NSC
GC 16867	11.77	17:45:36.02	−29:00:09.20	3628	0.76	−0.18	2.2	0.02	NSC
GC 16887	11.63	17:45:44.04	−28:59:27.66	3308	0.77	0.41	2.2	0.18	NSC
GC 16895	10.75	17:45:35.64	−29:00:47.00	3438	0.50	−0.13	2.4	0.07	NSC

Notes. We assume solar abundances of A(Fe) = 7.45 and A(Si) = 7.51 (Grevesse et al. 2007). General uncertainties are listed for each of the stellar parameters and the silicon abundances. The locations are Milky Way disk (MWD), nuclear star cluster (NSC), and nuclear stellar disk (NSD).
[a] GC 25 appears in other works and is listed as Id = 44 in Feldmeier-Krause et al. (2017) and Name = NE1–1 001 in Do et al. (2015) and Støstad et al. (2015). Note that the star listed as GC 25 in Nandakumar et al. (2018) is not the same star in spite of having the same name.
[b] GC 6227 and GC 10195 are possible background stars depending on whether they are intrinsically reddened.

3. Analysis

Our goal is to determine the $[\alpha/Fe]$-ratios as a function of metallicity for stars in the NSC and its vicinity. However, the spectra of the Galactic center stars show a surprising amount of features due to the presence of diatomic molecules, in particular, the CN molecule. To perform a good abundance analysis it is important to make sure all spectral features can be identified so a line list containing unblended lines can be constructed for good abundance analysis, see Section 3.1.

We analyze the M giant spectra using tailored synthetic spectra, calculating the radiative transfer through spherical model atmospheres. In order to derive abundances that are as accurate as possible, the fundamental input parameters for these stellar atmospheres must be well determined. These parameters are the effective temperature, T_{eff}, surface gravity, $\log g$, metallicity, [Fe/H], and the microturbulence, ξ_{micro}, of the stars. These are discussed in Sections 3.2–3.4.

In an earlier study, we analyzed a giant with $[Fe/H] \sim -1$ found in the vicinity of the NSC (Ryde et al. 2016b), measuring abundances for Mg, Si, Ca, and Ti. The remaining NSC giants are cooler and more metal-rich; molecules and blending severely limit the usable lines so that at our resolution we are able only to measure the α-element Si (see Section 3.5).

From three KECK runs, during the period 2015–2017, we have gathered spectra of a sample of 20 M giants that are all shown to be confined to the NSC and near vicinity (see Section 3.6).

3.1. Line List

In order to synthesize the spectra, an accurate line list is required. In the list provided by Thorsbro et al. (2018b) wavelengths and line strengths (astrophysical log gf-values) are updated using the solar center intensity atlas (Livingston & Wallace 1991). We have also made use of recent laboratory measurements of atomic line strengths of Mg I and Sc I (Pehlivan et al. 2015; Pehlivan Rhodin et al. 2017), as well as of Si I (Pehlivan Rhodin et al., 2020) in the K-band. Of approximately 700 identified, interesting spectral lines for cool stars, about 570 lines have been assigned new values.

As molecular lines have a crucial impact in terms of blending, we include molecular lines in the line list. For CN we include the list from Sneden et al. (2016), which is the most dominant molecule apart from CO, whose lines dominate in the 2.3 μm band head region. The CO line data are from Goorvitch (1994). At the shorter wavelengths of our spectra region, SiO, H_2O, and OH are important. Line lists for these molecules are included in our line list from, respectively, Langhoff & Bauschlicher (1993), Barber et al. (2006), and Brooke et al. (2016).
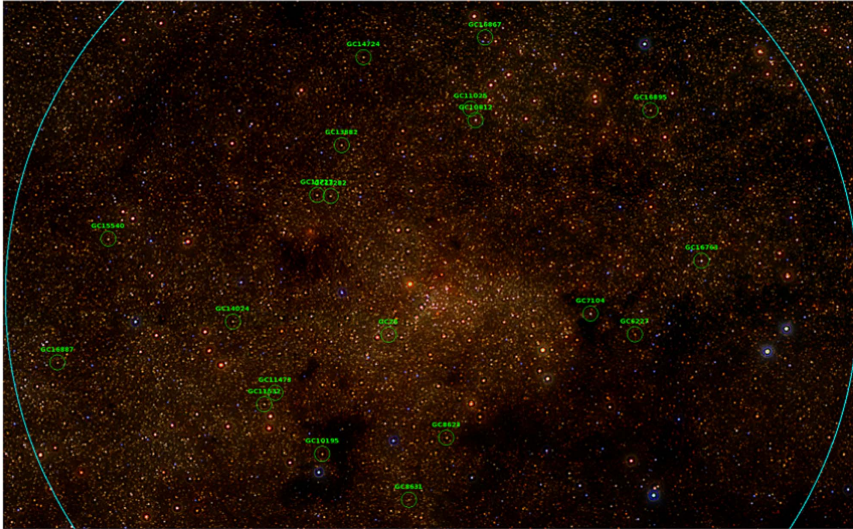
3

Figure 1. JHKs RGB image from the GALACTICNUCLEUS survey (Nogueras-Lara et al. 2018a, 2019b) marking the observed stars in the region inside the 3.5 pc projected distance from Sgr A* illustrated with the blue circle.
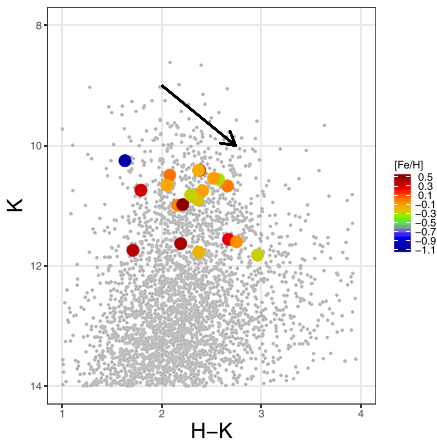

Figure 2. 2MASS K vs. H–K diagram in the NSC superimposed by our sample of 20 M giants colored by metallicity (see Section 3.4).

To identify clean spectral lines suitable for measurement, we examine synthetic model spectra of cool M giants to identify iron lines that are not blended with molecular features. The CN line list used (Sneden et al. 2016) has been shown to reproduce the observed CN spectrum very well, and can be used to identify blends. Unknown blends might still always be present

and special care has been taken when such possible mismatches are identified. Examples of lines that are not blended are illustrated in Figure 3, where an Fe I line and a Si I line are shown.

For the determination of Fe and Si abundances the lines shown in Table 2 have been identified as good lines with little or no blending.

3.2. Effective Temperature, T_{eff}

The effective temperatures of the stars in the MWD are obtained following Thorsbro et al. (2018a), where the temperatures from the APOGEE Data Release 14 (Blanton et al. 2017; Majewski et al. 2017; Abolfathi et al. 2018) were examined and then adopted.

To determine the temperatures of the stars in the Galactic center we rely on the method of Schultheis et al. (2016) as employed in Rich et al. (2017), which is based on using low-resolution SINFONI (Eisenhauer et al. 2003) spectra and measures an index of the CO band head at 2.3 μm. Rich et al. (2017) determined the effective temperatures for 17 of the 20 Galactic center stars in our sample. The same method is used for determining the temperature for the added stars, namely GC 8623 and GC 13727. We do not have SINFONI spectra for the GC 25 star and thus it remains undetermined using the CO band head method. The CO band head temperatures are shown in Table 3 in the "CO band" column.

To decrease the uncertainty in the determined temperatures for the stars in the Galactic center and to increase the correlation between the temperatures of the stars in the MWD stars and the stars in the Galactic center, we use the fact that there are strong Sc I lines in the K-band spectrum that
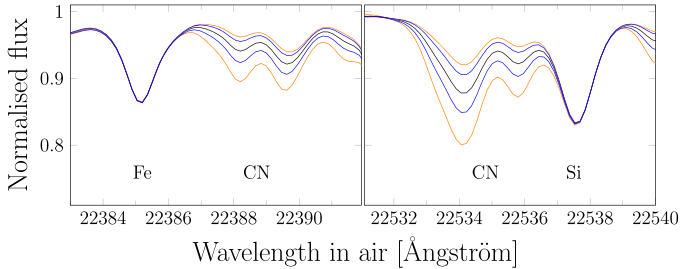
Figure 3. Synthetic model spectra for a star with solar metallicity at 3600 K effective temperature. The black line shows typical M giant abundances of carbon and nitrogen, the blue lines show the effect of varying the nitrogen abundance by ±0.2 dex, and the orange lines show a variation in the carbon abundance of ±0.2 dex. The Fe I line shown in the left plot and the Si I line in the right plot are not blended with CN molecules. For the stars we are investigating, CN blends are very common in the near-infrared, so finding unblended lines is crucial.

<table>
<tr><td colspan="3" align="center">Table 2
Lines Used for Abundance Determinations</td></tr>
</table>

Wavelength in Air (Å)	E_{exc} (eV)	log gf
Fe I		
21178.211	3.0173	−4.201
21238.509	4.9557	−1.281
21284.348	3.0174	−4.414
21851.422	3.6417	−3.506
22380.835	5.0331	−0.409
22385.143	5.3205	−1.536
22392.915	5.0996	−1.207
22419.976	6.2182	−0.226
Si I		
21354.249	6.2228	0.138
21368.693	7.3288	−1.905
21874.199	6.7206	−0.731
21879.345	6.7206	0.384
21924.981	7.0645	−1.269
22537.593	6.6161	−0.216

<table>
<tr><td colspan="4" align="center">Table 3
Analysis of the Effective Temperature of Stars in the Galactic Center</td></tr>
</table>

Star	CO band T_{eff} (K)	Scandium T_{eff} (K)	Mean T_{eff} (K)
GC 25	...	3383	3383
GC 6227	3800	3561	3681
GC 7104	3750	3563	3657
GC 8623	3415	3451	3433
GC 8631	3900	3897	3899
GC 10195	3500	3327	3414
GC 10812	3800	3990	3895
GC 11025	3400	3318	3359
GC 11473	3550	3489	3520
GC 11532	3500	3399	3450
GC 13282	3700	3386	3543
GC 13727	3372	3391	3382
GC 13882	3300	3387	3344
GC 14024	3650	3249	3450
GC 14724	3600	3364	3482
GC 15540	3600	3391	3496
GC 16763	3600	3419	3510
GC 16867	3650	3606	3628
GC 16887	3500	3116	3308
GC 16895	3450	3425	3438

are very temperature sensitive in the 3000–4000 K range (e.g., Thorsbro et al. 2018a). The effects of different scandium abundances, surface gravities, or metallicities are a second-order effect. Most of our observed stars are within this temperature range and the strengths of these lines should therefore be able to be used as a temperature indicator. We measure the equivalent widths for a set of scandium lines in the MWD stars for which the effective temperatures are known. We create four linear relations between the effective temperature and the equivalent widths of the four scandium lines at the following wavelengths in air: 21730 Å, 21812 Å, 21842 Å, and 22394 Å. Using the equivalent widths measured in the spectra of the Galactic center stars together with these empirical relations, and taking the average of the four results (having standard deviations on the order of 50 K), we can thus determine the effective temperature of the Galactic center stars. The effective temperatures determined this way are given in Table 3 under the column "Scandium."

Comparing the effective temperature values found in Table 3, and with a general uncertainty of 150–200 K, we find that the results from the different methods are in general agreement. We decide to take an average of the values, and

keep a conservative estimate of 150 K uncertainty for the effective temperature values. These temperatures are given in the "Mean" column in Table 3. For GC 25, we use the temperature determined from the Sc I lines.

3.3. Surface Gravity, log g, and Microturbulence, ξ_{micro}

Rich et al. (2017) demonstrated that in spite of the distance to the stars in the Galactic center being known to a good degree, the photometrically determined surface gravities are plagued with large uncertainties due to the patchy extinction. To determine surface gravity, log g, we instead benefit from the fact that isochrones of old (>1 Gyr) M giants are quite insensitive to the age of the star. This reduces isochrones to depend on surface gravity, effective temperature, and metallicity. We thus use a grid of Yonsei–Yale isochrones (Demarque et al. 2004) to determine log g given an effective temperature and metallicity. The construction and validation of this method is described in more detail in Rich et al. (2017).

5

The microturbulence, ξ_{micro}, that takes into account the small scale, nonthermal motions in the stellar atmospheres, is important for saturated lines, influencing their line strengths. We estimate this parameter from an empirical relation with the surface gravity based on a detailed analysis of spectra of five red giant stars ($0.5 < \log g < 2.5$) by Smith et al. (2013), as described in Rich et al. (2017).

The estimated uncertainty of 150 K for the effective temperatures propagates into an uncertainty of 0.3 for $\log g$ and 0.15 km s^{-1} for ξ_{micro}.

3.4. Metallicity, [Fe/H]

The metallicities of our stars are important not only for identifying the model atmosphere for a certain star but also for the metallicity distribution function (MDF), which is an important diagnostic for the discussion of the origin of the nuclear star cluster, see Section 4.

In order to determine metallicities we synthesize spectra and compare them to the observed spectra. We have chosen to use the spectral synthesis code Spectroscopy Made Easy (SME; Valenti & Piskunov 1996, 2012), which interpolates in a grid of one-dimensional (1D) MARCS atmosphere models (Gustafsson et al. 2008). These are hydrostatic model atmospheres in spherical geometry, computed assuming LTE, chemical equilibrium, homogeneity, and conservation of the total flux (radiative plus convective, the convective flux being computed using a mixing-length recipe). This code has the advantage that it includes a flexible χ^2 minimization tool for finding the solution that fits an observed spectrum the best in a prespecified spectral window. It also has a powerful continuum normalization routine. In cool star spectra, extra care is needed to normalize the spectrum in the region of a spectral line under consideration. The ubiquitous molecules and unavoidable residuals from the telluric line division necessitates a careful analysis line by line.

We recognize that using 3D atmospheric models would be an improvement over 1D atmospheric models (Scott et al. 2015b, 2015a). However, for this differential study we expect to see the same systematics to be present in both the Galactic center and the MWD stellar samples.

As a result of our updated temperatures and careful work on the line list, especially the new analysis of lines blended with CN, we reanalyze the [Fe/H] values given in Rich et al. (2017). The new [Fe/H] values are shown in Table 1, with a general estimated uncertainty of 0.15 dex. A comparison of our new [Fe/H] distribution function (MDF) with that of Rich et al. (2017) is shown in Figure 4.

Principally due to our new treatment of CN blending, our iron abundances have changed compared to earlier work; for example, the most metal-rich star now is [Fe/H] = +0.5, compared to +0.64 in Rich et al. (2017). We consider the present abundance distribution reported in this work to be the best current measurement of [Fe/H] and its range in the NSC.

3.5. α-Element Abundance Determination

The α-element abundances can potentially be measured from several lines from different species. However, considering the line strengths and number of unblended lines, there are only a few elements possible in the available wavelength region at the spectral resolution considered. The available Mg I lines are heavily blended with CN molecular lines and the strengths of
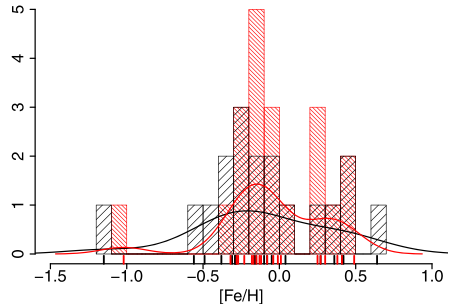

Figure 4. Determined metallicity distribution function (MDF) in red compared to that of Rich et al. (2017) in black. The reanalysis of the stellar parameters in this work does not significantly change the MDF of the nuclear stellar cluster.
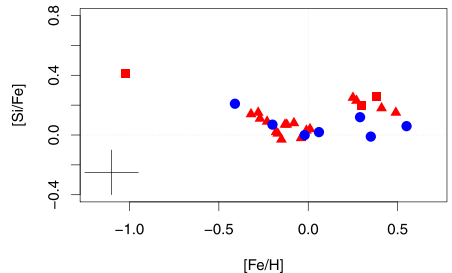

Figure 5. [Si/Fe] vs. [Fe/H]. Red triangles and squares are nuclear star clusters and nuclear stellar disk stars; blue disks are the Milky Way disk stars.

the Ti I and Ca I lines increase conspicuously with cooler effective temperature, broadly similar to the Sc I lines discussed in detail by Thorsbro et al. (2018a). This behavior argues strongly for non-LTE effects affecting the line strengths more than the abundances. Since no non-LTE corrections are available for these elements in the temperature range that our stars span, these lines cannot yet be used for determining the abundances. Si I, however, has several suitable lines and most importantly, non-LTE departure coefficient calculations show that departure from LTE is not important for Si I lines in the stellar parameter space of the stars in our sample. We verified this by examining the departure coefficients in MARCS model giant stars, using the atomic model presented in Amarsi & Asplund (2017), which utilizes the rather efficient inelastic hydrogen collisions of Belyaev et al. (2014).

The α-element abundance is therefore determined from the unblended Si I lines available (Table 2) with a general estimated uncertainty of 0.15 dex. Typical spectra are shown in Figure 6. The silicon abundances are shown in Figure 5 with the Galactic center stars marked with red triangles and squares, the latter for those not identified to be in the NSC (see Section 3.6), and the MWD stars are marked with blue disks.

We now examine more closely those metal-rich stars with Si enhancement. Figure 6 shows our observed spectra for the metal-rich subset giving an extra sanity check on the
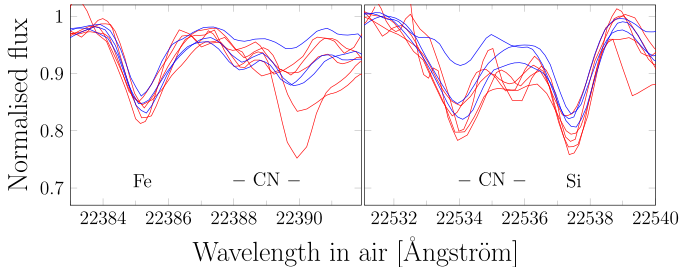
Figure 6. Observed spectra of the subset of stars from our sample with supersolar metallicities showing an unblended Fe I line and an unblended Si I line. Blue spectra for Milky Way disk stars, and red spectra for Galactic center stars. The Si I lines are visibly deeper for the Galactic center stars compared to the Milky Way disk stars, while the Fe I lines show negligible variation.

abundance results. The plot indicates stronger silicon features when comparing the Galactic center stars to the MWD stars, but the Fe I line does not show the strong difference we see in the Si I line. This figure shows that, independent of any abundance analysis, we can see that Si appears to be enhanced in the Galactic center for this subset of stars.

3.6. Stellar Dynamics and Positions

We examine the stellar dynamics of the three stars added to our data set to verify if they belong to the NSC. Second, we also check with "metal-rich" stars, [Fe/H] > 0.1, that differ in their position or dynamics.

As in Ryde et al. (2016a) and Rich et al. (2017) we use the H–K color, which is nearly only caused by extinction for testing whether the stars are currently in the NSC in the line-of-sight direction. We find that the $v_{\rm rad}^{\rm LSR}$ for the added stars GC 25, GC 8623, and GC 13727 are, respectively, 83, −20, and −125 km s^{-1} from the Keck spectra. These velocities are consistent with the lower precision values in Fritz et al. (2016). For the proper motions we use Fritz et al. (2016) as we did previously; see Figure 7. The new stars are all likely members of the NSC; see Figure 7.

As is visible in Figure 7 we do not find differences between the three added stars or the different metallicity groups. All stars seem to belong to the same hot system with a weak rotation aligned with the Galaxy. The sample, especially of stars with proper motions, is still too small to detect minor differences. We note that three stars, GC 10812, GC 7104, and GC 11473, have a preferred location in the NSD, of which the latter two are in the metal-rich set. Two of the stars, GC 6227 and GC 10195, could possibly be background stars, depending on if they are intrinsically reddened. While effects like motion can lead to exchange between the NSC and the NSD, it is still prudent to account for the possibility that some of these stars may reside in the NSD when explaining the enrichment pattern. However, there is still a need for a Galaxy model that includes all four central components (Sgr A*, the NSC, the NSD, and the bar/bulge) to better constrain the location of the stars. Mixing of stars is also a concern to take note of, at the projected distance of 2 pc from Sgr A* there may be about one NSD star for every three to four NSC stars (Gallego-Cano et al. 2020).

In the line of sight it seems that there could be a larger metallicity range in the NSD than in the NSC, since, of the three stars there, none are normal metallicity stars. Given the

low number of stars, this could be possible by pure chance since Do et al. (2015) and Feldmeier-Krause et al. (2017) find metal-poor stars that are at least projected NSC members.

4. Results and Discussion

A new analysis of iron lines including the most comprehensive currently available CN line list confirms that our sample's most metal-rich star has [Fe/H] $\sim$ +0.5. Our work continues the trend of recent work (Ryde & Schultheis 2015; Rich et al. 2017; Nandakumar et al. 2018) that finds stars with metallicity higher than solar but no evidence in the NSC for extreme metallicities. We therefore cannot confirm the assertion of Do et al. (2015) and Feldmeier-Krause et al. (2017) that stars in the NSC have [Fe/H] at or very close to +1 dex.

We have also reported the first trend of [Si/Fe] versus [Fe/H] for giants in the NSC and its vicinity. Below solar metallicity, we largely confirm the initial study of similar giants in the nuclear disk by Ryde & Schultheis (2015). However, our new results show for the first time a jump in [Si/Fe] to +0.2 dex, for [Fe/H] > 0. This particular trend has not been observed in any other stellar population. We emphasize that the sample size is small and the uncertainties of the abundances for Si and Fe in quadrature are $\sim$0.2 dex, so it is clear that a confirmation using a larger sample, and additional α-element lines is an essential next step. In Figure 8 we compare the [Si/Fe] abundance ratio as a function of [Fe/H] distribution of our samples of NSC (red triangles), NSD (red squares), and MWD (blue triangles) stars with those of giants (gray dots; Johnson et al. 2014) and microlensed dwarfs (black dots) in the bulge (Bensby et al. 2013). We find that our NSC and MWD samples fit the lower envelope of the bulge star distribution up to about solar [Fe/H]. The supersolar stars in the NSC and NSD show enhanced Si abundance compared to our disk and bulge stars.

It is also interesting to compare the properties of the NSC with those of the complex stellar system Terzan 5 in the bulge, which has multiple populations spanning 1.3 dex in metallicity (e.g., Origlia et al. 2011, 2013). Of special note are the two populations at [Fe/H] = −0.3 dex and [Fe/H] = +0.3 dex; these two populations have [Si/Fe] = +0.34 and [Si/Fe] = +0.03, respectively, with some stars in the metal-rich group having subsolar [Si/Fe]. The ages of these populations have been constrained by Ferraro et al. (2016) and Origlia et al. (2019). The subsolar component with α-enhancement was dated at 12 Gyr, while a younger turnoff of age 4.5 Gyr appears
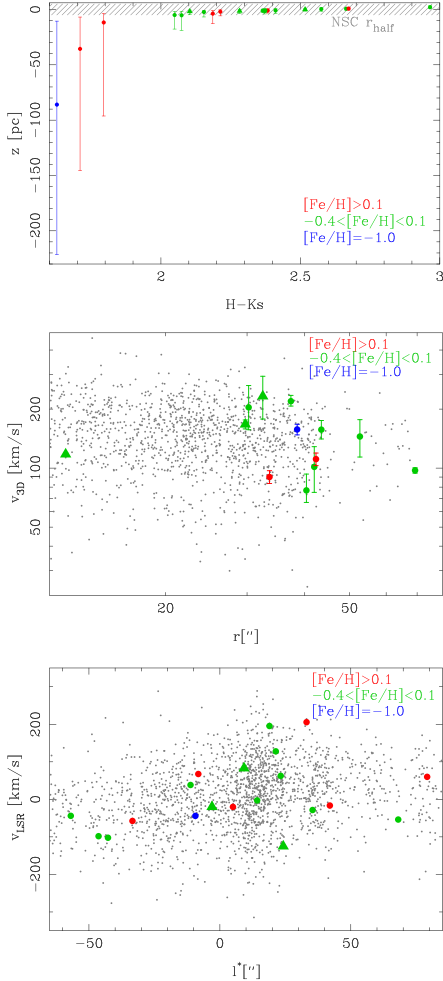
7

Figure 7. Comparison of sample stars in dynamic and position properties, in all plots the three new stars are plotted as triangles and the old ones as solid circles. The color indicates the metallicity group. Top: the line-of-sight position of all stars compared to the NSC. The NSD covers the full displayed range. Middle: total velocity; not all stars are shown here, because some are missing proper motions. Bottom: LSR corrected line-of-sight velocity vs. Galactic longitude relative to Sagr A*. Only stars outside the central 10″ are shown, since there the black hole increases velocities.

to be responsible for the metal-rich component with about solar-scaled alpha. The trend in [α/Fe] versus [Fe/H] appears reversed in the NSC compared to Terzan 5, with the α-enhancement rising at high metallicity, but other α-elements
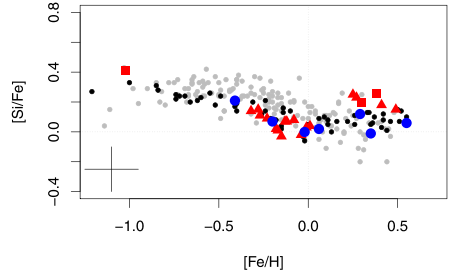
Figure 8. [Si/Fe] vs. [Fe/H]. Red triangles and squares are nuclear star clusters and nuclear stellar disk stars; blue disks are the Milky Way disk stars; gray dots are bulge giants from Johnson et al. (2014); black dots are microlensed bulge dwarfs from Bensby et al. (2013).

need to be measured before drawing firm conclusions. The contrast of these two systems is of great interest, and illustrates how chemical evolution can play out differently, even in systems of very similar metallicity.

4.1. Chemical Enrichment Scenarios

Assuming that the enhancement in Si is also present in other α-elements, the origin of the NSC populations is even more intriguing and we can speculate on possible formation and chemical enrichment scenarios. Some of the key questions for this investigation is ages of stars and the source of gas for star formation.

As per the discussion on Terzan 5 above, the subsolar and supersolar metallicity stars of the NSC can be seen as two groups of stars, and it would be interesting to ponder if there is a clear age dichotomy between them. Unfortunately, isochrone dating of the NSC is not possible because currently we can only observe bright giants near the tip.

We use chemical evolution models (Matteucci 2012; Grieco et al. 2015) to explore the chemical enrichment history of the NSC as traced by the subsolar metallicity stars with about solar-scaled alphas and supersolar metallicity stars with enhanced α-elements. The models assume that at the very early epoch of the galaxy and bulge formation a star formation episode occurred with punctual (and probably local) high star formation rates, i.e., mini-starburst activity. The type-II super-novae formed during such a burst would then inject α-elements within a few megayears The depth of the gravitational potential well of the Galactic center could help retain or rapidly reaccrete this enriched gas (Emsellem et al. 2015), and possibly form the population presented above, before the outbreak of SNe Ia (that would lower the [α/Fe] content of the interstellar medium). This early and massive star-forming episode could be followed by a recent starburst that occurred a few gigayears ago (Pfuhl et al. 2011; Nogueras-Lara et al. 2019a, R. Schödel et al. 2020, in preparation), but the origin of the gas and its retention in the NSC remain a challenge.

We first explore a model where a starburst is initiated by a sudden accretion of gas, either primordial or slightly enriched, which results in a dilution of chemical abundances (e.g., Fe). The model is illustrated in Figure 9, where the dilution of chemical abundances appears on the plot as a horizontal line followed by an increase of the [α/Fe] ratio. This is due to the
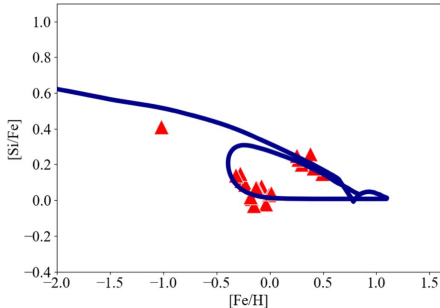
8

Figure 9. Chemical evolution model with a sudden accretion of primordial gas 2.5 Gyr ago adopting a Salpeter (1955) IMF. The blue line shows the [Si/Fe] vs. [Fe/H] trend of the gas from which stars are formed. Simplified, the line follows a time line from the upper left, down toward the bottom right as gas is consumed by star formation and enriched by Type II SNe and SNe Ia. A sudden infall of primordial or slightly enriched gas dilutes the gas resulting in a horizontal line toward the left. As the density of the gas increases the star formation increases, for instance, in a burst if the gas infall is rapid enough, at which an enrichment of Si by Type II SNe occurs until the time when the burst is diluted by the Type I SNe. During periods of low density, few or no stars are formed, and therefore we do not expect observe stars uniformly populating the track.

contribution of core-collapse SNe II in the starburst, followed by a decrease due to the Fe production from SNe Ia. This behavior appears as a loop, as one can see in Figure 9. This kind of behavior has been shown also by Johnson & Weinberg (2019) studying starbursts and by Spitoni et al. (2019) and Calura & Menci (2009) in connection with the Galactic disk. In this scenario the super-solar NSC stars could be either as old or as young as the subsolar stars.

To trigger a recent starburst episode, gas needs to be accreted either from other regions of the Galaxy or from an extragalactic origin. In the former case, torques from the bar drive gas inflows toward the center. It is, however, not clear why such inflow should be intermittent (as required to explain a sudden burst). Simulations of the Milky Way show that discrete accretion events could be due to the fragmentation of the inflowing gas from the central molecular zone (CMZ) at the inner Lindblad resonance (Renaud et al. 2013; Krumholz & Kruijssen 2015). The other possibility is the accretion of gas from extragalactic origin, for instance from a satellite galaxy tidally stripped during a passage near the Milky Way's center, i.e., on a rather radial trajectory. The gas stripped from a low-mass galaxy would have very low metallicity, whereas the gas from the CMZ could be near or above solar metallicity (Morris & Serabyn 1996).

Alternatively, we explore a different chemical evolution model where we suppose a pause in the star formation (see Figure 10 where pauses of several lengths are assumed). In these cases, no extra infall event is assumed, but the star formation simply starts again after the stop. As one can see from Figure 10, in this case there is also a loop but not a horizontal decrease of [Fe/H]. Here, the loop results from α-elements decreasing during the pause as Fe continues to be produced by SNe Ia, although less than in the star formation regime. When star formation reignites the [α/Fe] ratio increases and then decreases, as explained above.
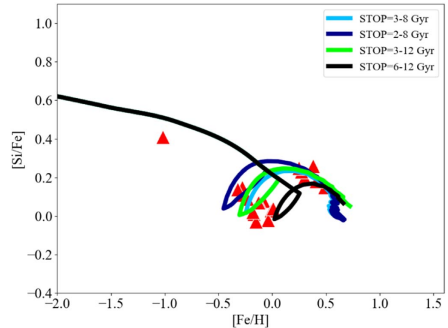

Figure 10. Chemical evolution models varying the temporal extent of the stop in star formation with a Salpeter (1955) IMF. All the cases are characterized by a reignition of the SF after the stop. See the description in Figure 9 for how to interpret the line.

The main differences between the two scenarios are the extra infall (starburst) and the efficiency of star formation. In the burst case, there is extra infall and the efficiency is high both before and during the starburst, whereas in the case of the pause in the star formation the efficiency is lower especially at the beginning but high after the reignition. The reason for this is that with a high star formation efficiency, as in some models of the classical bulge/bar (Matteucci et al. 2019), the gas is consumed quickly leaving too little to trigger star formation after the pause (a similar behavior was suggested by Matteucci et al. 2019 for the bulge). In the case of the bulge it was suggested that buckling of the bar could be the agent responsible for the pause in star formation.

Further investigations into modeling the alpha enrichment of supersolar metallicity stars in the NSC and vicinity is called for, and we will investigate this in an upcoming paper.

5. Conclusions

We report the first trend of [Si/Fe] versus [Fe/H] for giants in the nuclear star cluster and vicinity. The new trend differs clearly from the local disk; giants with supersolar metallicity show a +0.2 dex enhancement in [Si/Fe] relative to the stars in the local disk. Such an enhancement is also exceeding the values measured in the bulge.

In agreement with many studies of the inner and outer bulge, we find the most metal-rich stars in the NSC to reach [Fe/H] = +0.5, and exhibit no evidence of more extreme composition.

We emphasize that our current sample size is modest, and it is now of critical importance to increase the sample size, and to seek confirmation of the trend using other alpha elements. This will allow us to perform a detailed analysis of the origin and evolution of the NSC populations by exploring different chemical enrichment scenarios.

9

Facility: KECK:II (NIRSPEC).

Software: SME (Valenti & Piskunov 1996, 2012), RED-SPEC (Kim et al. 2015), IRAF (Tody 1993), BSYN & EQWIDTH (Gustafsson et al. 2008).

ORCID iDs

B. Thorsbro https://orcid.org/0000-0002-5633-4400
N. Ryde https://orcid.org/0000-0001-6294-3790
R. M. Rich https://orcid.org/0000-0003-0427-8387
M. Schultheis https://orcid.org/0000-0002-6590-1657
F. Renaud https://orcid.org/0000-0001-5073-2267
E. Spitoni https://orcid.org/0000-0001-9715-5727
T. K. Fritz https://orcid.org/0000-0002-3122-300X
A. Mastrobuono-Battisti https://orcid.org/0000-0002-2386-9142
L. Origlia https://orcid.org/0000-0002-6040-5849
F. Matteucci https://orcid.org/0000-0001-7067-2302
R. Schödel https://orcid.org/0000-0001-5404-797X

References

Abolfathi, B., Aguado, D. S., Aguilar, G., et al. 2018, ApJS, 235, 42
Amarsi, A. M., & Asplund, M. 2017, MNRAS, 464, 264
Antonini, F., Capuzzo-Dolcetta, R., Mastrobuono-Battisti, A., & Merritt, D. 2012, ApJ, 750, 111
Arca-Sedda, M., Capuzzo-Dolcetta, R., Antonini, F., & Seth, A. 2015, ApJ, 806, 220
Barber, R. J., Tennyson, J., Harris, G. J., & Tolchenov, R. N. 2006, MNRAS, 368, 1087
Belyaev, A. K., Yakovleva, S. A., & Barklem, P. S. 2014, A&A, 572, A103
Bensby, T., Yee, J. C., Feltzing, S., et al. 2013, A&A, 549, A147
Blanton, M. R., Bershady, M. A., Abolfathi, B., et al. 2017, AJ, 154, 28
Böker, T. 2010, in IAU Symp. 266, Star Clusters: Basic Galactic Building Blocks Throughout Time and Space, ed. R. de Grijs & J. R. D. Lépine (Cambridge: Cambridge Univ. Press), 58
Brooke, J. S. A., Bernath, P. F., Western, C. M., et al. 2016, JQSRT, 168, 142
Calura, F., & Menci, N. 2009, MNRAS, 400, 1347
Capuzzo-Dolcetta, R. 1993, ApJ, 415, 616
Carr, J. S., Sellgren, K., & Balachandran, S. C. 2000, ApJ, 530, 307
Cunha, K., Sellgren, K., Smith, V. V., et al. 2007, ApJ, 669, 1011
Davies, B., Origlia, L., Kudritzki, R.-P., et al. 2009, ApJ, 694, 46
Demarque, P., Woo, J.-H., Kim, Y.-C., & Yi, S. K. 2004, ApJS, 155, 667
Di Matteo, P. 2016, PASA, 33, e027
Do, T., Kerzendorf, W., Konopacky, Q., et al. 2018, ApJL, 855, L5
Do, T., Kerzendorf, W., Winsor, N., et al. 2015, ApJ, 809, 143
Dong, H., Schödel, R., Williams, B. F., et al. 2017, MNRAS, 471, 3617
Eisenhauer, F., Abuter, R., Bickert, K., et al. 2003, Proc. SPIE, 4841, 1548
Emsellem, E., Renaud, F., Bournaud, F., et al. 2015, MNRAS, 446, 2468
Feldmeier-Krause, A., Kerzendorf, W., Neumayer, N., et al. 2017, MNRAS, 464, 194
Feldmeier-Krause, A., Neumayer, N., Schödel, R., et al. 2015, A&A, 584, A2
Ferraro, F. R., Massari, D., Dalessandro, E., et al. 2016, ApJ, 828, 75
Fritz, T. K., Chatzopoulos, S., Gerhard, O., et al. 2016, ApJ, 821, 44
Gallego-Cano, E., Schödel, R., Nogueras-Lara, F., et al. 2020, A&A, 634, 71
Genzel, R., Eisenhauer, F., & Gillessen, S. 2010, RvMP, 82, 3121
Goorvitch, D. 1994, ApJSS, 95, 535
Grevesse, N., Asplund, M., & Sauval, A. J. 2007, SSRv, 130, 105
Grieco, V., Matteucci, F., Ryde, N., Schultheis, M., & Uttenthaler, S. 2015, MNRAS, 450, 2094
Guillard, N., Emsellem, E., & Renaud, F. 2016, MNRAS, 461, 3620
Gustafsson, B., Edvardsson, B., Eriksson, K., et al. 2008, A&A, 486, 951
Johnson, C. I., Rich, R. M., Kobayashi, C., Kunder, A., & Koch, A. 2014, AJ, 148, 67
Johnson, J. W., & Weinberg, D. H. 2019, arXiv:1911.02598
Kim, S., Prato, L., & McLean, I. 2015, REDSPEC: NIRSPEC Data Reduction, v. 2.5., Astrophysics Source Code Library, ascl:1507.017
Kovtyukh, V. V., Andrievsky, S. M., Martin, R. P., et al. 2019, MNRAS, 489, 2254
Krumholz, M. R., & Kruijssen, J. M. D. 2015, MNRAS, 453, 739
Langhoff, S. R., & Bauschlicher, C. W. 1993, CPL, 211, 305
Launhardt, R., Zylka, R., & Mezger, P. G. 2002, A&A, 384, 112
Livingston, W., & Wallace, L. 1991, An Atlas of the Solar Spectrum in the Infrared from 1850 to 9000cm⁻¹ (1.1 to 5.4 micrometer) (Tucson, AZ: National Solar Observatory)
Loose, H. H., Kruegel, E., & Tutukov, A. 1982, A&A, 105, 342
Majewski, S. R., Schiavon, R. P., Frinchaboy, P. M., et al. 2017, AJ, 154, 94
Mapelli, M., Hayfield, T., Mayer, L., & Wadsley, J. 2012, ApJ, 749, 168
Mastrobuono-Battisti, A., Perets, H. B., Gualand ris, A., Neumayer, N., & Sippel, A. C. 2019, MNRAS, 490, 5820
Matsunaga, N., Fukue, K., Yamamoto, R., et al. 2015, ApJ, 799, 46
Matteucci, F. 2012, Chemical Evolution of Galaxies (Berlin: Springer)
Matteucci, F., Grisoni, V., Spitoni, E., et al. 2019, MNRAS, 487, 5363
McLean, I. S. 2005, in High Resolution Infrared Spectroscopy in Astronomy, ed. H. U. Käufl, R. Siebenmorgen, & A. F. M. Moorwood (Berlin: Springer), 25
McLean, I. S., Prato, L., McGovern, M. R., et al. 2007, ApJ, 658, 1217
Milosavljević, M. 2004, ApJL, 605, L13
Minniti, D., Contreras Ramos, R., Zoccali, M., et al. 2016, ApJL, 830, L14
Morris, M., & Serabyn, E. 1996, ARA&A, 34, 645
Najarro, F., Figer, D. F., Hillier, D. J., Geballe, T. R., & Kudritzki, R. P. 2009, ApJ, 691, 1816
Nandakumar, G., Ryde, N., Schultheis, M., et al. 2018, MNRAS, 478, 4374
Neumayer, N. 2017, in IAU Symp. 316, Formation, Evolution, and Survival of Massive Star Clusters, ed. C. Charbonnel & A. Nota (Cambridge: Cambridge Univ. Press), 84
Neumayer, N., Seth, A., & Boeker, T. 2020, arXiv:2001.03626
Nogueras-Lara, F., Gallego-Calvente, A. T., & Dong, H. 2018a, A&A, 610, A83
Nogueras-Lara, F., Schödel, R., Dong, H., et al. 2018b, A&A, 620, A83
Nogueras-Lara, F., Schödel, R., Gallego-Calvente, A. T., et al. 2019a, NatAs, 3, 377
Nogueras-Lara, F., Schödel, R., Gallego-Calvente, A. T., et al. 2019b, A&A, 631, A20
Origlia, L., Massari, D., Rich, R. M., et al. 2013, ApJL, 779, L5
Origlia, L., Mucciarelli, A., Fiorentino, G., et al. 2019, ApJ, 871, 114
Origlia, L., Rich, R. M., Ferraro, F. R., et al. 2011, ApJL, 726, L20
Pehlivan, A., Nilsson, H., & Hartman, H. 2015, A&A, 582, A98
Pehlivan Rhodin, A., Hartman, H., Nilsson, H., & Jönsson, P. 2020, A&A, submitted
Pehlivan Rhodin, A., Hartman, H., Nilsson, H., & Jönsson, P. 2017, A&A, 598, A102
Pfuhl, O., Fritz, T. K., Zilka, M., et al. 2011, ApJ, 741, 108
Ramírez, S. V., Sellgren, K., Carr, J. S., et al. 2000, ApJ, 537, 205
Renaud, F., Bournaud, F., Emsellem, E., et al. 2013, MNRAS, 436, 1836
Rich, R. M., Ryde, N., Thorsbro, B., et al. 2017, AJ, 154, 239
Ryde, N., Fritz, T. K., Rich, R. M., et al. 2016a, ApJ, 831, 40
Ryde, N., & Schultheis, M. 2015, A&A, 573, A14
Ryde, N., Schultheis, M., Grieco, V., et al. 2016b, AJ, 151, 1
Salpeter, E. E. 1955, ApJ, 121, 161
Schödel, R., Feldmeier, A., Kunneriath, D., et al. 2014, A&A, 566, A47
Schultheis, M., Ryde, N., & Nandakumar, G. 2016, A&A, 590, A6

10

Scott, P., Asplund, M., Grevesse, N., Bergemann, M., & Sauval, A. J. 2015a, A&A, 573, A26
Scott, P., Grevesse, N., Asplund, M., et al. 2015b, A&A, 573, A25
Seth, A. C., Neumayer, N., & Boeker, T. 2020, in IAU Symp. 351 Star Clusters: From the Milky Way to the Early Universe (Cambridge: Cambridge Univ. Press), 13
Smith, V. V., Cunha, K., Shetrone, M. D., et al. 2013, ApJ, 765, 16
Sneden, C., Cowan, J. J., Kobayashi, C., et al. 2016, ApJ, 817, 53
Spitoni, E., Silva Aguirre, V., Matteucci, F., Calura, F., & Grisoni, V. 2019, A&A, 623, A60
Støstad, M., Do, T., Murray, N., et al. 2015, ApJ, 808, 106

Thorsbro, B., Ryde, N., Rich, R. M., et al. 2018b, in IAU Symp. 334 Rediscovering our Galaxy, 13 (Cambridge: Cambridge Univ. Press), 372
Thorsbro, B., Ryde, N., Schultheis, M., et al. 2018a, ApJ, 866, 52
Tody, D. 1993, in ASP Conf. Ser. 52: Astronomical Data Analysis Software and Systems II, ed. R. J. Hanisch, R. J. V. Brissenden, & J. Barnes (San Francisco, CA: ASP), 173
Tremaine, S. D., Ostriker, J. P., & Spitzer, L., Jr. 1975, ApJ, 196, 407
Valenti, J. A., & Piskunov, N. 1996, A&AS, 118, 595
Valenti, J. A., & Piskunov, N. 2012, SME: Spectroscopy Made Easy, v. 533, Astrophysics Source Code Library, ascl:1202.013

11

95

Clues to galaxy evolution from spectroscopic observations of Galactic centre stars

In this thesis results from observations of stars in the Galactic centre are presented. The results show that there are some interesting differences between the stars in the Galactic centre and stars further out. These differences may help us understand how our Galaxy evolved, and may even provide clues to theories of galaxy formation and evolution.

Brian Thorsbro studied computer science at the University of Copenhagen and then worked for 15 years in the IT industry until he realised his passion for physics. He enrolled as a student at Lund University in 2012 and joined the infrared spectroscopy group as a doctoral student at Lund Observatory in 2016. Brian Thorsbro now looks forward to continuing his work in stellar spectroscopy in Astronomy.